Univerzita Karlova
Přírodovědecká fakulta

Studijní program: Biologie
Studijní obor: NFYZZIV (1511T003)

Filip Tomáška

Úloha inhibičních interneuronů při kódovaní komplexních zvuků sluchovou kůrou myši

The role of inhibitory interneurons in encoding of complex sounds by the auditory cortex of mouse

Diplomová práce

Vedoucí diplomové práce: RNDr. Rostislav Tureček, Ph.D.
Konzultant: Mgr. Ondřej Novák, Ph.D.

Praha, 2018

Prohlášení:

Prohlašuji, že jsem závěrečnou práci zpracoval samostatně a že jsem uvedl všechny použité informační zdroje a literaturu. Tato práce ani její podstatná část nebyla předložena k získání jiného nebo stejného akademického titulu.

V Praze, 13.08.2018

Podpis

Abstract

Recent findings suggest, that perception of acoustic stimuli in the mouse auditory cortex relies on categorization of object-based representations. Local neuronal populations in L2/3 of the mouse auditory cortex reportedly exhibit a limited number (1-3) of stable modes of response, each possibly evoked by multiple complex sounds of variable acoustic features. Stimulation using linear intensity mixing of sounds evoking different response modes revealed an attractor-like dynamic of the underlying representation. These modes of response were hypothesized to represent the neural correlate of perceptual categorization. We have developed an experimental protocol enabling chronic two-photon imaging of the previously described population coding under awake conditions. Using this protocol we acquired data suggesting that the pattern of population activity underlying a mode of response, is stable during a week-long timeframe. We have also recorded the neural activity of a local subpopulation of somatostatin-positive inhibitory interneurons (SST+ INs) during abrupt changes in cortical representation. Our preliminary results suggest that local SST+ INs exhibit maximal firing when the neural correlate of a mode of response is exhibited by the surrounding population of principal cells. In addition, we observed a transient increase in the synchronicity of response of single SST+ cells, concurrent with the switch in cortical representation. We hypothesize that the observed dynamics may reflect the attractor state of the underlying network. Based on the successful acquisition of preliminary results, we confirm that the developed experimental protocol enables recording of specific interneuronal subtypes during changes in cortical representation.

Key words: Auditory cortex, sound encoding, complex stimuli, inhibitory interneurons, optophysiology, attractor dynamics

Abstrakt

Výsledky nedávno publikovaných štúdii ukazujú, že vnímanie akustických stimulov v sluchovej kôre myši môže vykazovať charakter kategorizácie objektovo-založených reprezentácii. Lokálne populácie neurónov nachádzajúce sa v spojenej druhej a tretej vrstve sluchovej kôry myši, údajne vykazujú malý počet stabilných módov odpovedi (1-3), vyvolávaných viacerými komplexnými zvukmi s rozdielnymi akustickými vlastnosťami. Stimulácie za použitia batérie dvoch lineárne zmiešaných zvukov vyvolávajúcich rozdielne módy odpovede preukázali, že takto definované kôrové reprezentácie vykazujú atraktorovú dynamiku. Módy odpovedi môžu podľa autorov reprezentovať nervový korelát vnemových kategórii. Vyvinuli sme protokol, ktorý umožňuje dlhodobé pozorovanie vyššie popísaného populačného kódovania, za použitia dvojfotónovej excitácie u bdelých zvierat. Využitím tohto protokolu sme získali výsledky, ktoré naznačujú že kôrové módy definované konzistentnými populačnými odpoveďami vykazujú stabilitu v časovom horizonte jedného týždňa. Naše predbežné výsledky tiež naznačujú, že priemerná aktivita somatostatín-pozitívnych interneurónov (SST+ INs) behom náhlych zmien v lokálnej reprezentácii dosahuje maximum v priebehu prítomnosti nervového korelátu módu odpovede daného aktivitou excitačných neurónov. Naše dáta taktiež naznačujú, že aktivita jednotlivých SST+ buniek pri odpovedi na kroky z lineárneho mixu spojené s prechodom medzi módmi odpovedi, vykazuje vyššiu zhodu. Naša interpretácia pozorovaného správania spočíva v teórii, že ide o dôsledok dvoch možných stavov lokálnej atraktorovej siete. Na základe získaných pilotných dát sme potvrdili, že vyvinutý experimentálny protokol umožňuje nahrávanie odpovedí špecifického podtypu interneurónov, behom zmien v kôrovej reprezentácii.

Kľúčové slová: Sluchová kôra, kódovanie zvuku, komplexné stimuly, inhibičné interneuróny, optofyziológia, atraktorová dynamika.

List of abbreviations

DNA: Deoxyribonucleic acid
EPSP: Excitatory postsynaptic potential
IPSP: Inhibitory postsynaptic potential
GABA: γ-aminobutiric acid
L1-6: Layer 1-6
PC: Principal cell
IN: Interneuron
PV: Parvalbumin
SST: Somatostatin
5HT3aR: Ionotropic serotonin receptor
Vip: Vasoactive intenstinal peptide
FS: Fast-spiking
ChC: Chandelier cell
AIS: Axon initial segment
AP: Action potential
KCC: Potassium-chloride cotransporter
MPB: Multipolar basket cells
FFI: Feed-forward inhibition
TC: Thalamocortical
MC: Martinotti cell
Non-MC: Non-Martinotti cell
FBI: Feedback inhibition
NMDA: N-methyl-D-aspartate
GAD: glutamate decarboxylase
NGFC: neurogliaform cell
GABAA: Ionotropic GABA receptor
GABAB: Metabotropic GABA receptor
GIRK: G-protein-coupled inwardly rectifying potassium channels
GAT: GABA transporter
CCK: Cholecystokinin
A1: Primary auditory cortex
A2: Secondary auditory cortex
S1: Primary somatosensory cortex
V1: Primary visual cortex
M1: Primary motor cortex
AC: Auditory cortex
CC: Cortico-cortical
CS: Cortico-subcortical
CT: Cortico-thalamic
DM: Dorsomedial auditory field
DA: Dorsoanterior auditory field
DP: Dorsoposterior auditory field
IAF: Insular auditory field
AAF: Anterior auditory field
RF: Receptive field
STRF: Spatio-temporal receptive field
IRES: Internal ribosomal entry site
OGB-1: Oregon Green BAPTA 1
GEVI: Genetically-encoded voltage indicator
GECI: Genetically-encoded calcium indicator
CaM: Calmodulin
AAV: Adeno-associated virus
WPRE: Woodchuck hepatitis virus posttranscriptional regulatory element
SV40: Simian virus 40
syn: synapsin promoter
LSCM: Laser-scanning confocal microscopy
2PLSM: Two-photon laser scanning microscopy
2PA: Two-photon absorption
FOV: Field of view
ROI: Region of interest
PSTH: Post-stimulus time histogram
ACM: Averaged correlation matrix
GPCR: G-protein coupled receptor
CNS: Central nervous system
fps: frames per second

Table of Contents

1 Introduction

The orchestration of the activity of cellular ensembles forming tissues and organs is mostly organized, directly or indirectly, by neuronal populations of the central nervous system. The understanding of the language these populations communicate in when processing extrinsic and intrinsic signals relevant to the organism or when effectuating responses, could have similar ground-breaking consequences as those once generated by the deciphering of the genetic code. Therefore, the breaking of the *neural* code, in many aspects the most prominent mystery of present day physiology, possibly represents the next grand discovery with potential to define a generation of research.

The mammalian brain, with the neocortex as its crowning mystery, remains poorly understood mainly due to its unparalleled complexity in terms of development, organization and function. Every model aspiring to describe the mode of its operation, needs to do so with respect to its anatomical architecture and wiring. Further constraints are generated by the well-documented functional properties of single cells (such as firing rates or short-term synaptic dynamics), or large functional areas (such as their organization into primary and higher-order cortices). The lack of knowledge regarding the physiology of neuronal populations, is primarily caused by the challenges coupled with observations on such scale. Hopefully, recent and future advancements in neurobiological methods will provide tools enabling discoveries leading to the understanding of how information is represented and processed in the central nervous system, ultimately resulting in the capacity to causally intervene under pathological conditions.

2 Structure of interest

As a structure presumably responsible for cognitive abilities and a hallmark of human evolutionary success, the mammalian neocortex is capable of processing complex and highly specific information in distinct functional areas, while employing the same general pattern of cellular organization across different regions. The following chapters will discuss the architecture of the neocortex starting with the characterization of its main neuronal constituents, followed by their functional organization into layers and circuits. Finally, a specific model describing an auditory stimulus-coding strategy will be reviewed.

2.1 Cellular composition

There are two major neuronal subtypes residing in the neocortex. First, the excitatory, glutamatergic, spiny, principal neurons representing approximately 80% of all neocortical neuronal population. These cells are capable of forming synapses generating excitatory postsynaptic potentials (EPSP). Secondly, the inhibitory, GABAergic, smooth, mostly aspiny neurons representing the remaining 20% of total neocortical neurons. Synapses of these cells usually generate inhibitory postsynaptic potentials (IPSP) (DeFelipe and Fariñas, 1992;

Markram et al., 2004). Since inhibitory interneurons and their roles in functional microcircuits represent a substantial part of research described in this text, their properties will be discussed in more detail.

2.1.1 Excitatory neurons

Neocortical neurons forming excitatory synapses are the major (80%) neuronal constituent of the neocortex, responsible for 85% of local connections (DeFelipe and Fariñas, 1992; Douglas and Martin, 2007; Markram et al., 2004). Due to the presence of dendritic spines (short (1-2 μm) membranal compartments (Ballesteros-Yáñez et al., 2006)) excitatory cells are also often termed *spiny* and are, based on their morphology, further distinguishable into two groups: pyramidal cells and non-pyramidal cells (DeFelipe and Fariñas, 1992).

Pyramidal cells form apical dendrites, long axons and reside in all neocortical layers except L1 (DeFelipe and Fariñas, 1992), where their apical dendrites often terminate in tufts (Oberlaender et al., 2012). These cells include both upper and lower L2/3 pyramids with intracortical connectivity (Petersen and Crochet, 2013) and large pyramidal neurons found in L5 (Kasper et al., 1994) and L6 (Thomson, 2010) accounting for most of the output to subcortical regions from the neocortex. Spiny non-pyramidal neurons are classically described as star-shaped or of interneuronal morphology, due to their short, locally branching axonal projections (DeFelipe and Fariñas, 1992). These cells are mainly present in the L4 and include two subtypes: stellate cells, which completely lack an apical dendrite, and star pyramids, which do project a slender apical dendrite terminating in L2 (Oberlaender et al., 2012; Staiger et al., 2004). In general, excitatory neurons mostly form asymmetric (Gray type I) synapses targeting dendritic spines (Ballesteros-Yáñez et al., 2006; Colonnier, 1968; Gray, 1959).

In addition to being the guideline to neuronal migration during neocortical development (Rakic, 1972), local radial glia are a direct progenitor of neocortical principal cells (Tamamaki et al., 2001). Furthermore, it was shown that sister principal cells generated by asymmetrical division of radial glia exhibit transient electrical connections during development (Yu et al., 2012a). These are later transformed into chemical synapses, the incidence of which is significantly higher between clonal sisters when compared to random neighboring principal cells (35% in sister cells compared to 5-20% in random (Markram et al., 1997; Sjöström et al., 2001; Song et al., 2005)) (Yu et al., 2009). Thus, neocortical excitatory microcircuits seem to be lineage-dependent and of significantly nonrandom connectivity (Song et al., 2005). The main task of neocortical principal cells is to convey signals within and between various areas, in other words to effectively carry and drive the flow of information (Tremblay et al., 2016). To our current knowledge, principal cells of the neocortex cannot be categorized into genetically and functionally defined subclasses. Consequently, their characterization mostly relies on morphological properties and connectivity, which are largely layer-specific. Therefore, PC subtypes will be further discussed in the context of single layers (1.2.1 Lamination).

2.1.2 Inhibitory neurons

While neocortical principal cells (PCs) presumably act as carriers of information and drive the flow of data, the role of neocortical GABA(γ-aminobutyric acid)-ergic inhibitory interneurons (INs) most likely involves modulation and shaping of the incoming data flow (Tremblay et al., 2016). Besides the classical, fast synaptic transmission, neuromodulators such as acetylcholine, serotonin, noradrenalin and dopamine have been documented to play an important role in the neocortical function, via their IN-mediated influence (Kawaguchi and Shindou, 1998; Muñoz and Rudy, 2014).

Neocortical INs are of significant anatomical, morphological and electrophysiological diversity, including variable synaptic targeting and subtype-specific expression of genetic markers (Kawaguchi and Kubota, 1997; Kubota, 2014; Markram et al., 2004). This renders any categorization challenging and prone to duplication (The Petilla Interneuron Nomenclature Group (PING), 2008). The commonly accepted generalization states that INs represent 20% of total neocortical neurons, forming 15% of total synapses (symmetric (Gray type II) (Colonnier, 1968; Gray, 1959)). However, data from rat somatosensory cortex suggests that local numbers of INs can be as low as 10-15% (Meyer et al., 2011). Moreover, INs exhibit variable targeting patterns including the soma, the axon initial segment or dendritic shafts (Douglas and Martin, 2007; Kirkcaldie, 2012; Kubota, 2014).

As postulated by Cajal, relative numbers of these “short-axon” cells rise proportionally with the importance of cerebral tissue in evolution. Thus, larger numbers of INs are possibly correlated with the superior performance of human neocortex (Yuste, 2005). Contrary to principal cells, which are of local origin and undergo short migration of radial nature, INs originate in ganglionic eminences of the ventral telencephalon and migrate tangentially towards their final habitats during neocortical development (Guo and Anton, 2014; Lee et al., 2010). The indisputable importance of GABAergic INs within neocortical circuitry (Isaacson and Scanziani, 2011), highlighted by its early recognition, has been a strong driver for continuous research despite their notable variability and largely unsuccessful categorization efforts (Markram et al., 2004; The Petilla Interneuron Nomenclature Group (PING), 2008). Finally, advances in molecular genetics, most notably represented by site-specific recombination systems (Cre/lox, Flp/frt) incorporated into mice (Bockamp et al., 2002), led to the discovery of genetic markers linked with specific morphological and electrophysiological properties (Taniguchi et al., 2011; Tasic et al., 2016). Neocortical INs can be ultimately divided into three non-overlapping groups based on the expression of three main markers: parvalbumin (PV), somatostatin (SST) and the ionotropic receptor for serotonin (5HT3aR) (Kubota et al., 1994; Lee et al., 2010; Zeisel et al., 2015). The expression of these markers is accompanied by specific physiological or morphological properties, nevertheless, an apparent causal connection linking main marker expression to IN features remains, in many cases, unclear, while examples of cells exhibiting all features of a given category, although lacking the main marker have been documented (Taniguchi et al., 2013).

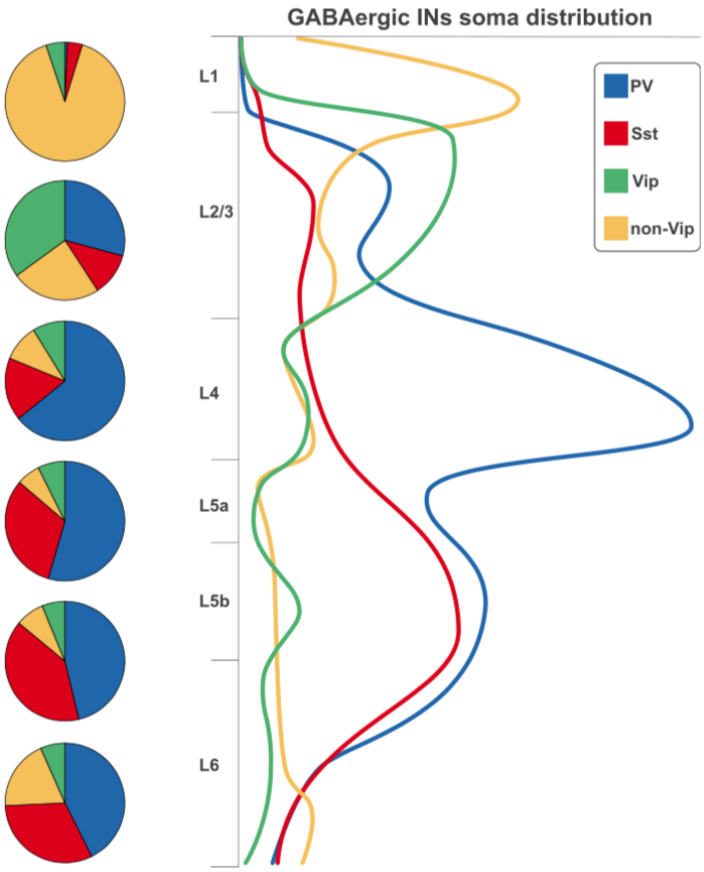

Fig. 1, **Laminar distribution of different interneuronal subtypes** (Tremblay et al., 2016). 5HT3aR INs are predominantly found in the supragranular layers (non-VIP+ INs in L1, VIP INs in L2/3). Although absent in L1, PV+ INs are the most abundant IN subtype of the neocortex. SST+ INs are present in all layers, most notably in the infragranular part of the neocortex.

2.1.2.1 Parvalbumin-positive INs

Parvalbumin (PV) is a calcium-binding protein involved in intracellular calcium homeostasis (Arif, 2009), and the main genetic marker for the largest population of neocortical INs, accounting for ~40% of total IN numbers in the neocortex (Fig. 1) (Tamamaki et al., 2003; Xu et al., 2010). With developmental origins in the medial ganglionic eminence (Guo and Anton, 2014), PV-positive INs include two main morphological subtypes: basket cells and chandelier cells.

2.1.2.1.1 Fast-spiking PV-positive basket cells

Fast-spiking (FS) PV-positive (PV+) basket cells are the most abundant IN subpopulation of the neocortex. Organized into an exclusive, electrically interconnected network (Galarreta and Hestrin, 1999; Gibson et al., 1999), FS basket cells form a multipolar dendritic arbor and exhibit fast, precise, reliable, non-adapting firing (Hu and Jonas, 2014; Kawaguchi, 1995; Taniguchi et al., 2013). This phenotype is driven by

their specialized cellular and membrane properties, including high membrane density of sodium channels (Hu and Jonas, 2014). Further electrophysiological features include low input resistance, low resting membrane potential with subthreshold gamma oscillation activity and the capacity to produce brief spikes with fast afterhyperpolarization supporting high-frequency firing _. Furthermore, both synaptic input to and output from PV+ basket cells is strongly depressing, thus enabling only brief and transient inhibition (Gupta, 2000; Reyes et al., 1998).

According to Ohms law, low input resistance of a membrane results in smaller changes in voltage upon the injection of current (the neurotransmitter-mediated opening of channels). Thus, FS basket cells require stronger stimuli in order to reach the depolarization threshold. In summary, electrical properties of basket cells result in a very fast time constant preventing EPSP summation except for strong near-simultaneous events, therefore enabling reliable coincidence detection and high-pass filtering applicable in the organization of data flow (Tremblay et al., 2016).

PV-positive basket cells form a locally branching axonal arbor, densely (200-1000 cells) and non-specifically innervating neighboring principal cells and INs (mainly other PVs, not SST+ (Pfeffer et al., 2013)). Target cells are contacted at multiple sites (5-15 per cell) of somatic or perisomatic localization (Kawaguchi and Kubota, 1997; Kubota, 2014). By targeting the perisomatic region of PCs (sites of dendritic integration), basket cells effectively control global excitability of the given principal cell and, since being electrically coupled to other local PV+ basket cells, may synchronize local neuronal networks and drive populational oscillations (Buzsáki and Wang, 2012; Freund, 2003; Keimpema et al., 2012; Papp et al., 2001). In addition to the mostly local inhibition generated by regular FS basket cells, a second class of large, presumably PV+, basket cells was reported to form translaminar and transcolumnar projections promoting layer synchronization (Keimpema et al., 2012; Lund et al., 1988; Lund and Yoshioka, 1991; Thomson, 2010). Somata of PV+ basket cells are found in all layers except L1, most densely in L4 (Fig. 1) (Tremblay et al., 2016).

2.1.2.1.2 Chandelier cells

The second main morphological subtype of neocortical PV+ INs are the axo-axonic chandelier cells (ChCs). The term “Chandelier” (Szentágothai and Arbib, 1974) describes the unique targeting properties exhibited by this IN subtype, mainly consisting of dense innervation of the axon initial segment (AIS) with rows of axon terminals termed “cartridges”, bearing resemblance to “a row of candles on a chandelier” (Fig. 2) (Howard et al., 2005; Tai et al., 2014). ChCs are significantly stereotypical in their axonal targeting, innervating exclusively the AIS of principal cells (up to 200 per ChC (Somogyi et al., 1982)). This suggests that ChCs play a substantial role in control over AP generation (Kawaguchi and Kubota, 1997; Kubota, 2014; Somogyi, 1977; Taniguchi et al., 2013). Their somata reside mainly in the upper L2 (from where they send dendrites to L1) and in both L5 and L6 (Taniguchi et al., 2013).

The electrophysiological profile of ChCs resembles that of FS basket cells including exclusive electrical coupling (Kubota, 2014; Taniguchi et al., 2013; Woodruff et al., 2011), promoting synchronizing impact over

larger populations. It is therefore not surprising, that ChCs have been implicated in the oscillation control (hippocampal theta rhythm) (Howard et al., 2005; Kubota, 2014). Interestingly, due to lower expression levels of potassium chloride contransporter 2 (KCC2) reported in the AIS of PCs, GABA-mediated chloride-channel opening may cause local depolarization (Szabadics, 2006).

Contrary to FS basket cells, ChCs are mostly driven by local PC activity and exhibit significantly lower spontaneous firing rates (Howard et al., 2005). Such features would support the hypothetical role of ChCs in the reduction of excessive excitation in local populations (Zhu et al., 2004). Furthermore, results showing an increase in spontaneous ChC firing rate following a decrease in GABAergic input would suggest a possible role of ChCs in monitoring and regulation of local GABA levels (Howard et al., 2005).

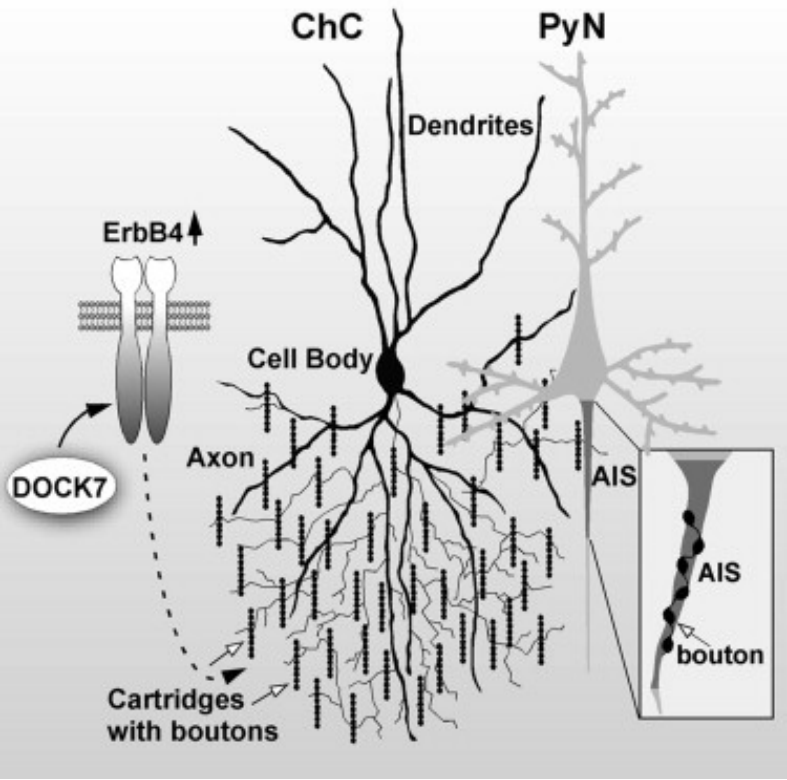

Fig. 2,. **A graphical representation of ChC morphology** (Tai et al., 2014). A detailed depiction of the cartridge-axon complex along with a schematic demonstration of the interaction between DOCK7 a (cytoplasmic activator of ErbB4), and ErbB4 (a tyrosine-kinase receptor) essential for successful development of the ChC phenotype.

2.1.2.2 Feed-forward inhibition

The following example illustrates the overall effect of the above-described properties of PV+ basket cells in a well-documented neocortical circuit. FS basket cells of L4 are the main IN subtype involved in feed-forward inhibition (FFI) of principal cells receiving thalamocortical input. The ascending thalamocortical (TC) projections terminate on both L4 principal cells and L4 FS PV+ INs. As a consequence of their locally branching non-specific and dense axonal plexus, most of the inhibition generated by local FS basket cells is directed towards the neighboring principal cells. Moreover, FS basket cells show a stronger response to TC input due to their specific expression profile (calcium-permeable AMPA receptors (Hull et al., 2009)) (Fig. 3A) (Ji et al., 2016; Zhou et al., 2012). Subsequently, upon stimulation by TC input, FS basket cells responds with fast, precise inhibition of the surrounding PCs. Due to the presence of an additional synapse (illustrated by the wiring diagram in Fig. 3A), basket cell-mediated inhibitory input on L4 PCs arrives with a 1-2 ms delay following the ascending TC input (Pouille, 2001). This creates a brief temporal window, during which a summation of synchronous EPSPs may occur on the PC and an action potential (AP) may be generated, until suppressed by the following onset of inhibition (Fig. 3B). PCs of this circuit therefore serve as coincidence detectors, gating solely near-synchronous thalamic input (Pouille, 2001). Such temporal filtering reportedly sharpens the temporal precision of sensory representations. To provide an example, the above-described dynamics were reported to participate in feature selectivity performed by the L4 of rodent barrel cortex (Pinto et al., 2003; Wilent and Contreras, 2005). Furthermore, the superior nature of PV+ basket cell recruitment prevents early PC saturation while increasing their sensitivity, which consequently enhances the signal-to-noise ratio of PC response (Fig. 3D) (Alonso and Swadlow, 2005; Pinto et al., 2000). This concept hypothetically underlies the improvement of acuity of frequency discrimination in mouse auditory cortex (AC) (Aizenberg et al., 2015). Short-term synaptic depression on both input and output synapses of basket cells causes the gradual extension of summation windows on PCs (Fig. 3C). This was hypothesized to play a role in the switch between two possible stages of stimulus recognition: from presence detection, to the “thorough” perception (Wang et al., 2010).

In summary, FS PV+ basket cells provide fast, efficient and precise inhibition within the local neuronal population and play an important role in the gating of sensory information through feed-forward inhibition by forcing coincidence detection and high-pass filtering on local PCs.

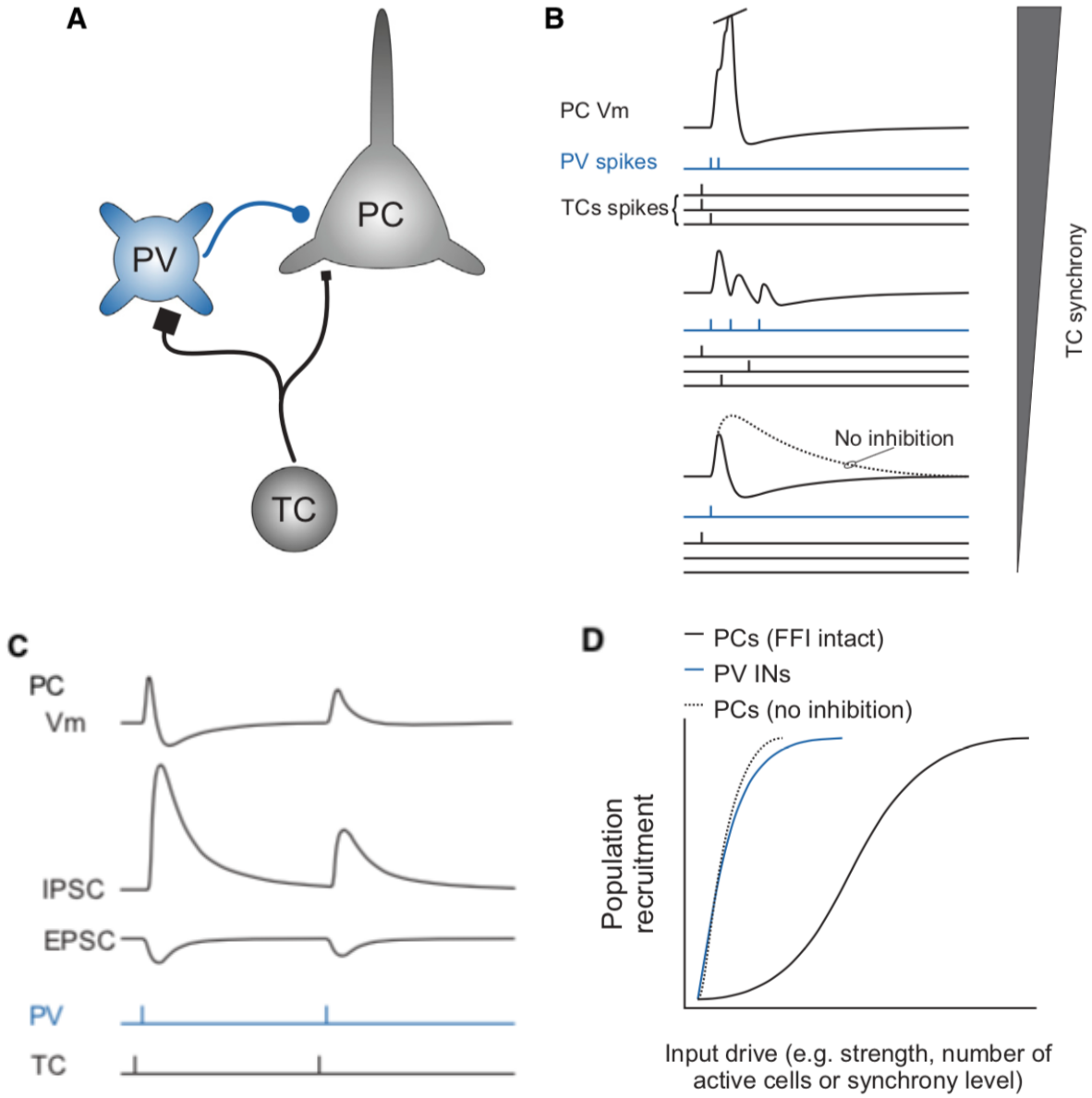

Fig. 3 **Feed-forward inhibition** (Tremblay et al., 2016). A: A wiring diagram of feed-forward inhibition. The same thalamic input produces stronger responses in PV+ basket cells (relative square size) due to their specialized membrane properties. B: Disynaptic inhibition of local principal cells produces a short delay in inhibition following TC input, thus creating a temporal window during which EPSP summation is possible. *Top*: Synchonous input may succeed in generating an AP. *Middle*: Strongly asynchronous TC input is prevented from generating EPSP summation. *Bottom*: A comparative representation displaying the strongly repolarizing effect of FFI on PCs. C: Strong short-term depression on both input and output synapses of FS basket cells results in a relatively fast decrease in the effectivity of FFI. D: Rapid recruitment of basket cells (PV+ INs) enhances PC sensitivity by preventing their rapid saturation (dotted).

2.1.2.3 Somatostatin-positive INs

Somatostatin (SST) is a polypeptide first discovered in the context of hypothalamic somatotropin (growth hormone) inhibition (Brazeau et al., 1973). Its main function involves inhibitory regulation of endocrine and exocrine secretion, predominantly employed in the gastrointestinal tract (Gahete et al., 2010). Moreover, SST acts as a neuromodulator in the CNS and is commonly employed as a co-transmitter by GABAergic cells. Its neuromodulatory effects are GPCR-mediated and include inhibition of neurotransmitter release in the presynaptic cell as well as generation of slow long-lasting inhibition in the postsynaptic cell (Liguz-Lecznar et al., 2016).

SST-positive (SST+) INs have developmental origins in the medial ganglionic eminence and represent the second largest group of neocortical interneurons (20-30% of total INs (Yavorska and Wehr, 2016)). Distinct functional properties of this group are largely determined by two elements: their targeting pattern and short-term dynamics of their excitatory inputs. Contrary to PV+ INs, SST+ INs exhibit dendritic targeting (predominantly dendritic shafts) (Dennison-Cavanagh et al., 1993; Lima and Morrison, 1989; Wang et al., 2004). Moreover excitatory input synapses on SST+ INs are significantly facilitating (Beierlein et al., 2003; Kapfer et al., 2007; Silberberg and Markram, 2007), a characteristic determined by the postsynaptic cell (the interneuron in this case), since a single PC can form both depressing and facilitating synapses depending on its synaptic partner (Buchanan et al., 2012; Reyes et al., 1998; Thomson, 2003). SST+ INs can be divided into two main morphological groups based on the laminar localization of their axonal arborization: Martinotti cells and non-Martinotti cells.

2.1.2.3.1 Martinotti cells

Somata of Martinotti cells (MCs) (Fig. 4 *bottom*) reside in L2/3, L5 and L6. Their dendrites arborize locally and are of bi- or multipolar morphology. In addition to the targeting basal dendrites of the local neuronal population, axons of MCs project to L1, where they branch in a wide axonal plexus (Kubota, 2014) targeting apical dendrites (including spines (Chiu et al., 2013)) of pyramidal cells that reside in L5 (Wang et al., 2010). MCs form chemical synapses with PCs and other INs (PV+ and Vip+). Connections between MCs are, however, strictly electrical (contrary to PV+ basket cells, which are chemically interconnected and, therefore, inhibit each other) (Mahesh M. Karnani et al., 2016; Pfeffer et al., 2013).

The electrical properties of MCs are also somewhat opposite of those of PV+ basket cells. Membranes of MCs exhibit high input resistance, high resting membrane potential, and slow time constant. Further promoted by the strong short-term facilitation of their input synapses, the above-listed features support EPSP summation (Kapfer et al., 2007). Firing patterns employed by MCs include burst firing, regular firing and low-threshold firing (Kubota, 2014). Furthermore, cholinergic input was reported to strongly modulate MC excitation (there is no such effect on FS basket cells) (Fanselow et al., 2008; Kawaguchi, 1997).

2.1.2.3.2 Non-martinotti cells

Non-martinotti cells (Non-MCs) (Fig. 4 *top*) represent SST+ INs lacking an axonal plexus in L1. Located in L4 and L5, non-MCs direct most of their axonal projections to L4 neurons, predominantly L4 PV+ INs, thus suggesting their role in disinhibition of the thalamorecipient (L4) layer (Ma et al., 2006; Xu et al., 2013). In comparison with MCs, electrophysiological properties of non-MCs are of higher variability, including firing patterns typical of MCs (low-threshold spiking) (Beierlein et al., 2003) and firing profiles resembling those of fast-spiking basket cells (Ma et al., 2006). Non-MCs also exhibit facilitating excitatory input, show strong depolarizing response to cholinergic input and, similarly to other types of INs, are electrically interconnected (Amitai et al., 2002).

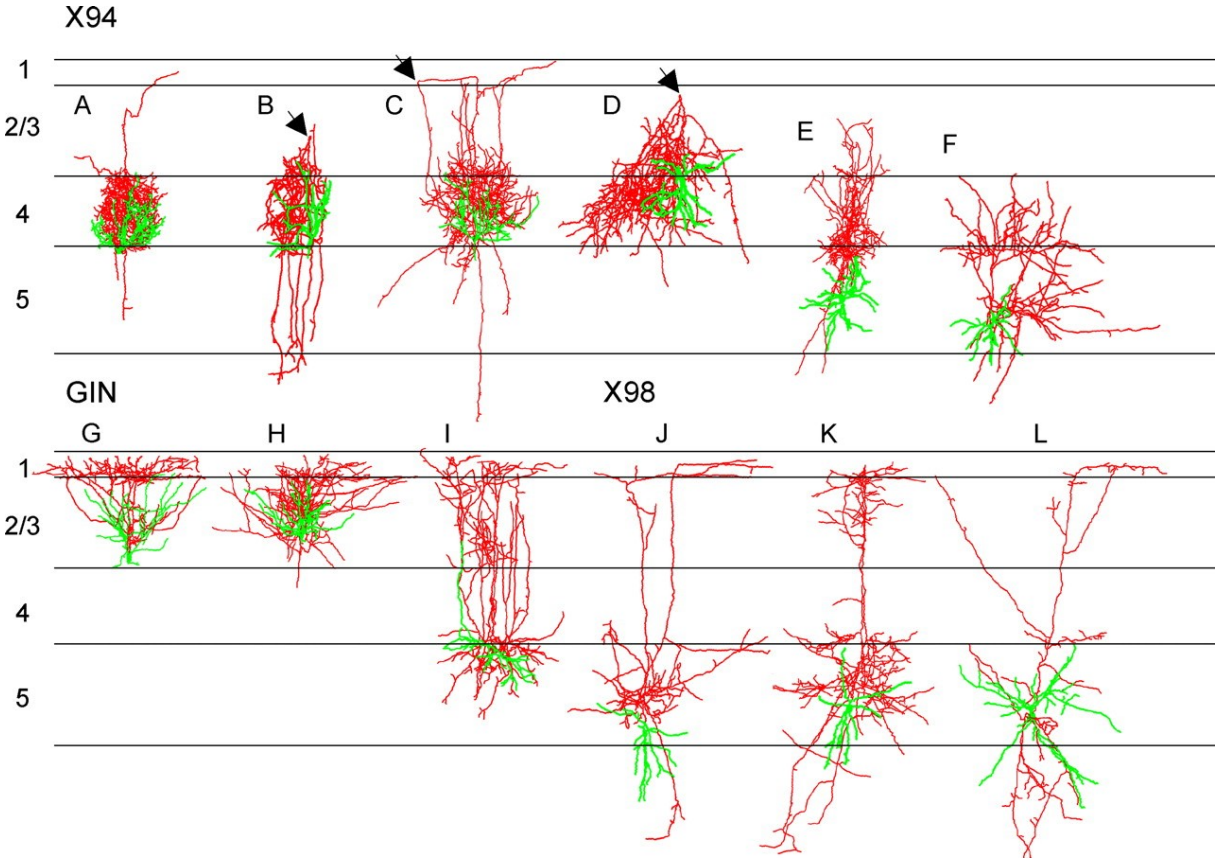

Fig. 4 **Morphological reconstructions of non-Martinotti cells (*top*) and Martinotti cells (*bottom*)** (Ma et al., 2006). Dendrites are green, the axon is red. Arrows represent the turning point of an axon of a non-MC on its way back to L4 .

2.1.2.4 Feedback inhibition

The well-described circuit motif of feedback inhibition (FBI) will be discussed in the following paragraphs, in order to illustrate the functional consequences of the above-listed properties of SST+ cells in comparison with PV+ INs.

Both PV+ and SST+ INs "promiscuously" innervate all possible synaptic targets within their spatial domains, thus creating a dense, non-specific net of inhibition upon local PCs (Fino and Yuste, 2011; Packer and Yuste, 2011). Consequently, upon excitation an IN does not only inhibit the PC from which the excitation has originated, but also other local PCs within the radius of its axonal plexus (Tremblay et al., 2016). Therefore, the same inhibitory circuitry mediates both the feedback inhibition of the PCs driving the IN activity, and the lateral inhibition of the PCs which do not excite the given IN. These laterally inhibited PCs may reside locally, or may be targeted by specialized populations of GABAergic neurons projecting onto their dendrites or somata from elsewhere (Helmstaedter et al., 2008; Kätzel et al., 2011). This concept is widely employed by various systems, examples of which include: surround suppression mediated by SST+ INs in the visual cortex (Adesnik et al., 2012), cell assembly or neuronal population selection (Roux and Buzsáki, 2015), role in the generation of gamma oscillation (FS basket cells) (Buzsáki and Wang, 2012) and attractor networks of hippocampal grid cells (Couey et al., 2013). In a FBI wiring diagram (Fig. 5A), a PC forms excitatory connections with an IN, while being reciprocally targeted. As previously discussed, electrical properties and short-term dynamics of excitatory input represent the main functional differences between PV+ and SST+ INs, subsequently shaping the dynamics of recurrent inhibition.

Low capacitance of PV+ IN results in their fast responses to excitatory input, which gradually diminish due to the strongly depressing character of excitatory input synapses and due to the fast time constant preventing EPSP summation (Fig. 5B *left up*). In the case of SST+ INs, the high membrane potential causes that non-synchronous excitatory input initially drives subthreshold events. However, due to a slow time constant enabling EPSPs to summate and strongly facilitating input synapses, SST+ INs gradually depolarize (Fig. 5B *bottom left*), until reaching the action potential threshold (Fig. 5B *bottom right*) (Kapfer et al., 2007; Pouille and Scanziani, 2004). This temporal dichotomy in inhibition also carries a spatial component, owing to different targeting patterns of PV+ and SST+ INs. As reported for hippocampal PCs, a high-frequency stimulus (100 Hz) delivered to the local population results in immediate perisomatic inhibition, gradually substituted by dendritic inhibition (Pouille and Scanziani, 2004). As discussed in the context of feed-forward inhibition (FFI), PV+ basket cells are intrinsically reliable coincidence detectors and their activity is best driven by synchronous input. Consequently, this IN subtype mainly mediates FBI in response to coordinated firing of a larger number of PCs (Kwan and Dan, 2012), with the capacity to alter the overall timing of local PC activity, by regulating their sodium based somatic depolarization (Tremblay et al., 2016). On the other hand, SST+ INs are capable of integrating positive changes in firing rates from as little as single PCs (Kapfer et al., 2007; Kwan and Dan, 2012), thus serving as local detectors and suppressors of bursting activity. This proposed role is supported by

the dendritic nature of SST+ IN targeting. It suggests regulatory effect over dendritic integration by shunting NMDA receptor-based spikes on dendritic shafts, and inhibition of calcium-based potentials locally generated in order to relay dendritic depolarizations to the otherwise distant AIS (dendritic initiation zone is further discussed in 2.2.1.1.4 Layer 5) (Fig. 5E) (Miles et al., 1996; Royer et al., 2012).

In summary, PC+ basket cells are assumed to temporally segregate local neuronal populations into functional cell assemblies using FBI (Fig. 5C) (Buzsáki and Wang, 2012). On the other hand, SST+ INs are expected to generate a local non-specific net of inhibition suppressing extensive bursting activity. Such environment hypothetically favors a winner-takes all, attractor-like network dynamic, where an optimally stimulated PC (or an assembly of PCs) could drive the SST+ IN strongly enough to inhibit its neighbors via disynaptic inhibition (Fig. 5D) (Silberberg, 2008). In contrast to FFI, the excitation driving FBI originates locally. However, it is important to note that INs involved in FFI and FBI do not represent separated populations. Both PV+ and SST+ INs may receive local and thalamocortical input at the same time, which would implement them in both inhibitory circuits simultaneously. In summary both FFI and FBI represent concepts of functional organization rather than physically separated wiring patterns (Roux and Buzsáki, 2015).

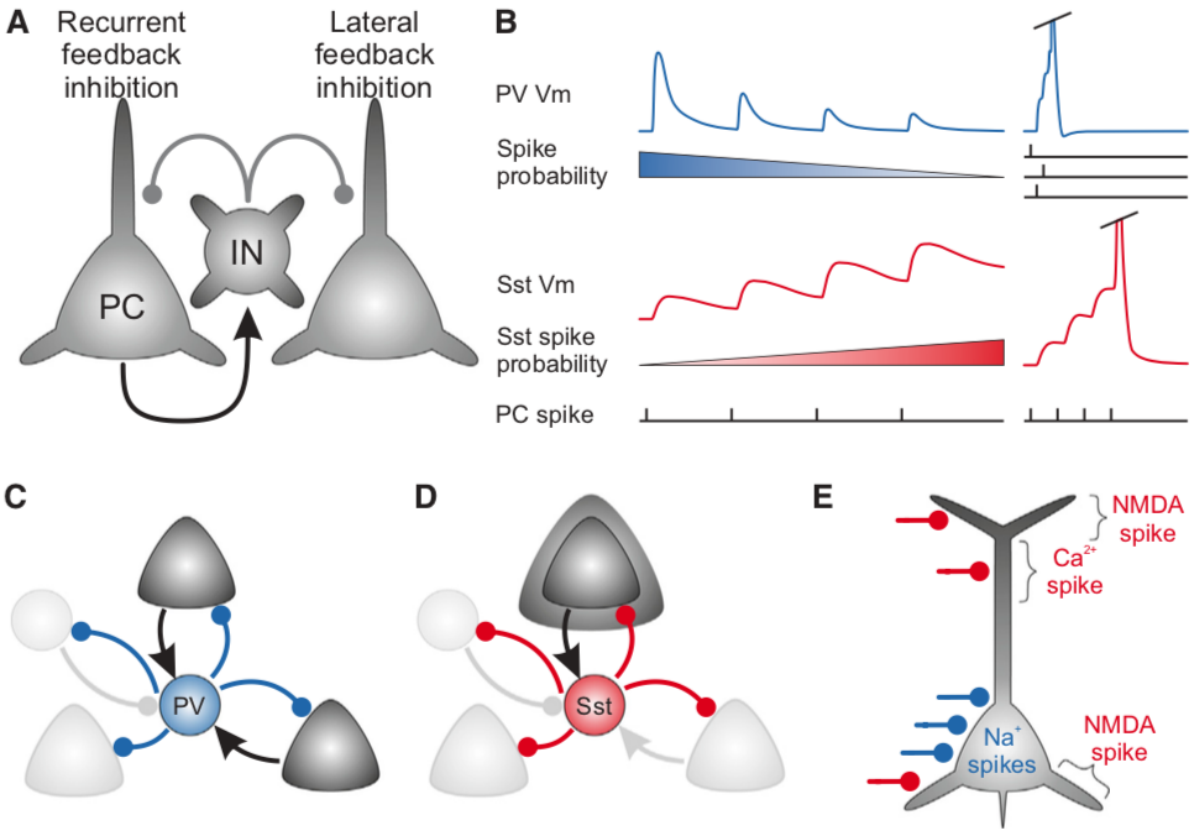

Fig. 5 **Feedback inhibition** (Tremblay et al., 2016). A: A general wiring diagram of feedback inhibition. Locally generated excitation depolarizing an interneuron (IN), results in feedback inhibition of the stimulating

principal cell (PC) and lateral inhibition of other local PCs due to dense and non-specific nature of IN targeting. B: Electrical and synaptic properties of PV+ (*top*) and SST+ (*bottom*) INs determine their response to excitation input from a PC. The amplitude of EPSP during continuous spiking diminishes in the case of PV+ INs (top left) while it grows in the case of SST+ INs (bottom left). Successful somatic depolarization of a PV+ IN is achieved if synchronous input arrives from multiple cells (*top right*). An SST+ IN can be depolarized by a single PC if enough EPSP are provided repeatedly for successful summation. C: PV+ basket cells are driven by synchronously active PCs, while inhibiting the rest of the population. D: SST+ INs provide tonic inhibition favoring attractor dynamics, where the PC with the strongest drive inhibits all others. E: A graphical representation of axonal targeting for PV+ (blue) and SST+ (red) INs, specifying the nature of inhibited depolarizations.

2.1.2.5 5HT3aR-positive INs

The third and the most heterogeneous group among GABA-ergic INs consists of cells expressing a functional ionotropic serotonin receptor (5HT3aR) as their main marker (Fig. 8). 5HT3aR+ INs originate in the caudal ganglionic eminence and represent the remaining 30% of all glutamate decarboxylase (GAD) (a marker of GABAergic cells) positive cells of the neocortex (Lee et al., 2010). In addition to the susceptibility to serotonin-mediated excitation, all types of 5HT3aR+ INs express nicotinic receptors and may therefore be depolarized by cholinergic input (Férézou et al., 2002; Lee et al., 2010). 5HT3aR+ INs are the dominant IN subtype in supragranular layers, while being the only neuronal subtype present in L1 (Fig. 1) (Lee et al., 2010; Rudy et al., 2011). 5HT3aR+ INs are further divided into two groups based on the expression of the vasoactive intestinal peptide (Vip).

2.1.2.5.1 Vip-positive 5HT3aR+ INs

The vasoactive intestinal peptide (Vip) is a short neuropeptide, a member of the glucagon/secretin family, modulating neural activity in both central and peripheral nervous system (White et al., 2010). Outside of the nervous system, Vip-mediated signalization regulates physiological and pathophysiological processes taking place in digestive, reproductive, respiratory and cardiovascular systems (Umetsu et al., 2011).

Vip-positive (Vip+) INs represent ~ 40% of total 5HT3aR+ INs and are dividable into two morphological categories: bipolar and multipolar. The small somata of bipolar Vip+ INs are mainly located in L2/3 (60%) while other layers of the neocortex collectively account for 40% (Fig. 1, Fig. 6) (Prönneke et al., 2015). Predominantly of vertically-oriented bipolar morphology, projections of these cells span in a translaminar, but horizontally confined fashion. Dendrites of bipolar Vip+ INs with somas located in L2/3 reach L1 but do not target infragranular layers. Dendrites of bipolar Vip+ INs residing in infragranular layers form dendritic projections in both supra- and infragranular layers. However, in terms of axonal projections, supragranular bipolar Vip+ INs have descending axons targeting the whole neocortex, while those of deeper layers form axons

confined to L5 and L6. In summary, bipolar Vip+ INs of infra and supragranular layers exhibit inverse projectional organization (Bayraktar et al., 2000; Kubota, 2014; Prönneke et al., 2015). Further notable properties of bipolar Vip+ INs include preferential targeting of SST+ INs, a very high input resistance (enabling responses to weak stimuli including TC drive (Lee et al., 2010)) and various firing patterns (Caputi et al., 2009; Jiang et al., 2015). In terms of nomenclature, bipolar Vip+ INs are commonly referred to as bitufted or double-bouqet cells (DeFelipe et al., 2006).

Vip+ INs not exhibiting a bipolar phenotype tend to form dendrites of multipolar morphology and reside in the upper L2 and in deep layers of the neocortex. These cells include small Vip- and cholecystokinin-positive (Cck+) basket cells with locally and horizontally projecting axons forming basket like innervation (Caputi et al., 2009; Wang, 2002). In addition, Vip-positive (Vip+) INs were reported to induce local vasodilatation, thus directly coupling neural activity with the vascular system (Cauli et al., 2004).

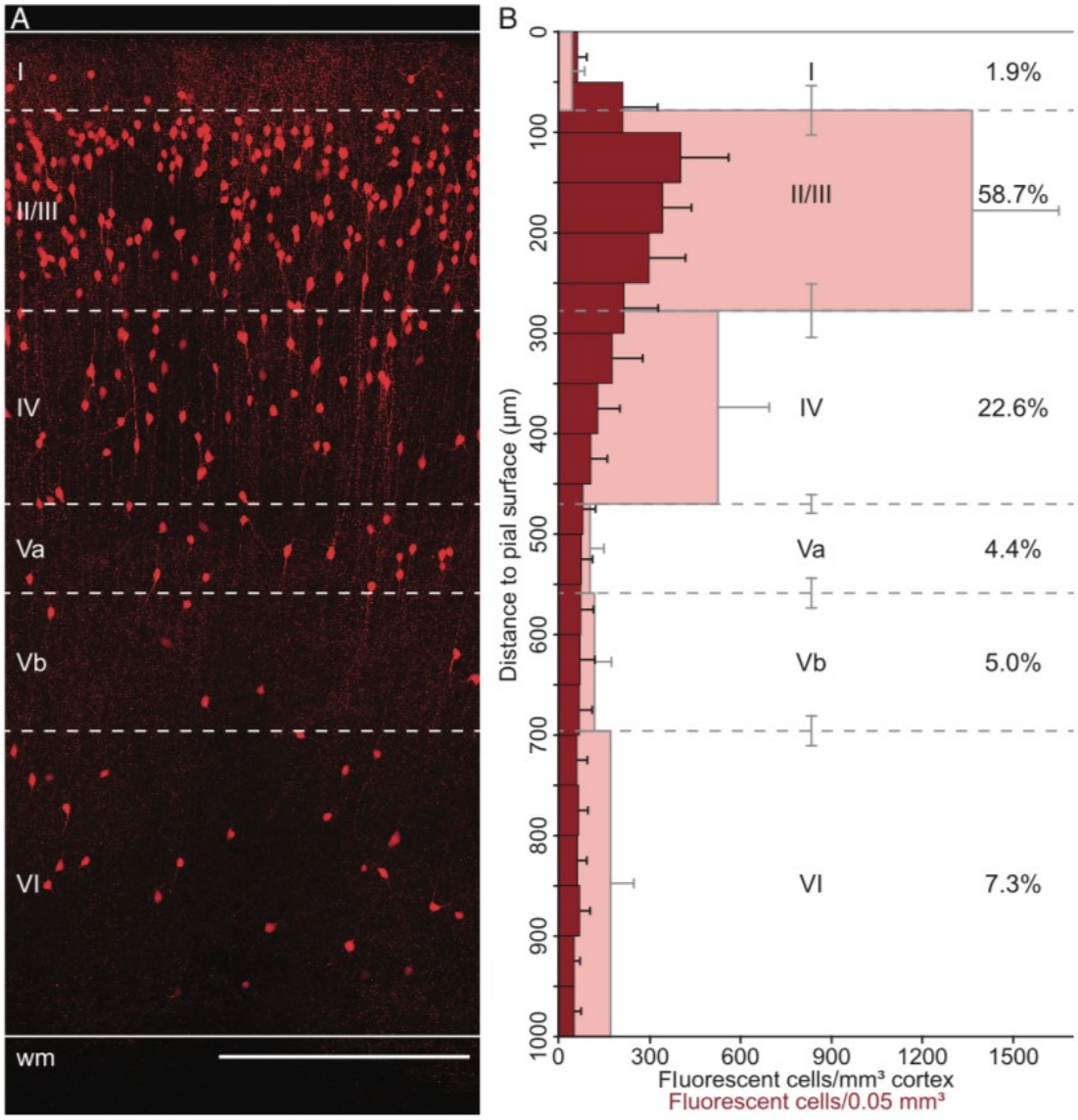

Fig. 6 **Vertical distribution of Vip+ cells in the neocortex** (Prönneke et al., 2015). A: Vip+ cells expressing a red fluorescent protein tdTomato show uneven distribution along neocortical layers. Lateral projection of a z-

stack acquired from a 300µm thick coronal section. B: Relative Vip+ cell density across the neocortex determined based on 150 samples similar to A show that Vip+ cells are preferentially located in L2/3 (60%).

2.1.2.5.2 Non-Vip-expressing 5HT3aR+ INs

Non-Vip-expressing INs represent ~60% of the total neocortical 5HT3aR+ IN population, while being the almost exclusive neuron type of L1 (90%) (Lee et al., 2015; Rudy et al., 2011). Non-Vip+ INs do not bear strict group-specific features but are divided into three subgroups, which do: neurogliaform cells, single-bouquet cells, and large Cck+ basket cells.

Neurogliaform cells (NGFCs) are an IN-subtype of specific morphological properties and synaptic transmission present in all layers of the neocortex, while being the almost exclusive residential neuronal subtype of L1 (Tremblay et al., 2016). NGFCs have a small soma and an especially dense local dendritic field consisting of frequently branched dendrites (Hestrin and Armstrong, 1996; Kawaguchi et al., 2006; Kubota, 2014; Oláh et al., 2007). Their axons, exhibit high densities of terminal boutons and form a fine but dense axonal plexus (longest axons of non-pyramidal cells) of mostly local nature (with the exception of L1 NGFCs (elongated NGFCs, which form axonal arborizations extending beyond their anatomical columns) (Hestrin and Armstrong, 1996; Jiang et al., 2013; Kawaguchi and Kubota, 1997; Kubota, 2014).

NGFCs exhibit a late-spiking firing pattern with slowly devolving depolarization (Kawaguchi, 1995), a feature often used for their identification in electrophysiological recordings. Furthermore, NGFCs have been reported to form electrical synapses with other IN subtypes, thus suggesting their implication in integration of the otherwise electrically separated interneuronal networks (Simon et al., 2005). In addition to the above-described morphological and electrophysiological features, it is the, to a large extend consequent, nature of the chemical synaptic transmission, which differentiates NGFCs from the rest of IN subtypes. Contrary to other GABAergic INs of the neocortex, NGFCs produce slow, long-lasting IPSPs in their target cells (PCs and other INs), through the combined activation of GABAA (a chloride channel mediating fast hyperpolarization) and GABAB (a G-protein-coupled receptor mediating slow hyperpolarization through the activation of G-protein-coupled inwardly rectifying potassium channels (GIRK) Kiv3.2) receptors (Gähwiler and Brown, 1985; Lüscher et al., 1997; Oláh et al., 2007; Tamás et al., 2003). Since GABAB receptors are usually located extrasynaptically, their activation is typically induced by extensive synaptic transmission leading to GABA spillover (Scanziani, 2000). Nevertheless, NGFCs are not equipped to deliver long-lasting firing that would oversaturate synaptic GABA transporters (GAT) tasked with GABA intake (Gonzalez-Burgos, 2010). Therefore, in addition to regular, Gray type 2 synaptic connections, NGFCs form synapses with larger synaptic clefts (Szabadics et al., 2007), while their axons include terminal boutons with no clear postsynaptic partner, presumably in order to facilitate GABA diffusion (Oláh et al., 2009). Single-bouquet cells (SBCs) are the second neuronal subtype residing in L1, mainly its inner part. In comparison to NGFCs, SBCs do not mediate volume transition and target L2/3 INs based on excitatory drive from L2/3 PCs (Lee et al., 2015).

The non-Vip Cholecystokinin-positive (Cck+) basket cells are of larger overall morphology (soma, axonal and dendritic projections) than those Vip-positive (Galarreta et al., 2004; Karube et al., 2004). Given their name, large Cck+ basket cells exhibit somatic and perisomatic targeting and, therefore, were extensively compared to PV+ basket cells of the same targeting pattern. While networks of PV+ basket cells likely mediate fast, reliable regulation of network synchronicity and oscillations (Buzsáki and Wang, 2012; Pouille, 2001), the role of Cck+ basket cells has been implicated in the translation of mood-related signals of subcortical origin (illustrated by the strong serotonergic drive from raphe nuclei), to local neuronal populations (Freund, 2003; Freund and Katona, 2007). This is supported by the fact that Cck+ basket cells, unlike their PV+ counterparts, are sensitive to serotonin (as part of the 5HT3aR+ group), acetylcholine (via postsynaptic nicotinic receptors) and also presynaptically express cannabinoid receptors (CB1).

2.1.2.6 Disinhibition

Networks containing neurons forming inhibitory connections with PC-targeting GABAergic INs, represent the wiring base for the disinhibition circuitry (Fig. 7A). In the context of neocortex, such targeting is most dominantly exhibited by bipolar Vip+ INs of the superficial layers, preferentially targeting SST+ INs of L2/3 (reported for primary somatosensory (S1) (Lee et al., 2013), auditory (A1) (Pi et al., 2013) and visual (V1) cortices (Pfeffer et al., 2013)). As a consequence of their horizontally-confined axonal morphology (Prönneke et al., 2015), bipolar Vip+ INs may mediate focal disinhibition in a similarly columnar fashion (Fig. 7C) (M. M. Karnani et al., 2016). However, in order to exert spatially confined disinhibition with functional relevance, the input driving bipolar Vip+ INs must be of causally-related origin. As documented in sensory cortices, cortico-cortical feedback from higher-order regions preferentially targets Vip+ INs, membrane properties of which further promote facilitated depolarization by this excitatory input (Lee et al., 2010). The primary motor cortex (M1), targeting the S1 barrel cortex may serve as an example of such wiring (Lee et al., 2013). Local electrophysiological data show, that SST+ INs of the barrel cortex exhibit higher levels of activity during rest (no whisker stimulation) as opposed to the significant inhibition of their firing during periods of active or passive whisker movement. Moreover, the latter situation is accompanied by an elevation in the activity of surrounding PCs (Gentet et al., 2012). Glutamatergic input from the cingulate cortex targeting V1 provides another example of disinhibition-mediated top-down modulation by feedback projections from higher-order areas (Gonchar and Burkhalter, 2003; Zhang et al., 2014). In addition to feedback projections, Vip+ bipolar INs were also reported to receive direct thalamic input, which suggests their possible role in feed-forward sensory-dependent disinhibition of supragranular populations (Lee et al., 2010).

Besides the spatially restricted disinhibition induced by direct excitatory input, bipolar Vip+ INs are also sensitive to neuromodulatory projections of mainly subcortical origin. Consequently, there seems to be another, neuromodulatory, system mediating the disinhibition that is less spatially restricted and acts on a more global scale (Fig. 7B) (Fu et al., 2014). For illustration, locomotion, as a global state of the organism, seems to cause global disinhibition in sensory cortices (visual, auditory), via cholinergic input (from the basal forebrain)

activating nicotinic receptors located on membranes of Vip+ INs. Other neuromodulatory systems are also suspected to act in a similar manner (Fu et al., 2014).

In summary, the disinhibition mediated by Vip+ INs can be both spatially limited and widespread depending on the nature of the input. Glutamatergic excitatory input from higher-order structures (feedback) or from primary thalamic nuclei (feed-forward) both result in spatially precise disinhibition often leading to an increase in representation acuity. Neuromodulatory input from subcortical areas on the other hand, result in less-specific, widespread changes in neocortical activity by increasing the overall gain of entire areas.

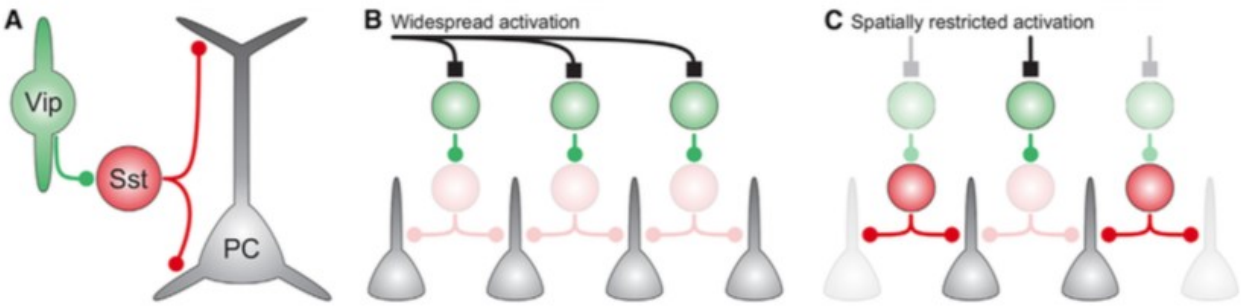

Fig. 7 **Feedback inhibition** (Tremblay et al., 2016), A: A wiring diagram demonstrating the identities of and connectivity between neurons involved in disinhibition. B: Neuromodulatory input on bipolar Vip+ INs results in a widespread disinhibition of global effect. C: Excitatory input (cortico-cortical or thalamocortical) on bipolar Vip+ INs results in spatially confined disinhibition of a limited number of local PCs.

Advancements in molecular genetics enabled significant progress in the categorization of INs into non-overlapping groups of specific function within the networks of neocortex. PV+ basket cells are considered to represent the “clockwork” of the neocortex given their pivotal role in oscillation generation and sensory gating through feed-forward inhibition. SST+ INs are expected to form an adaptive blanket of feedback inhibition enabling attractor-like competition and selection of the most active cells/cell assemblies. And finally, Vip+ bipolar INs could create “holes” in the above-mentioned blanket of inhibition based on current cognitive circumstances.

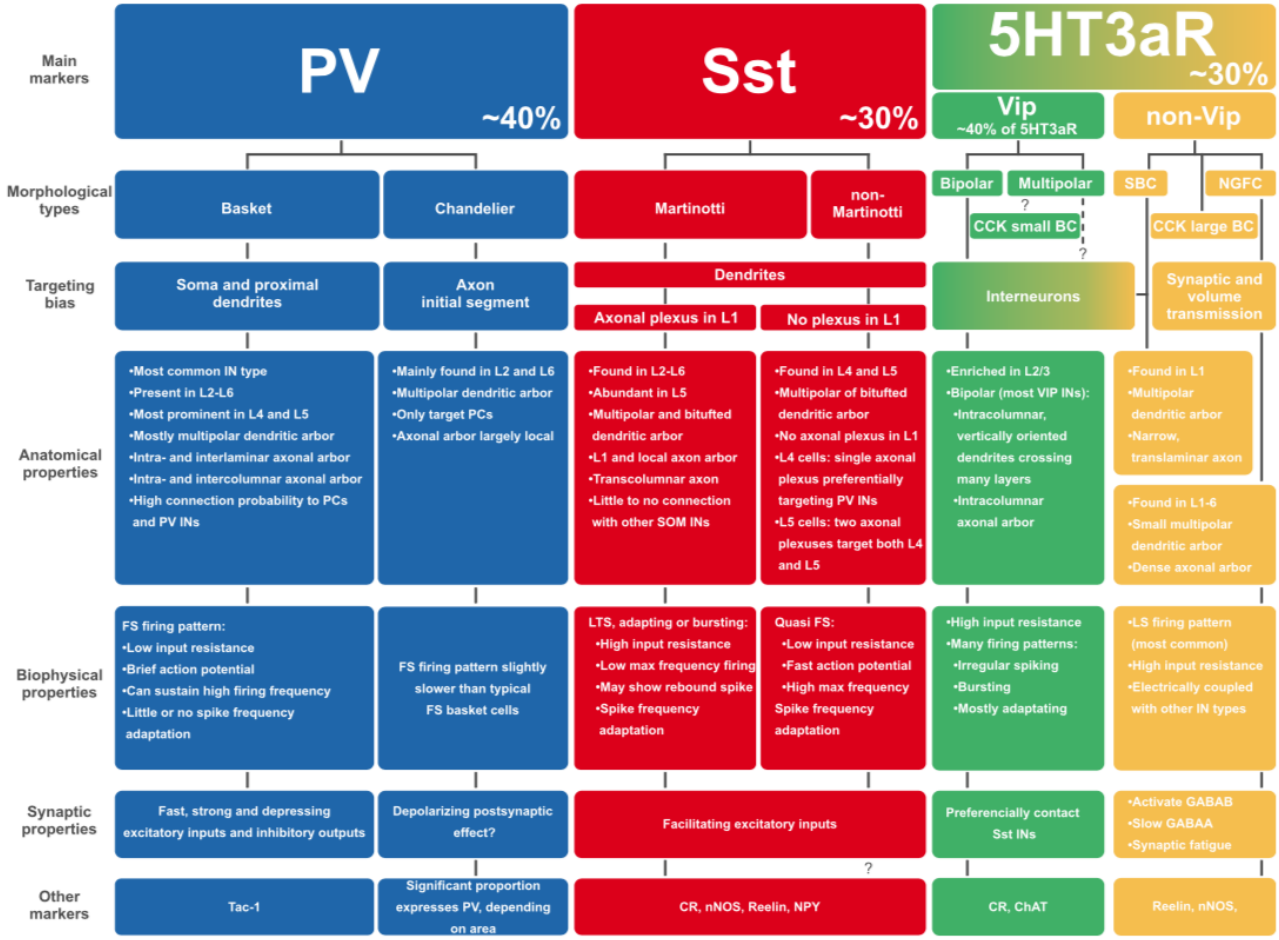

Fig. 8 **Classification of neocortical interneurons** (Tremblay et al., 2016). Virtually all neocortical INs express one of three non-overlapping molecular markers. Further subdivisions of these groups include the previously characterized morphological, electrophysiological and other subtypes.

2.2 Functional architecture

The hypothesis that the neocortex could be assembled from universal building blocks was first postulated by the early neuroanatomists and further developed in the second half of the twentieth century. Neocortical neurons are morphologically and functionally organized into six layers (Douglas and Martin, 2004), thus exhibiting universal horizontal architecture. However, a strict vertical pattern of organization common to the entire neocortex remains elusive as the notion of cortical columns as functional units has been largely abandoned (Costa et al., 2010).

2.2.1 Lamination

Layer-dependent differences in cellular density and morphology, provided early neuroanatomists including Meynert (Seitelberger, 1997) and Brodmann with information leading to the characterization of the neocortex as a six-layered structure (Skoglund, 1997). Layer 4 is often referred to as the granular layer, due to the morphological features of its cellular constituents. Consequently, layers above L4 are frequently termed supragranular layers while layers located deeper than L4 are commonly termed infragranular. During development, cortical layers are generated by successive migration of neurons from the ventricular zone towards pial surface, while surpassing previously arriving cells (Ogawa et al., 1995). Furthermore, neurons of different layers exhibit distinct input/output patterns, ultimately resulting in layer-specific physiological properties (Douglas and Martin, 2004; Gilbert and Kelly, 1975). The existence of such layer-specific organization suggests the possible role of neocortical lamination as a scaffold used to organize and limit the way neocortical neurons form connections, in order to achieve optimal wire use (Chklovskii et al., 2002; Douglas and Martin, 2004; Mitchison, 1991).

The relative thickness of different layers seems to be largely invariant across different sensory cortices of the mouse neocortex. Layers 1, 2/3 and 4 represent 50% of total thickness, while Layers 5 and 6 both contribute with 25% (Anderson et al., 2009). Nevertheless, the six-layered nature of neocortical organization is still subject to considerable variability across the whole neocortex (for example the output-oriented primary motor cortex is often termed agranular for its apparent lack of L4 (Yamawaki et al., 2014)). Therefore, a depiction of neocortical lamination exhibiting strict functional and anatomical boundaries represents a significant simplification and needs to be considered with respect to the local context (Shipp, 2007).

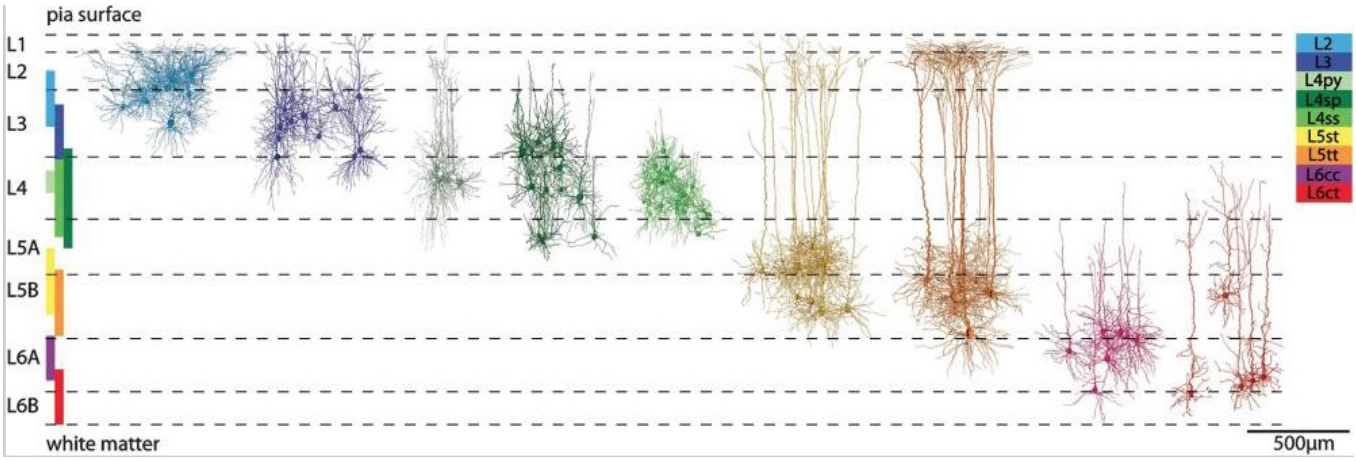

Fig. 9 **Glutamatergic excitatory cells of the neocortex** (Oberlaender et al., 2012), A schematic representation of different cellular morphology of glutamatergic excitatory cells present in the neocortex. py: pyramid, sp: star pyramids, ss: spiny stellate, st: slender-tufted (L5 cortico-cortical), tt: thick-tufted (L5 cortico-subcortical), cc: corticocortical, ct: corticothalamic.

2.2.1.1.1 Layer 1

From the morphological point of view, Layer I, or the *molecular* layer, of the neocortex is mostly comprised of apical dendrites of cortical neurons, as well as axons of both cortical and subcortical origin (Larkum, 2013; Rubio-Garrido et al., 2009). Contrary to other layers, L1 contains only a very sparse population of neurons (Garcia-Munoz and Arbuthnott, 2015; Shipp, 2007). In mice, its thickness is ∼125 μm (Petersen and Crochet, 2013).

L1 is the first layer to appear during neocortical ontogenesis as the *marginal zone* and is essential for further neocortical development (Marín-Padilla, 1998; Muralidhar et al., 2014). From between E10,5 and E12,5, a special class of interneurons, the Cajal-Retzius cells, migrate into the marginal zone and mediate the transient localized production of *reelin* (Kwon et al., 2011) an extracellular matrix protein essential for successful cortical lamination (Del Río et al., 1997; Ogawa et al., 1995). Glutamatergic Cajal-Retzius cells are no longer present in the mature neocortex (Ma et al., 2014), instead the only neurons present in mature L1 are GABAergic interneurons almost exclusively belonging to the 5HT3aR group (mainly non-VIP) (Fig. 1) (Lee et al., 2015; Rudy et al., 2011). L1 of a mature neocortex is where local (10%) and long-distance (90%) projections including higher-order structures converge on a relatively small number of interneurons, thus suggesting its role in top-down feedback of cortical processing (Cauller, 1995; Gilbert and Sigman, 2007; Larkum, 2013).

2.2.1.1.2 Layers 2 and 3

The *external granular* (L2) and *external pyramidal* (L3) layers consist of neurons, which were the last to migrate into the developing neocortex. While L2 and L3 are morphologically discernable in human samples, their distinction in rodents is more challenging. Therefore, rodent L2 and L3 are collectively referred to as L2/3 (Meng et al., 2017). The mouse L2/3 is a ∼300 μm thick structure densely populated by pyramidal neurons of two morphological subtypes. PCs residing closer to the pial surface exhibit apical dendrites with short, horizontally stretched dendritic trees (Fig. 9) (Oberlaender et al., 2012). Pyramids located deeper within the L2/3 develop apical dendrites with vertical alignment terminating in L1 (Fig. 9) (Oberlaender et al., 2012; Petersen and Crochet, 2013). Furthermore, multiple subtypes of inhibitory interneurons, mainly cells of the 5HT3aR group (with a slight bias towards VIP-expressing) supported by a lower number of PVs (Fig. 1) reside in L2/3 (Rudy et al., 2011).

In terms of neurophysiology, projections to and from L2/3 provide connections between different neocortical areas and regions, thus forming the foundation for an information integration nod located in L2/3 (Petersen and Crochet, 2013). Excitatory neurons of L2/3 were shown to exhibit sparse, spatially focused and generally lower evoked and spontaneous activity when compared to the higher and spatially distributed overall activity reported for neurons of the granular layer (O'Connor et al., 2010; Petersen and Crochet, 2013; Sakata and Harris, 2009). Moreover, the receptive fields of neurons belonging to L2/3 show greater heterogeneity in comparison to those of L4 neurons (Bathellier et al., 2012; Winkowski and Kanold, 2013). Due to the above

listed properties, neurons of L2/3 exhibit higher stimulus selectivity, including that to complex stimuli (Petersen and Crochet, 2013).

2.2.1.1.3 Layer 4

Neurons of L4, the *internal granular* layer, are the main neocortical target for thalamic input (Douglas and Martin, 2004; Gilbert and Wiesel, 1979) (originating from the medial geniculate nucleus in the case of AC (Cetas et al., 1999)). Although this notion may be contested by the fact that thalamic innervation has also been reported for all other layers (Cetas et al., 1999; Constantinople and Bruno, 2013; Ji et al., 2016; Rubio-Garrido et al., 2009), L4 still receives the strongest thalamic drive (Constantinople and Bruno, 2013; Ji et al., 2016). Thalamocortical projections target both excitatory neurons and GABAergic interneurons (Feldmeyer, 2012; Ji et al., 2016). The strength of thalamic innervation terminating on PV interneurons (the most abundant IN type of L4 (Tremblay et al., 2016)) surpasses those terminating on all other cell-types including excitatory neurons. This enables strong sensory-evoked feed-forward inhibition, resulting in precise and reliable synchronization of L4 pyramidal activity (Ji et al., 2016; Zhou et al., 2012). Thalamocortical projections constitute only 5-20% of excitatory synapses on L4 neurons, while the rest presumably originates from local cortical circuits (Douglas and Martin, 2007; Feldmeyer, 2012). However, axon terminals originating from thalamic nuclei preferentially target perisomatic regions of L4 neurons, thus possibly increasing the efficiency of thalamic drive over that of locally originating input (Richardson et al., 2009).

In general, most (58% in rat somatosensory cortex (Staiger et al., 2004)) L4 excitatory neurons of sensory cortices, belong to the group of *spiny stellate cells* (Fig. 9). Dendritic trees of these cells are limited to L4, lack the apical dendrite and their axons project vertically while arborizing in L4 and L2/3 (Costa and Martin, 2011; Feldmeyer, 2012; Oberlaender et al., 2012). Another spiny neuronal subtype found exclusively in L4 are the *star pyramidal cells* (Fig. 9) (representing 25% of excitatory cells in L4 of rat somatosensory cortex (Staiger et al., 2004)). Star pyramids do form an apical dendrite, although not terminating further than L2 and with no tuft (Oberlaender et al., 2012). These two cell types are further complemented by L4 pyramids, with apical dendrites terminating in tufts located in L1 (Oberlaender et al., 2012), representing 17% of excitatory principal cells in the somatosensory cortex of a rat (Staiger et al., 2004). Contrary to other sensory cortices, the majority of L4 excitatory neurons of the AC does exhibit apical dendrites, a hallmark for L4 of the auditory cortex across species (Richardson et al., 2009; Smith and Populin, 2001).

The concept of L4 as the main thalamorecipient layer further relaying the incoming input towards supragranular layers has been originally proposed half a century ago (Gilbert and Wiesel, 1979) and remains relevant to this day (Callaway, 2004; Dantzker and Callaway, 2000; Douglas and Martin, 2004). However, such generalization of function will always represent a mere simplification since connections to, within and from the neocortex are too complex to be described in such a straightforward way.

2.2.1.1.4 Layer 5

Layer 5, the *internal pyramidal* layer, consists of large pyramidal cells, dividable into two groups based on their connectivity, morphology and physiology. First, the *cortico-cortical* (CC), or *slender-tufted* cells (Fig. 9), projections of which (besides other neocortical regions) include transcallosal cortico-cortical targets and striatum (Kasper et al., 1994; Ramos et al., 2008). CC cells are characterized by a smaller soma, a thin apical dendrite with a simple ramification often terminating below L1 and a regular pattern of action potential (AP) firing (Groh et al., 2010; Hefti and Smith, 2000; Kasper et al., 1994) Secondly, the *cortico-subcortical* (CS), or *thick-tufted* cells (Fig. 9) exhibiting projection patterns terminating in structures within the thalamus, the colliculi, or within various nuclei located in the brainstem (Bourassa and Deschênes, 1995; Hallman et al., 1988; Kasper et al., 1994; Kim et al., 2015). CS cells fire APs in bursts, have a larger soma and a thick apical dendrite with a complex dendritic tuft primarily ramifying in L1, along with additional branching in other layers (Groh et al., 2010; Hefti and Smith, 2000; Kasper et al., 1994). L5 pyramids are also directly targeted by thalamocortical input, thus suggesting a possible role in the integration of direct sensory input arriving from the thalamus, and processed information, which has already passed through L4 and supragranular layers (Constantinople and Bruno, 2013; Ji et al., 2016).

In order to increase the relevancy of depolarizations on distant apical dendrites, membranes of pyramids with dendritic tufts in L1 employ a specialized strategy ensuring reliable signal transduction to the axon initial segment. These measures include a dendritic initiation zone capable of driving a plateau-shaped Ca^{2+}-based action potential, effectively relaying synaptic input, which would have otherwise produced a subthreshold depolarization due to its distance from the axon initial segment (Larkum, 2013; Schiller et al., 1997; Yuste et al., 1994). However, these features are not exclusive to pyramids of L5, as similar dendritic spikes have been observed in the apical dendrites of L2/3 pyramidal cells (Larkum et al., 2007).

In addition to the dense, non-specific local inhibition, L5 PV+ FS basket cells also specifically target neurons of L2/3, possibly promoting synchronization of these layers (Lund et al., 1988). In addition, SST+ INs create a network targeting dendritic initiation zones of L5 pyramids, mediating disynaptic lateral inhibition. Since input from active pyramids has a facilitating effect on SST+ INs, their activity results in strong inhibition of neighboring pyramids (Kätzel et al., 2011; Silberberg and Markram, 2007) (see 1.1.2.4 Feedback inhibition).

2.2.1.1.5 Layer 6

Layer 6, or the *multiform* layer is, in terms of cell morphology, the most heterogeneous among neocortical layers (Chen et al., 2009). Complemented by cells of lower L5, L6 pyramids represent the biggest neocortical population with corticothalamic (CT) connectivity (Jones and Wise, 1977). However, L6 CT cells only represent 30-50% of L6 pyramids, with corticocortical (CC) cells and claustrum-projecting cells accounting for the rest (Thomson, 2010). L6 CC pyramid cells (Fig. 9, Fig. 10) are of diverse morphology (inverted, upright, bipolar) and develop long axonal arbors limited to deep layers targeting other cortical areas. Their projection pathways include those that originate in higher-order sensory cortices and target the

corresponding lower-order cortex in order to provide feedback, or those that originate in the somatosensory cortex while targeting motor cortices (Bai et al., 2004; Thomson, 2010). L6 CT cells (Fig. 9) develop axon collaterals and dendritic tufts that both target layers located directly above (Bortone et al., 2014; Kim et al., 2014; Thomson, 2010). Moreover, L6 CT cells are further divided into two subtypes based on their thalamic targeting and position within the layer: Firstly, L6 CT cells located in the upper part of L6 project back into the primary thalamic area from which the local network is innervated, while sending collaterals to the reticular thalamic nucleus (nRT) (Fig. 10) (Bourassa and Deschênes, 1995; Thomson, 2010). Secondly, L6 CT cells residing in the lower part of L6, also reciprocally target their thalamic counterparts. In addition, these pyramids target other, for example association-related, thalamic regions (Fig. 10) (Deschênes et al., 1998; Thomson, 2010). The third group of claustrum-projecting L6 pyramids was originally discovered in cat visual cortex and can be morphologically distinguished based on a thin apical dendrite reaching L1 (Fig. 10) (Katz, 1987; Thomson, 2010).

Pyramids of L6 are, similarly to those of L5, directly targeted by axons of thalamic neurons. Moreover, the inactivation of L4 does not affect responses of L5 nor L6 neurons to the upstream stimulation of thalamic efferents, thus suggesting that thalamocortical projections innervate infragranular and supragranular layers via two independent pathways (Constantinople and Bruno, 2013). A population of large basket cells residing in L6 projects to L4, while their counterparts in L4 reciprocally innervate L6 (a motif also found in L5 and L3), thus promoting synchronized inhibition of these two layers (Lund et al., 1988; Lund and Yoshioka, 1991; Thomson, 2010). Furthermore, L6 CT pyramids have been reported to target a specific subclass of inhibitory INs located in deep layers (West et al., 2006). These fast-spiking PV-positive inhibitory neurons belong to a specialized group of long-range projecting INs (Tremblay et al., 2016), capable of developing a rich axon arbor targeting all layers and delivering strong disynaptic inhibition throughout the cortical column (Bortone et al., 2014).

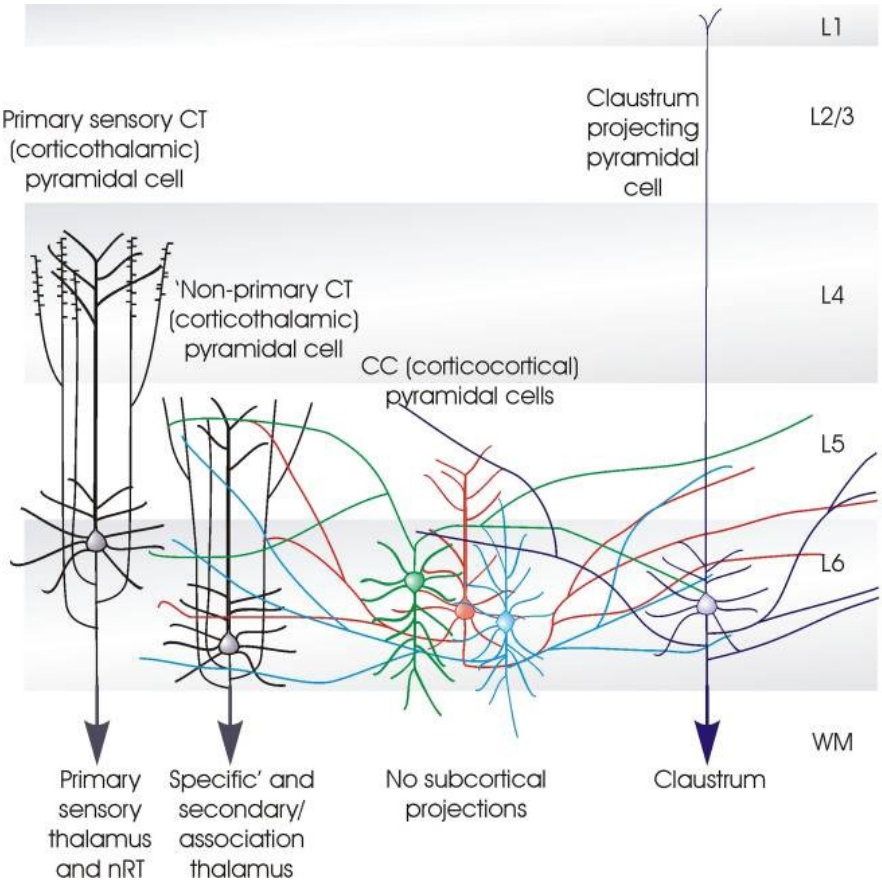

Fig. 10 **Pyramidal neurons of layer six** (Thomson, 2010). A schematic representation of the morphological properties and connectivity used to characterize different L6 pyramidal subtypes.

2.2.2 Canonical circuit

Electrophysiological recordings in the somatosensory cortex of a feline model revealed vertically clustered (columnar) organization (Mountcastle, 1957), further supported by findings from the visual cortex (Hubel and Wiesel, 1962). In addition, intracellular injections of horseradish peroxidase into previously electrophysiologically characterized cells provided further anatomical proof pointing towards radially organized architecture (Gilbert and Wiesel, 1989, 1983, 1979), thus fortifying the hypothesis that cortical columns may represent an universal functional module of the neocortex (Hubel and Wiesel, 1974; Mountcastle, 1997). However, the columnar organization hypothesis has also been subject to criticism due its inconsistency, illustrated by its apparent lack in rodent neocortex (Horton and Adams, 2005; Murphy and Berman, 2004) or the seeming discrepancy between functional maps and detailed neuroanatomy (Costa et al., 2010; Douglas and Martin, 2007). Thus, some authors propose that due to the high variability of columnar organization between and within species or even within the visual cortex of one individual, cortical columns lack functional relevance completely (Douglas and Martin, 2007, 2004; Horton and Adams, 2005). In conclusion, cortical columns seem to have been rejected as a general module employed in the functional construction of neocortex (Costa et al., 2010).

Although there is apparently no modular block that could dissect the whole architecture of the neocortex into independent components, the anatomical properties surrounding neocortical connections imply general motifs describable as the "canonical circuit" (Fig. 11). Raw thalamic input targets mainly neurons of L4 (Ji et al., 2016), which channel this flow to the superficial layers in a feed-forward manner. Here PCs of L2/3 integrate and process the incoming signal (preprocessed by L4, or arriving directly form the thalamus) along with neocortical intra- and interareal feedforward inputs (Dantzker and Callaway, 2000; Douglas and Martin, 2004). In addition, feedback projections from L5 and from L2/3 of other areas delivers wider context with possible predictive value (Larkum, 2013). Therefore, the most probable role of L2/3 networks is to, based on the input (of both cortical and subcortical origin) and in cooperation with other neighboring and distally located L2/3 networks (Fig. 11), probe all possible representations and select those in accord with the current circumstances (Douglas and Martin, 2004). Next, the processed information is directed towards deeper layers where the interpretation of the incoming thalamic input is further handled (also possibly directed towards higher-order cortices where it forms a part of the significant intracortical input to L4).

Pyramids of L5 represent the final level of signal processing before the output leaves the neocortex and drives subcortical actions (Douglas and Martin, 2004; Kim et al., 2015). In addition, CC pyramids of L5 project reciprocal connections to the upstream L2/3 networks, possibly in order to outline the limitations of the explored input interpretations, according to the output already generated (or, in the case of inter-areal L2/3 targeting, to provide contextual feedback regarding output from their respective area). Finally, L5 PCs target the cortico-thalamic pyramids of L6 (receiving also cortico-cortical feedback), through which feedback to the thalamic nuclei driving the neocortical input, is achieved. (Douglas and Martin, 2004; Thomson, 2010). Upon observation of the flow of information with respect to the laminar organization of the neocortex, a general pattern emerges. The feed-forward information flow representing extrinsic information terminates in the middle layer (L4). Additionally, feedback information of internal origin enters the circuit through the outer layers (Larkum, 2013).

The above-described model of basic neocortical circuitry proposes a simplified framework respecting the anatomical and physiological features of cells along with their spatial organization. Nevertheless, the proposed connectivity is not exclusive as there are many exceptions such as thalamic input targeting every layer (Deschênes et al., 1998) or countless others. In summary, the canonical circuit represents a general set of connectional trends found throughout the neocortex and symbolizes the currently available approximation to the forever sought universal building block.

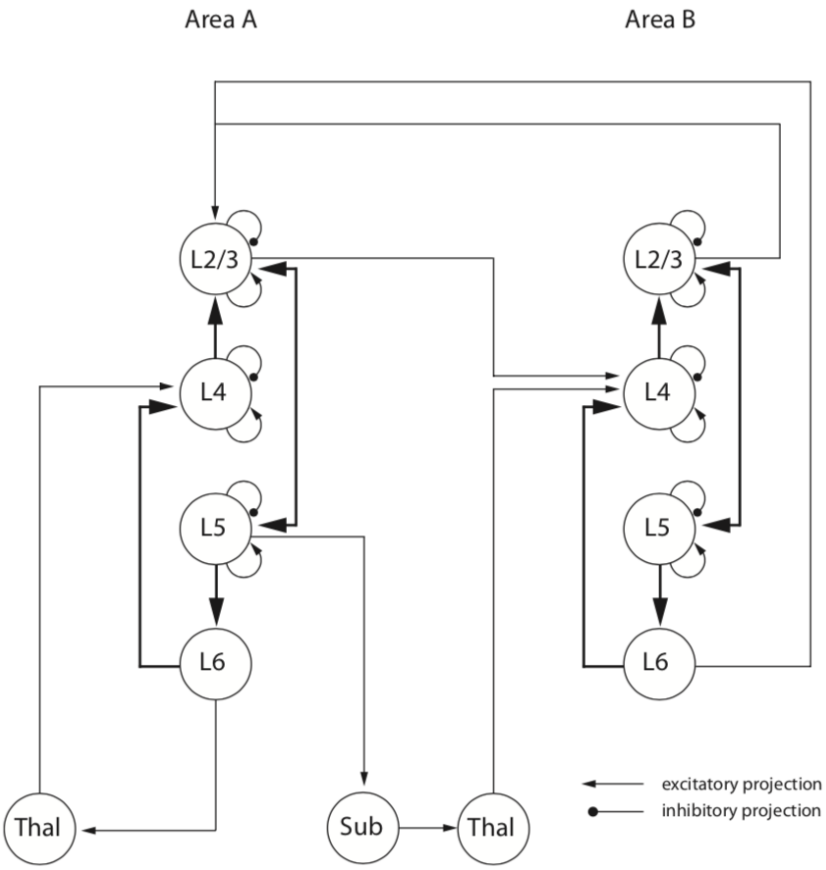

Fig. 11 **Canonical circuit** (Costa et al., 2010). A schematic representation of the "canonical circuit" adapted from previous works of Rodney Douglas and Kevan Martin (Douglas et al., 1989; Douglas and Martin, 2004).

2.3 Neocortical arealization

The mammalian neocortex is organized ("arealized") into specialized fields shaped by their spatial context and input (Arai and Pierani, 2014). The basic layout of the mammalian neocortex is comprised of four primary cortices: somatosensory (S1), visual (V1), auditory (A1) and motor (M1). These, with the exception of M1 controlling motor output, relay sensory information from the periphery to higher-order areas (Arai and Pierani, 2014).

So far, seven auditory fields were identified: the primary auditory cortex (A1) and the anterior auditory cortex (AAF) represent the core, primary region of the mouse auditory cortex (AC), primarily receiving raw thalamic input. The secondary (A2), dorsoposterior (DP), dorsomedial (DM) and dorsoanterior (DA) auditory cortices form a surrounding "belt" of higher-order cortices (Fig. 12). The seventh region, the insular auditory field (IAF), is located rostrally and is anatomically a part of the insula (Baba et al., 2016; Tsukano et al., 2015). Five of the seven auditory fields are tonotopically organized: A1, A2, AAF, DM and IAF (Baba et al., 2016). To our current understanding, A1, AAF and A2 respond uniformly to the whole frequency spectrum (5-80kHz) (Tsukano et al., 2015), while the IAF responds preferentially to lower frequencies, and the DM AC favors

ultrasonic sounds over 40kHz (Fig. 12) (Sawatari et al., 2011; Tsukano et al., 2015). Higher-order cortices are hypothesized to process complex, object-based stimuli (Bizley and Cohen, 2013), representations of which are less determined by their frequency composition (Issa et al., 2014). However, tonotopic maps of auditory fields, even their existence in some cases, are still subject to change since the nature of AC arealization evolves significantly with advancements in the available methodology (Baba et al., 2016; Issa et al., 2014; Sawatari et al., 2011; Stiebler et al., 1997; Tsukano et al., 2015).

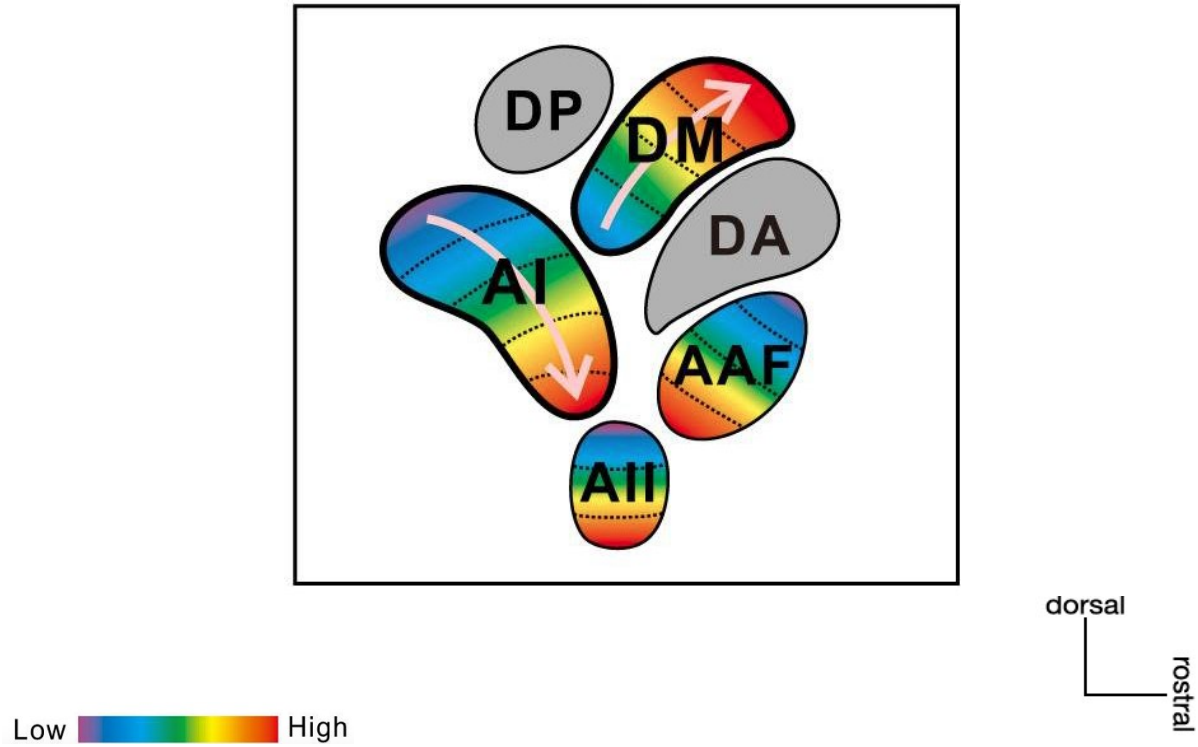

Fig. 12 **Graphical representation of different auditory fields of the right hemisphere with their respective tonotopic organization** (Tsukano et al., 2015). A1 and AAF represent the core of auditory cortex. The remaining fields are of higher order and are commonly referred to as the "belt" area.

2.4 Neocortical representation of complex auditory stimuli

2.4.1 Filter-based models of auditory representation

The initial translation of sounds from physical properties of air into neural signal takes place in the mammalian cochlea; a transductor capable of decomposing a heterogeneous, natural-sound waveform into separate frequencies (Robles and Ruggero, 2001). Consequently, structures involved in the lower levels of the auditory pathway, such as the inferior colliculus, exhibit according tonotopic organization with separated frequency bands (Barnstedt et al., 2015).

The classical approach to auditory research operates with pure tones. These largely artificial stimuli have proven to be extremely useful in the uncovering of the initial stages of sound coding (Barnstedt et al., 2015; Robles and Ruggero, 2001; Theunissen and Elie, 2014). The same batteries of simple tones also led to the

description of tonotopic organization in higher-order structures including the auditory cortex (Stiebler et al., 1997; Tsukano et al., 2015). Responses of neurons in sensory cortices often exhibit organization into receptive fields (RFs), as reported for the visual cortex (Alonso and Swadlow, 2005; Rust et al., 2005), somatosensory cortex (Estebanez et al., 2012) and auditory cortex (Theunissen and Elie, 2014). Based on these responses to pure-tone stimuli, the classical hypothesis of auditory representation states that auditory percepts are encoded by single neurons exhibiting maximal firing rates in response to a specific value of a given parameter, thus effectively supporting the "neuron doctrine" postulated by Barlow (Barlow, 1972; Frégnac and Bathellier, 2015). In describing the frequency-dependent response dynamic of a neuron including its temporal component, spectro-temporal receptive fields (STRFs) provide the most complete overview of single-neuronal tuning (Aertsen et al., 1981; Christianson et al., 2008; Theunissen et al., 2000). However, the significant variance between STRFs obtained by pure-tone stimulations and STRFs of the same neuron obtained in response to natural sounds demonstrates the non-linearity of single-neuron responses, while questioning the relevance of such pure tone stimulation in the study of a system, to which these are largely artificial and behaviorally irrelevant (Machens et al., 2004; Theunissen et al., 2000; Theunissen and Elie, 2014).

RF-based decomposition of perception implies a strict bottom-up hierarchy where neurons (through their RFs) function as linear filters operating with a static non-linear component (Priebe and Ferster, 2012). Although a relevant concept in the context of lower auditory pathway (inferior colliculus) (Andoni et al., 2007), models attempting to predict neocortical responses to complex or natural sounds solely using RFs of single neurons fail in achieving so, which limits their relevancy to simple or specific stimuli only (Fig. 13). Based on the acquired evidence, it seems that auditory perception is more likely to be represented as auditory objects (Bizley and Cohen, 2013) rather than through the extraction of singular acoustic features, a notion incompatible with the proposed dedicated coding (Nelken, 2004).

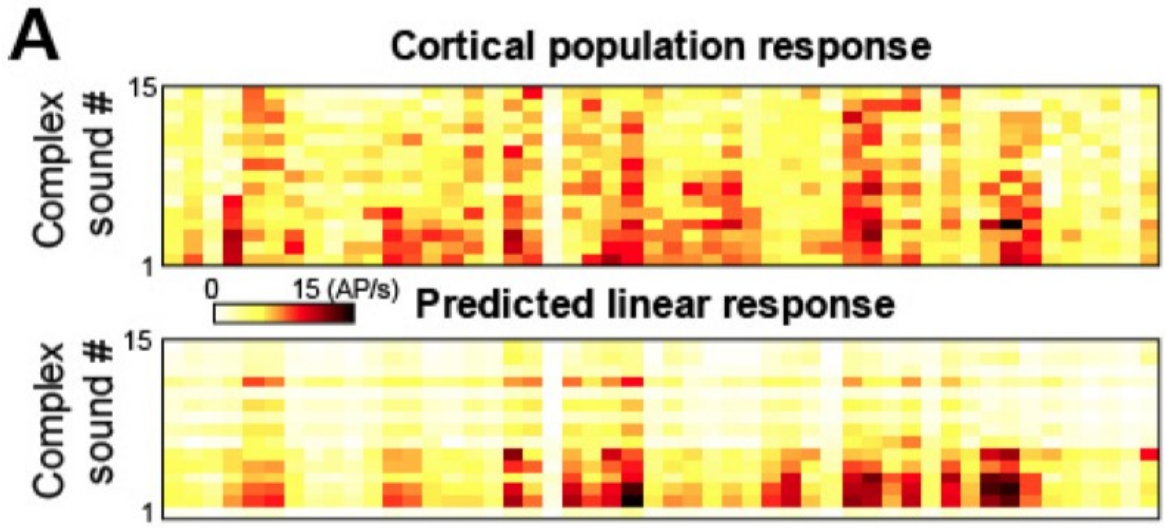

Fig. 13 **Neurons of the auditory cortex exhibit non-linear responses to complex sounds** (Bathellier et al., 2012). Responses of a defined neuronal population predicted based on the assumption that single neurons act as linear filters decomposing the sound wavelengths (*bottom*). The actual responses recorded from these neurons (*top*) show that the neural representation of complex sounds exhibits substantial nonlinearities, thus contesting the classical view regarding auditory cortex function.

In summary, the main issue with RFs and their predictive or descriptive capacity is the non-linearity in responses to complex stimuli, presumably caused by extrinsic inputs converging on neocortical neurons (Bathellier et al., 2012). Examples of such influences include the context of the stimulus, rate and intensity of stimulation and the current state of the animal (Atiani et al., 2009; Christianson et al., 2011; Deneux et al., 2016; Eggermont, 2011; Kato et al., 2015; Ulanovsky et al., 2004). Therefore, the proposed filter-based coding strategy employed by lower parts of the auditory pathway does not correspond to the observed response dynamics of neocortical PCs and needed to be reevaluated.

2.4.2 Population coding of perceptual categories

The failure of the dedicated, filter-based coding model to reliably describe stimulus-evoked activity of the auditory cortex has inspired the search for more viable alternatives. Distributed coding exhibits greater robustness and resistance to imperfections in signal transduction, a convenient feature in the context of the intrinsically noisy nature of neural transmission (Erickson et al., 1996; Rothschild et al., 2010).

The Hopfield network was proposed as a theoretical model for neuronal computation based on input-dependent evolution of recurrent neuronal networks into discrete, stable attractor states (Hopfield, 1982). The attractor network is a nonlinear dynamical system that, based on arriving input and the nature of its connections, can evolve into one or more discrete attractor-final states, transition among which requires the resetting of the

network and subsequent evolution in the updated context. In the context of neural representation, an attractor-state represents a pattern, or a state of activity of a given neuronal population. The spontaneous evolution toward the attractor-final state can be seen as evolution towards an energy minimum (a basin of attraction) (Fig. 14) represented by an activity pattern imposed on single cells by the current circumstances. The "energy level" corresponds to the level of compliance of the population activity to the demands forced by the arriving input and the local synaptic profile. Due to the nature of the attractor network, transitions between these representations are abrupt and no half-states exist (Bar-Yam, 1997). Such basins of attraction may represent a robust way of perceptual category representation, resistant to behaviorally irrelevant variances. In theory, generalized classification of sensory input provides a much more viable and flexible framework for sensory discrimination, while tolerating object-based representation proposed as the likely alternative to acoustic feature selection in the context of auditory processing (Miller et al., 2003; Nelken et al., 2003; Russ et al., 2007; Seger and Miller, 2010).

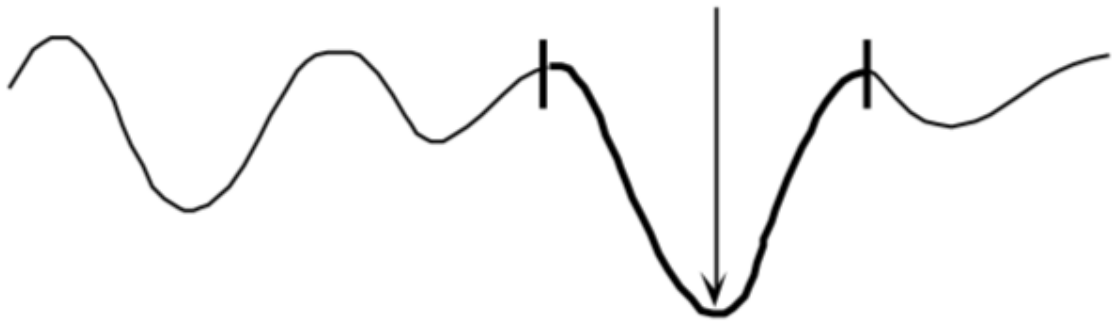

Fig. 14 **A graphical representation of a simple energy landscape used to illustrate the properties of an attractor network** (Bar-Yam, 1997). The highlighted section represents a basin of attraction created by long-term potentiation of local synapses. The possible principle of categorization may consist of the notion that neuronal representations falling anywhere within the highlighted area naturally evolve into the representation represented by the energy minimum (arrow).

Neocortical architecture of superficial layers includes specifically interconnected recurrent networks of neuronal units under a non-specific net of inhibition. Moreover, it has been experimentally demonstrated that the architecture of the neocortex supports non-linear activity (Maass et al., 2007; Wang, 2008) and population coding in the auditory cortex (Loebel et al., 2007). These features hypothetically qualify the neocortex as fit for possible attractor-like dynamics under Hopfield network conditions. Attractor-like dynamics have first been observed in the hippocampal navigational apparatus describing the population activity of place cells (Redish, 1999; Wills et al., 2005) and head-direction cells (Zhang, 1996). Furthermore, similar discrete dynamics of possible perceptual categories have been described for sensory perception in the olfactory bulb (Niessing and Friedrich, 2010) and finally the auditory cortex (Bathellier et al., 2012).

2.4.3 Discrete categorization of sounds by the auditory cortex

Necortical representation of auditory stimuli reportedly involves small numbers of highly active neurons (Hromádka et al., 2008), exhibiting synchronous firing, dependent on stimulus intensity and identity (Bathellier et al., 2012). Although individual cells of these neuronal ensembles show high inter-trial variability in evoked activity (Fig. 15A *top*), the "core" response pattern is not only invariant, but also remarkably universal since being evoked by multiple stimuli of different acoustic properties (Bathellier et al., 2012). Moreover, it was shown that each of the observed neuronal populations (for example 72 neurons in Fig. 15) is capable of producing a limited number (1-3) of such modes (Fig. 15) (patterns) of response, transition among which is abrupt and lacks an intermediate state of any kind (Fig. 16) (Bathellier et al., 2012). These attractor-like dynamics support the previously postulated hypothesis, that the auditory cortex represents sounds as objects through perceptual categorization (Bathellier et al., 2012; Nelken et al., 2003). This notion was further supported by behavioral experiments showing, that discrimination between stimuli evoking the same response mode is significantly harder to learn, when compared to the discrimination between stimuli belonging to two separate modes (Fig. 17) (Bathellier et al., 2012).

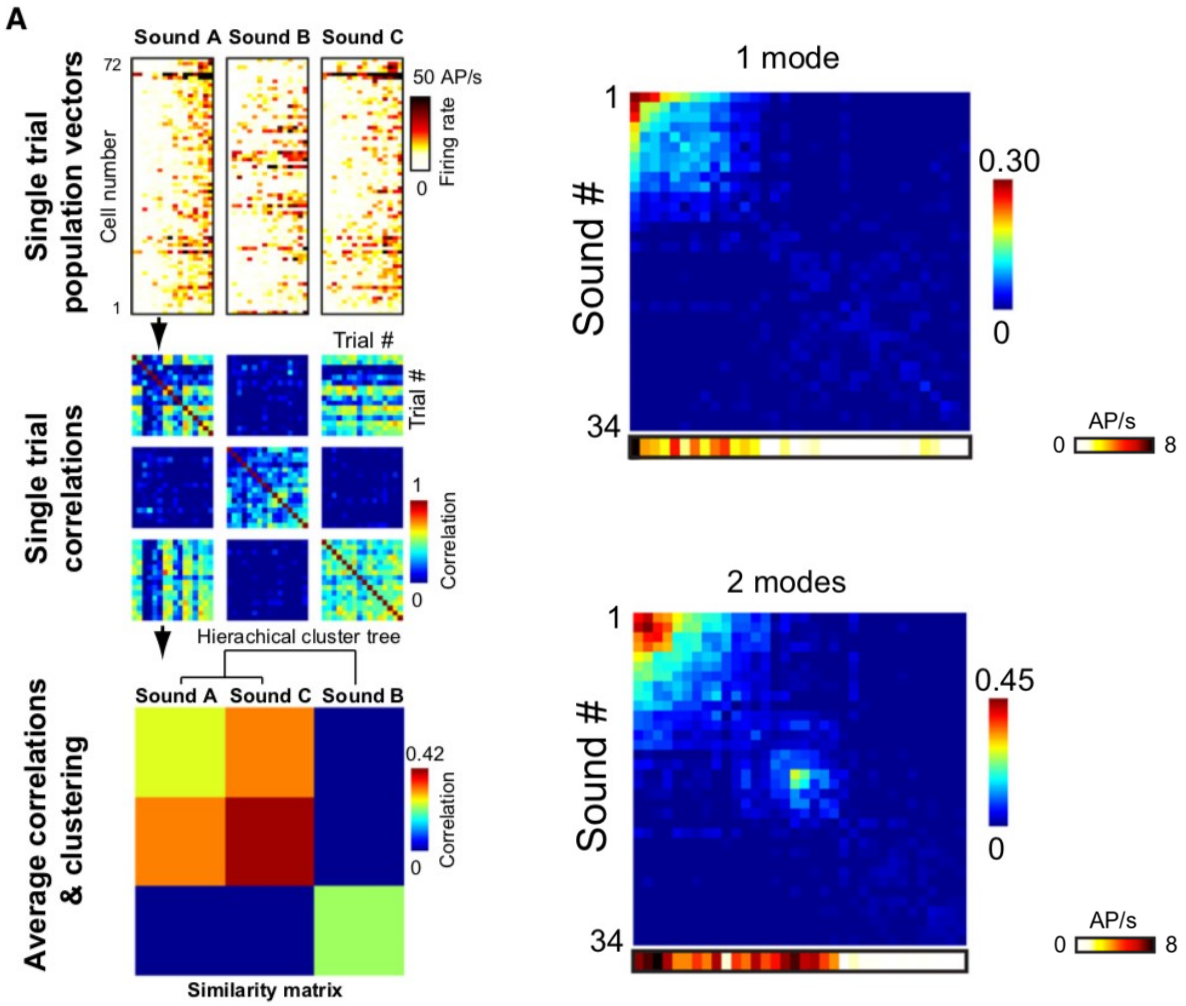

Fig. 15 **The analysis pipeline used to detect and visualize the organization of modes of response to a stimulation battery of complex sounds** (Bathellier et al., 2012). *Left, top*: Each bracket corresponds to the stimulus-evoked activity of 72 neurons represented in the form of population vectors (columns) in 20 trials (rows). Trials are arranged by mean population activity. Note the trial-to-trial heterogeneity of response with an underlying invariant pattern common to sounds A and C, but different in the case of sound B. *Left, middle*: A correlation matrix where single-trial population vectors (1x72 vectors) are cross-correlated. The top left square represents single trials of sound A and their similarity to other trials of the same sound (high overall correlation). Top middle square describes the similarity between single trials of sound A compared to sound B (low overall correlation). Top right square illustrates the high overall similarity between the pattern of response elicited by sounds A and C. *Left, bottom:* If every square from *left, middle* is represented by its average value of correlation and the resulting pixels are clustered together based on their similarity a graphical representation of different "teams" of sounds evoking different modes of response is generated (Sounds A and C = mode 1, Sound B = mode 2). *Right*: Clustered average correlation matrices reveal the number of invariant patterns of response and the identity of sounds evoking them. *Top*: A population with a single mode of response. *Bottom*: a population with two modes of response.

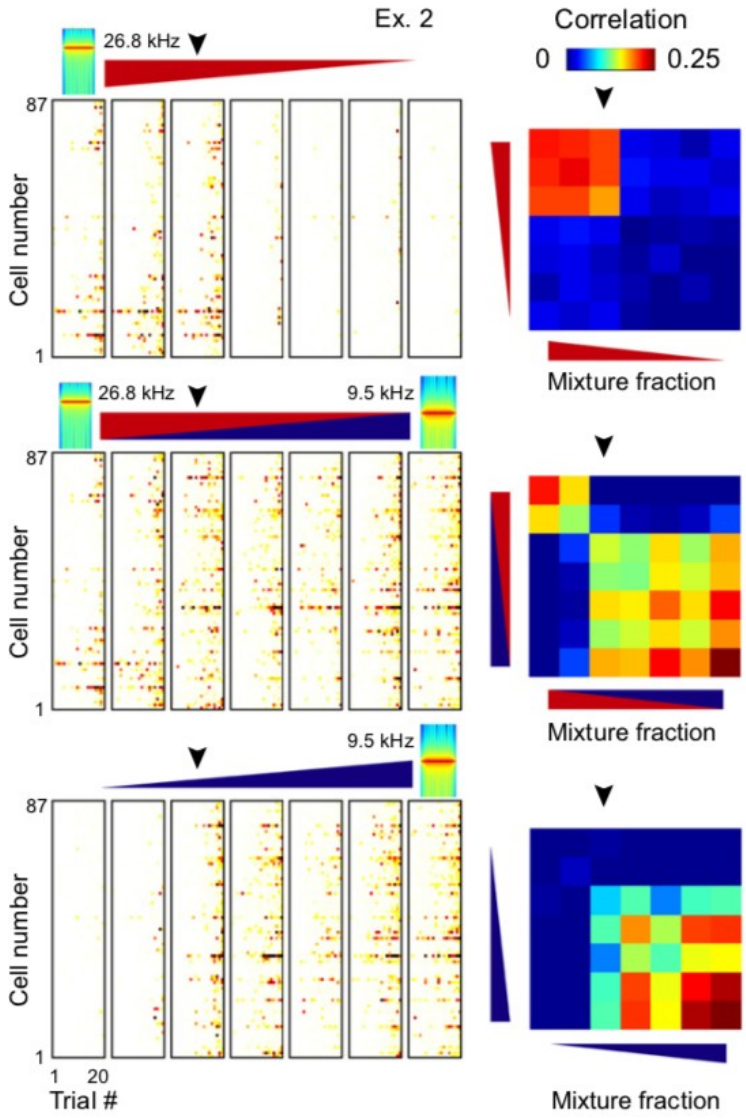

Fig. 16 **Attractor-like dynamics of the response modes based on linear mixes of sounds** (Bathellier et al., 2012). Specialized stimulation batteries were constructed for neuronal populations where the existence of two modes was observed, using linear intensity mixes of two sounds previously attributed to different modes. These mixes were presented to the neuronal ensemble and abrupt changes in representation were observed (middle). The comparison of responses to solely intensity modulated non-mixed sounds (top, bottom) and to the mixing setting (middle) shows, that the switch is not only intensity dependent, but shows signs of competition between two representations as well.

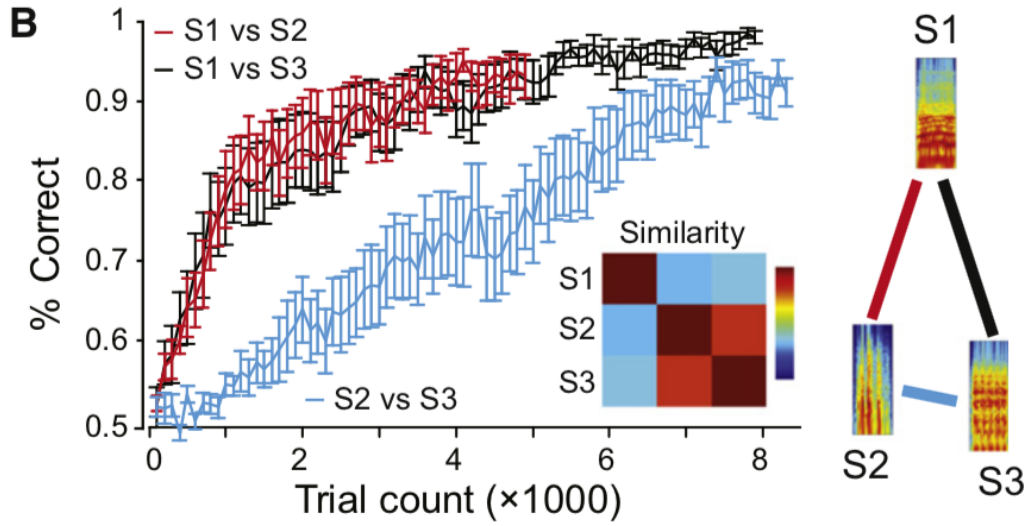

Fig. 17 **A behavioral test assessing the possible link between response modes and categorization** (Bathellier et al., 2012). A go/no-go paradigm was employed in order to probe the subjects ability to discriminate sounds from the same (S2 and S3) and from different (S1) response modes. When the subject approached the licking tube a sound was played and followed either by a reward or by an air-puff. The learning curves show the evolution of the capacity to discriminate two sounds during training. Learning curves describing the efficacy of discrimination in the case of S1 and S2 or S3 are steeper, presumably due to their different response modes. Conversely, discrimination of S2 and S3 exhibits a much shallower learning curve, thus suggesting that these stimuli may evoke similar perceptual categories.

In order to visualize and examine the nature of population coding employed by the AC, Bathellier et al, developed the following methodology: Neural activity in the form of spiking probability was recorded from a local population of L2/3 neurons. The firing rate of each neuron recorded in a 250ms time-bin following the stimulus was averaged and single-trial population vectors were constructed for the whole battery of stimuli (Fig 15A). A side-by-side visualization of these single-trial population vectors coupled into groups by sound, may reveal a pattern of response (if present), consistent across trials. In order to test the consistency of the response pattern, all single-trial population vectors were cross-correlated in a correlation matrix. The mean value of correlation between single trial population vectors evoked by the same sound, represents the overall stability of the representation. Moreover, single-trial vectors evoked by different sounds of the stimulation battery are also cross-correlated in different brackets of the matrix. The mean value of correlation between these, describes the similarity of the representation evoked by the two sounds. For example, the correlation matrix in Fig. 15A is constructed from single trial population vectors organized into three groups by sound that are plotted above. Cross-correlation of all of these vectors reveals intra- and inter-sound similarity of the evoked pattern of activity. The diagonal brackets representing the level of autocorrelation exhibited by responses evoked by different sounds reveal, that all three stimuli evoke a stable representation. By setting an autocorrelation threshold, sounds not evoking a stable pattern of response in the given FOV (usually true for most stimuli of the battery) can be filtered. Furthermore, brackets in rows of the correlation matrix test the similarity of a sound-evoked

representation to those evoked by the remaining sounds of the battery. In the case of Fig. 15A, the sound A-related response pattern shows high similarity to the response pattern evoked by Sound C. The cortical representation of Sound B is consistent (high autocorrelation), but unique and not similar to those of sounds A and C. By averaging trial-by-trial correlation coefficients in brackets representing intra- and inter-sound comparisons of population coding, a much more informative representation in the form of an averaged correlation matrix (ACM) is constructed. Moreover, brackets of the ACM can be reorganized via hierarchal clustering into groups of stimuli with high intra-cluster cross-correlation. A clustered ACM therefore provides a comprehensible readout about the number of modes of response exhibited by the FOV and about the identities of sounds evoking these conserved patterns. Examples of clustered ACMs acquired using a battery of 30+ sounds show that most of the presented stimuli do not evoke a stable pattern of response in the local population (Fig. 16 *right*), and those that do can be clustered into a small number of groups (one or two) based on their cortical representation.

In summary, Bathellier et al. have provided coherent experimental data suggesting that the processing of acoustic stimuli by the auditory cortex is based on discrete perceptual categorization, the neural correlates of which are represented by attractor-final states of the underlying recurrent network (Bathellier et al., 2012).

3 Experimental aims

1) Development of a protocol enabling the observation of population coding of complex sounds as described by Bathellier et al. 2012, using genetically-encoded calcium indicators.

2) Assessment of the activity of interneuronal subtypes accompanying abrupt changes in population coding as described by Bathellier et al. 2012.

4 Materials and methods

4.1 Materials

4.1.1 Drugs

Lidocaine, used for local anesthesia, was subcutaneously administered during skin and muscle removal. Its mode of action involves silencing of pain afferents through non-selective inhibition of voltage-gated sodium channels and consequent blockage of action potential generation and propagation (Derry et al., 2014).

Atropine, a competitive antagonist of muscarinic receptors, was used to counter bronchoconstriction and mucus secretion (possibly blocking the airways), both regulated by acetylcholine (Alagha et al., 2014). Atropine was subcutaneously injected prior to the surgery.

Dexamethasone, a glucocorticoid receptor agonist with anti-inflammatory effects (Tsurufwi et al., 1984), was used to prevent brain swelling. Dexamethasone was administered subcutaneously as pre-medication.

Carprofen, a non-steroidal inhibitor of cyclooxygenase and phospholipase A2, has anti-inflammatory, antipyretic and analgesic activity and is applied primarily in veterinary medicine (Snow et al., 2014). Carprofen was administered subcutaneously for seven days following the surgery, in order to reduce post-operative pain and inflammation.

Eye ointment (opthalmoseptonex) was used in order to prevent eye damage since mice do not close their eyes when under anesthesia.

Povidone iodine (betadine) was used to clear the surgical field from any microorganisms (naturally present on skin surface), in order to prevent surgical-site infections. Its mode of action consists of releasing free iodine from the polymer it is bound to (povidone), which in turn penetrates the cell wall and oxidizes microbial molecules (Dumville et al., 2015).

4.1.2 Fixation

Cyanoacrylate glue (Loctite Super Attak) was used to fixate the skin onto the skull, to fixate the aluminium headbar in a suitable position, and to sculpt an immersion-holding reservoir surrounding the cranial window.

A custom-made aluminium headbar was glued onto the skull of the animal in order to maximally suppress movement of the field of view.

4.1.3 Experimental animals

Subjects of the following experiments were male and female transgenic mice with interneuron subtype-specific (Cre-dependent) expression of the red fluorescent protein tdTomato. Mice were prepared through cross-breeding of either of two cell-type specific driver lines: SST-IRES-Cre (Jackson laboratory stock n.018973)), or PV-IRES-Cre (Jackson laboratory stock n.012358), and the flex-tdTomato reporter line (Jackson laboratory

stock n.007909). Age of the subjects varied between 6-18 weeks. A total number of 103 mice (PV/tdT = 30, SST/tdT= 73) were subjected to the surgical protocol discussed in section 4.3. All of the performed procedures were approved by the ethical committee of the Institute of Experimental medicine, Czech Academy of Sciences.

4.2 Tools enabling *in vivo* neural imaging

4.2.1 Fluorescent reporters of neural activity

Neural activity reporting via fluorescent probes can be currently achieved using small organic molecules or genetically-encoded protein-based indicators. The visualization of action potentials can be accomplished either directly through membrane-bound voltage-sensitive reporters, or indirectly by reporting on large calcium transients associated with neuronal depolarization (Kerr et al., 2005; Lütcke and Helmchen, 2011).

Historically, organic dyes represented the optophysiological method of choice due to their fast kinetics and good signal-to-noise ratio, both largely superior to those of their early genetically-encoded counterparts. Probes based on calcium chelators, such as Oregon green BAPTA-1 (OGB-1) (Grynkiewicz et al., 1985), support single-AP detection at cellular resolution if combined with 2PLSM (Grewe et al., 2010; Paredes et al., 2008). Membrane bound voltage-sensitive dyes on the other hand, enable meso- and macroscopic imaging with remarkable temporal resolution (Lütcke and Helmchen, 2011). However, regular upgrades of protein-based probes created by genetic engineering have been recently able to match the long unrivaled properties of organic dyes (Chen et al., 2013). Consequently, OGB-1 and other small organic molecules have been replaced by the significantly less toxic, genetically targetable protein indicators compatible with chronic experiments (Lütcke and Helmchen, 2011).

Although the calcium-independent genetically-encoded voltage indicators (GEVIs) provide superior temporal resolution and subthreshold sensitivity at single-cell level (properties beyond of what is possible for reporters dependent on concentration dynamics of intracellular calcium), they are not yet available for 2PLSM and, therefore, cannot be effectively employed in imaging below superficial layers (Lin and Schnitzer, 2016). As a consequence, genetically-encoded calcium indicators (GECIs) represent the state-of-the-art method for *in vivo* neural activity imaging.

A grand majority of studies in neuroscience aiming to record neural activity with single-AP and single-cell resolution uses single-fluorophore GECIs of the GCaMP (Nakai et al., 2001) family, mainly the GCaMP6 generation (Chen et al., 2013). The architecture of GCaMP indicators is based on the linkage of a circularly permuted GFP linked to calmoduline (CaM) from one side and to M13 (a short peptide originally from myosin light-chain kinase) from the other. Conformational changes induced in the event of a calcium ion binding to CaM, result in superior fluorescence of the probe (Mank and Griesbeck, 2008; Nakai et al., 2001). The GCaMP6 family includes three variants: slow (6s), medium (6m) and fast (6f). The GCaMP6s variant produces superior changes in fluorescence in response to neural activity, but due to its slow decay-time cannot reliably distinguish single APs in moderately firing neurons (Fig. 18). The GCaMP6f variant on the other hand, is not as potent in

terms of signal strength but has the fastest decay-time resulting in single-AP resolution comparable to that of OGB-1 (Chen et al., 2013) (Fig. 18). As of recently, a new generation of upgraded GCaMP GECIs, the GCaMP7 family, has been developed and is expected to become the indicator of choice for neural imaging (Dana et al., in preparation).

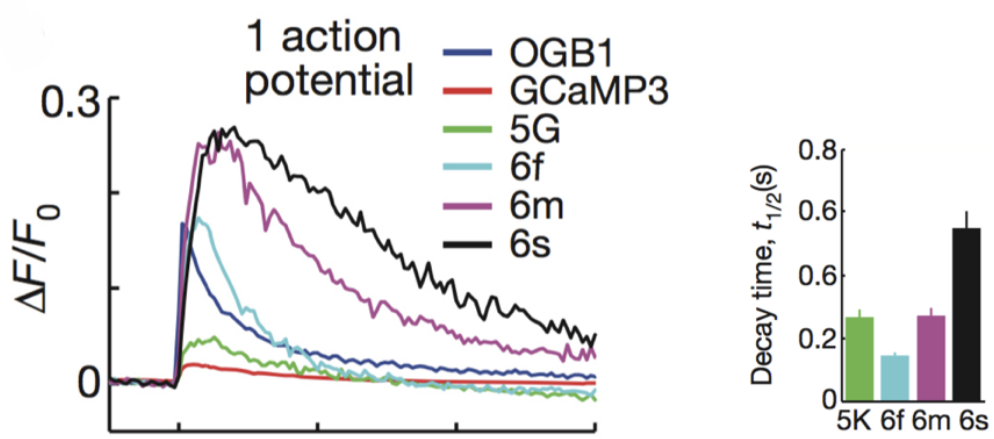

Fig. 18 **A comparative representation of properties of selected calcium indicators** (Chen et al., 2013). *Left*: Fluorescent traces representing the amount of signal generated in response to a single action potential along with the slope of its decay. GCaMP6s produces the largest change in fluorescence, however, exhibits a long decay time (*right, black*) ($t_{1/2}$ ~ 0.5s). Consequently, 6s lacks the ability to resolve single APs. GCaMP6f generates weaker contrast (*left*), but has faster kinetics (*right, turquoise*) supporting single AP resolution under reasonable frequencies.

4.2.2 Viral vector

Adeno-associated viral (AAV) vectors are based on a group of non-pathogenic single-stranded DNA viruses (parvoviruses), whose coding sequences responsible for site-specific genome integration (*rep*) were replaced by an expression cassette (Büning et al., 2008). Consequently, experimentally used AAV vectors exhibit episomal persistence providing transient expression of the inserted sequence, while lacking the possibly harmful mutagenic effects of larger lentiviral vectors (Karra and Dahm, 2010). Furthermore, different AAV serotypes exhibit specific tropisms and transduction properties (Büning et al., 2008; Watakabe et al., 2015), thus providing an additional, although largely unspecific, level of targeting. The commercially available GCaMP6-containing AAV vectors offer different serotypes and cell-type-specific promoters including variants with transcription-translation STOP cassettes compatible with the Cre/lox-mediated excision (Kuhlman and Huang, 2008). This enables both tissue-specific (promoter-determined) and cell-subtype-specific (based on genetic markers such as SST) expression. In order to enhance the post-transcriptional stability of the coding sequence, a WPRE (Woodchuck Hepatitis Virus Posttranscriptional Regulatory Element) is commonly included at the

3'end of the insert (Zufferey et al., 1999). The expression cassette is usually terminated by the SV40 (simian virus 40) polyadenylation signal, employed due to its conveniently short sequence considering the limited length (~5 kbp) (Karra and Dahm, 2010)) of inserts supported by AAV vectors (Choi et al., 2014).

Calcium imaging in all experiments described in this text was performed using calcium indicators, genes of which were delivered using following vectors: AAV1.syn.GCaMP6s.WPRE.SV40 (Penn Vector Core Catalog number AV-1-PV2824) and AAV9.syn.GCaMP6f.WPRE.SV40 (Penn Vector Core Catalog number AV-9-PV2822).

4.3 Surgical procedures

In order to acquire optical access to the structure of interest, a chronic cranial window (Holtmaat et al., 2009; Trachtenberg et al., 2002) was implanted over the auditory cortex (AC) following the injection of the viral vector in all of the experimental mice. The operation protocol was as follows:

Isoflurane-anesthetized mice (isoflurane(%)/oxygen mix: 4% induction phase, 1-2% maintaining phase) were placed on a heated pad (38°C) and premedicated with subcutaneous injections of atropine (0.05ml, 1mg/kg) and dexamethasone (0.05ml, 2.5mg/kg) in order to prevent endotracheal accumulation of mucus and to reduce brain swelling respectively. Eyes of the subjects were treated with opthalmoseptonex. Next, the surgical field covering the parietal area of the skull was cleared of hair and treated with betadine and lidocaine. Skin was removed, the now-accessible parietal bone was cleared of remaining tissue and a custom-made aluminium headbar was glued onto the dry skull using cyanoacrylate glue. In the following step, *m.temporalis* was excised and the surrounding skin was glued onto the skull so that a patch (preferably of most caudal and ventral position possible) of the temporal bone would remain accessible.

The AC is located under the caudal side of the parietal bone, 2 mm from the occipital edge of the cortex and dorsal from the *sinus petrosus*. However, its exact location varies significantly from animal to animal and cannot be decisively located based on spatial cues (Stiebler et al., 1997). A 3,5mm wide craniotomy over the presumptive AC-containing area was performed using a small burr-tip dental drill. Cold saline was frequently applied during this process in order to prevent thermal damage to the underlying tissue (Yuan et al., 1994). The circular-sized bone "cut-out" was gently removed and cold saline was applied on the uncovered brain tissue with intact *dura mater*. The administration of the viral vector was preferably performed using a Nanoject III injector (Drummond Scientific) enabling injections of a defined volume, administered at 1nl/s. Successful expression of GCaMP6s delivered using the AAV1 serotype required 7-10 injections of 80nl. On the other hand, the number of injections required when using the AAV9 serotype was 4-6, while the volume represented 200nl.

Finally, after the final injection, the craniotomy was sealed with a 3mm round glass coverslip, gently pressed against the tissue and fixated using cyanoacrylate glue. The total duration of the above-described procedure was approximately four hours. The success rate of the microsurgery was rather low at 30-50%. Throughout post-surgical care, 0.7ml (2.5mg/ml) of carprofen was daily administered in the seven days following the surgery.

4.4 Calcium imaging

4.4.1 Optical imaging and two-photon excitation

Neural activity has classically been recorded using electrophysiological methods directly probing the changes in membrane voltage of neurons. The lack of an intermediary translating electrical events into fluorescent signal renders electrophysiological methods extremely reliable in both temporal precision and electrical sensitivity. However, juxtacellular electrophysiological recordings enabling targeting of genetically defined neurons are restricted to small numbers of cells, while extracellular recordings capable of recording local populations (up to tens of neurons), lack means of sufficient identification (Buzsáki, 2004; Chorev et al., 2009; Lütcke and Helmchen, 2011).

Optophysiological methods enable recording of mainly suprathreshold neural acitivty in genetically defined neuronal populations with single-cell resolution (Knöpfel et al., 2006), although with lower temporal resultion. Therefore, the optophysiological approach to neural activity recording is, in many ways, complementary to that of electrophysiology. The state-of-the-art optophysiological method for *in vivo* neural activity recording is two-photon calcium imaging. The double variability introduced through the visualization of a transient calcium concentration peak accompanying an AP, renders calcium imaging significantly less reliable in terms of temporal resolution (Pologruto et al., 2004). Nevertheless, it is sufficient enough to provide a reliable readout of neuronal suprathreshold activity, presumed to represent the most relevant output in terms of information coding (Lütcke and Helmchen, 2011).

Laser scanning optical microscopy employs fluorescent probes in order to generate contrast and visualize various cellular or tissue features including the anatomy of cellular compartments or changes in membrane voltage. Fluorescence is generated in two steps. First, the fluorophore is excited upon absorption of a photon of fluorophore-specific wavelength. The subsequent relaxation of the molecule is accompanied by the emission of a photon of a different wavelength (Fig. 19) (Drobizhev et al., 2011).

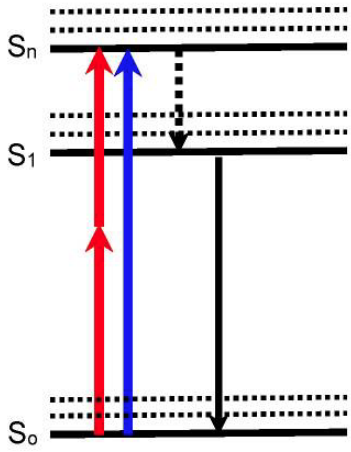

Fig. 19 **Jablonski diagram of single- and two-photon excitation** (Drobizhev et al., 2011). A schematic representation of single (blue) and two-photon (red) excitation resulting in an invariant outcome in the form of emission of a photon of a fluorophore-specific wavelength.

The laser beam of excitation light scanning the sample is focused into a pixel-representing focal point, from which its intensity linearly decreases with distance. Consequently, out of focus fluorescence is generated above and under the focal plane, resulting in contamination of relevant signal (Fig. 20 *left*). In laser scanning confocal microscopy (LSCM), the undesired out-of-focus emission is filtered by a pinhole granting passage only to ballistic photons arriving from the focal plane. (Combs, 2010; Helmchen and Denk, 2005). However, if the focal plane is located further along the z-axis, the photons emitted from the focal point are more likely to be scattered by the increasing number of molecules present in the superficial layers of the sample. Due to the alteration of their original trajectories (failure to remain ballistic), these photons are filtered by the pinhole and, therefore, the amount of detected signal decreases with increasing depth (Helmchen and Denk, 2005). In addition to scatter, excitation light of wavelengths used in linear excitation exhibits a relatively high probability of absorption by biological tissue when compared to the near-infrared light. Due to the above-listed reasons, LSCM cannot effectively image structures located deeper than 100 μm (Combs, 2010).

Two-photon absorption (2PA) is a phenomenon involving the simultaneous (within a femtosecond) arrival of two photons, resulting in the combination of their power and subsequent excitation of the fluorophore normally excited by a single photon of roughly half their wavelength (Fig. 19) (Combs, 2010; Helmchen and Denk, 2005; Zipfel et al., 2003). The most important prerequisite to 2PA is high spatial density of photons. In the context of 2PLSM, sufficient density is achieved through the use of an objective with a high numerical aperture (NA=0.95), coupled with the use of a pulsed laser. Due to its non-linear dependence on the linearly decreasing intensity of the laser beam, the probability of two-photon excitatory transition, decreases exponentially (fourth power (Denk et al., 1990)) with distance from the focal point (Helmchen and Denk, 2005; Zipfel et al., 2003). As a consequence, the intensity of excitation light required for 2PA is not present outside of the focal point, effectively limiting the generation of fluorescence to a femtoliter volume (Fig. 20) (Dunn et

al., 2000). Since no out-of-focus fluorescence is generated, all photons emitted by the sample at the given time can be assigned to the currently illuminated pixel, regardless of scattering. In summary, two-photon laser-scanning microscopy (2PLSM) (Denk et al., 1990) represents a method capable of fast, high-resolution, deep-tissue imaging of genetically defined neuronal populations located as deep as 1mm below the pial surface (Helmchen and Denk, 2005). In combination with genetically-encoded calcium indicators, 2PLSM represents the most efficient tool currently available for *in vivo* neuronal imaging in the neocortex of the mouse.

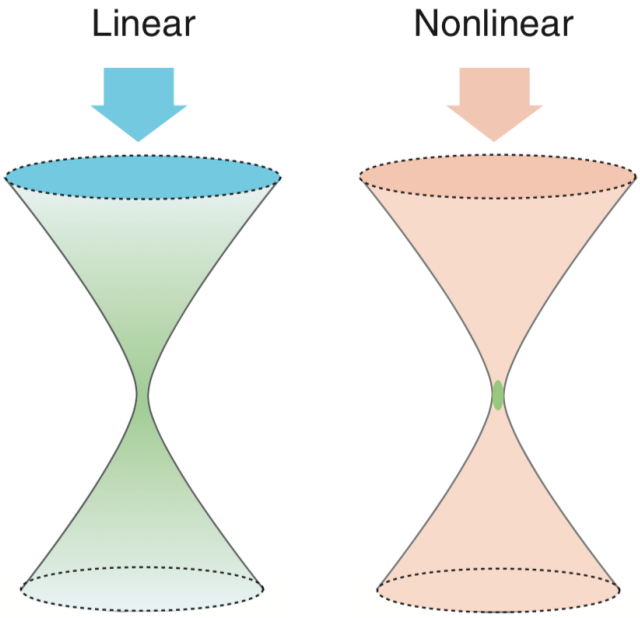

Fig. 20 **Spatial profile of fluorescence generation using single- and multi-photon excitation** (Helmchen and Denk, 2005). A schematic representation illustrating the difference in spatial localization of fluorescence generation achieved by linear (LSCM) and nonlinear (2PLSM) excitation.

4.4.2 Experimental protocol

All imaging was performed using an Ultima IV Two-photon laser-scanning microscope (Prarie Technologies) equipped with a Chameleon Ultra II tunable pulsed laser (Coherent) operating at 920 nm (80Hz, 140fs wide pulses with 12.5ns interpulse time). A minor part of the dataset was recorded using, galvanometric mirrors capable of scanning a 256x256 field of view (FOV) at 3Hz driven from the PrarieView imaging software. Since April 2018, the experimental setup was upgraded with a resonant scanner (Sutter) supporting scanning of 512x512 FOVs at 30Hz and with the Scanimage imaging software (MATLAB based package Vidrio Technologies). Mice expressing GCaMP6f were imaged using the upgraded microscope.

Prior to the imaging session, the mouse was briefly anesthetized (isoflurane) in order to be headfixed under the microscope and placed in a heated plastic tube. All imaging was performed using a 20x water immersion objective (XLUMPLFLN 20XW, Olympus).

First, a FOV with cells responding to improvised acoustic stimulation (clicks, cracks) was located and segmented into single cell-shaped regions-of-interest (ROI) using tools available in both imaging programs. Changes in fluorescence in each ROI were recorded upon stimulation. All FOVs presented in results were located within L2/3 (150-200μm below the pial surface).

Acoustic stimulation was presented using a battery of 39 stimuli (at 85-90 dB) used in the original study (Bathellier et al., 2012), kindly provided by dr. Bathellier. The stimuli included pure tones and complex sounds containing a wide range of frequencies and modulations. Stimuli were delivered using an E-MU 1212M sound card, a Denon PMA-535R amplifier and an ultrasonic speaker (Raal). Stimuli were presented in pseudorandom order with a 3 second (GCaMP6s), or 1 second (GCaMP6f) interstimulus interval. One recording consisted of 8-10 repeats.

In cases of FOVs exhibiting 2 or more modes of response, one sound was selected from each mode and a linear intensity mix (10% steps) of these two stimuli was generated in MATLAB. The resulting battery of 11 sounds was delivered to and neuronal responses were recorded from the same FOV. If tdTomato labeled inhibitory interneurons were not ideally positioned within the original FOV, another set of recordings was performed targeting interneurons specifically.

Changes in fluorescence were processed in a “Two-photon Processor” MATLAB package (Tomek et al., 2013) using the “peeling” algorithm (Grewe et al., 2010) in the case of GCaMP6s, or the “foopsi” algorithm (Vogelstein et al., 2010) in the case of GCaMP6f and translated into spike probabilities. Next, population recordings were analyzed using the statistical pipeline proposed by Bathellier et al., and described in section 2.4.3. Average firing rates during 250-500ms-long time bins from post-stimulus time histograms (PSTHs) of all imaged neurons were organized into single-trial population vectors. These were then cross-corelated in a correlation matrix and correlation coefficients for single-trials of the same stimuli were averaged. Stimuli expressing subthreshold autocorrelation were removed (the value of the threshold varied between 0,05-0.2). Next, hierarchal clustering was performed on the average-correlation matrix constructed as discussed in section 2.4.3. The resulting clusters of stimuli represent response modes described in the original study (Bathellier et al., 2012).

The activity of interneurons was first analyzed using PSTHs consisting of spike probabilities extracted from fluorescent traces by the “foopsi” algorithm. Spike extraction from GCaMP6f is more likely to ignore smaller events than to generate false-positive APs. SST+ INs presumably integrate the activity of the whole local population and, therefore, should not exhibit responses to stimuli as strong as certain PCs. Consequently, most of the information concerning the (inherently less dynamic) firing profile of single SST+ INs was filtered by spike extraction. All INs exhibited similar levels of GCaMP expression and, therefore, should produce similar changes in fluorescence in response to depolarization. Thus, the activity of single SST+ cells and their populations can analyzed using stimulus-evoked fluorescent traces directly. Similarity of the evoked activity in the context of single cells was analyzed in the following steps: First, a correlation matrix cross-correlating all single-trial response traces was constructed. Next, by averaging correlation coefficients between trials of the same sound, an averaged correlation matrix (ACM) was generated much like in the case of population vectors.

The resulting ACM reflects the similarity of responses evoked by different sounds in a single cell. The average synchronicity profile of response across the population was visualized by creating a mean ACM from all local SST+ cells.

5 Results

5.1 Optimization of the experimental protocol

The method introduced by dr. Bathellier and his colleagues in their study regarding discrete neocortical representation of auditory stimuli has employed a synthetic calcium indicator called OGB-1 (Grynkiewicz et al., 1985) (Bathellier et al., 2012). However, experiments using OGB-1 are restricted to those of acute nature, due to the gradual removal of the dye actively executed by the stained cells of the FOV (Stosiek et al., 2003). In order to render the experimental conditions more physiological and compatible with chronic experiments, we replaced OGB-1 with genetically-encoded calcium indicators of the GCaMP6 family (the current field standard) (Chen et al., 2013). Therefore, the first experimental aim of this thesis was to replicate the original experimental findings by Bathellier et al. (discussed in section 2.3.4) using GECIs instead of synthetic dyes.

5.1.1 GCaMP6s

Research in the hosting laboratory has been focused on changes in tuning properties of single interneuronal subtypes following acoustic trauma (Novák et al., 2016) and conditioning-induced plasticity (Zelenka et al., in preparation) in the AC. While the first study was performed using OGB-1, the latter has employed GCaMP6s. Therefore, an experimental protocol specifying the viral titer and number of injections required for optimal expression was already developed by the time the following experiments were performed (8-10 injection sites, injection volume:~80nl).

The switch from OGB-1 to GCaMP6 bears important consequences in terms of acquisition speed. While OGB-1 fills the whole cell including the nucleus, GCaMP6 exhibits cytoplasmic localization and its presence in the nucleus reportedly causes aberrant activity (Chen et al., 2013). Consequently, OGB-1 stained cells can be imaged in a “Linescan” mode, where the laser beam scans the FOV along a user-defined scanning path, collecting only few representative pixels per cell, which enables high scanning rates (up to 100Hz) using mirror galvanometers. On the other hand, the unevenly distributed expression of GCaMP requires full-frame scanning and subsequent segmentation of the FOV into single-cell ROIs. This leads to a substantial loss of scanning speed as the same setup capable of 100 fps on linescan mode, reaches 3 fps at 256x256 with raster scanning.

Despite the initially low success rate of surgeries, we were able to image 17 mice exhibiting solid GCaMP6s expression. Out of these, two were exhibiting two or more modes of response across multiple sessions with the autocorrelation threshold (representing the similarity of population response evoked by a given stimulus between trials) at 0.05. However, further analysis revealed extreme variability in terms of the identity of mode-related sounds. Interestingly, no “switching of teams” was recorded as the stimuli were organized into

two exclusive pools (Fig. 23A). Visualization of single-trial population responses to single sounds (Fig. 21 *right*) seemingly (coupled together by hierarchal clustering) evoking the same response pattern, did not provide evident motifs of activity resembling those presented in the original study (Fig. 15A or Fig. 16). The average firing rate of the stimulus-evoked activity was highly variable from trial to trial (Fig. 23B) (as previously reported (Bathellier et al., 2012; Hromádka et al., 2008)). We further noticed that stimuli clustered into mode 1 exhibited low overall firing rates. In contrast, sounds clustered into mode 2, generally evoked strong population activity. In order to further examine the validity of these observations, we rearranged the stimulation battery based on average stimulus evoked population firing rate evoked in each session. Stimuli of the first mode placed in the low-firing end of the spectrum, while sounds of mode two were placed among the strong-firing inducing stimuli (Fig. 22).

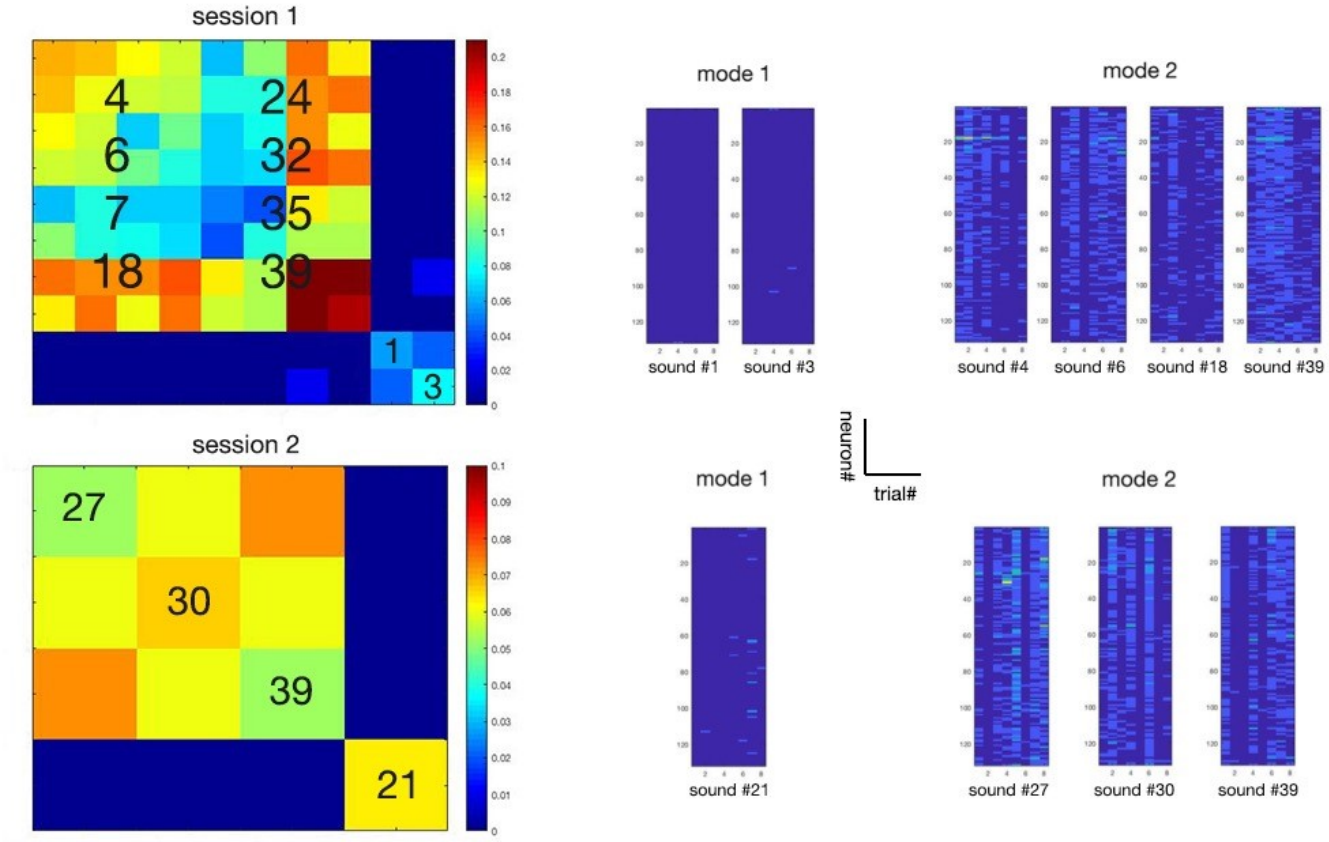

Fig. 21 **A representative example of clusters observed in mice expressing GCaMP6s** *Left*: Clustered averaged correlation matrices from the same FOV in two immediately following sessions performed under matching conditions. The identities of sounds are extremely variable as well as the number of stimuli capable of passing the autocorrelation threshold. *Right*: Single trial population vectors for sounds clustered into mode 1 or mode 2. Sounds 1 and 3 of the first session as well as sound 21 of the second session are clustered into mode 1 based on consistently weak population responses. Sounds clustered into mode 2 in both sessions do not exhibit a tangible pattern of activity. The detected similarity in the elicited population response seems to have been generated by high overall activity of the whole FOV.

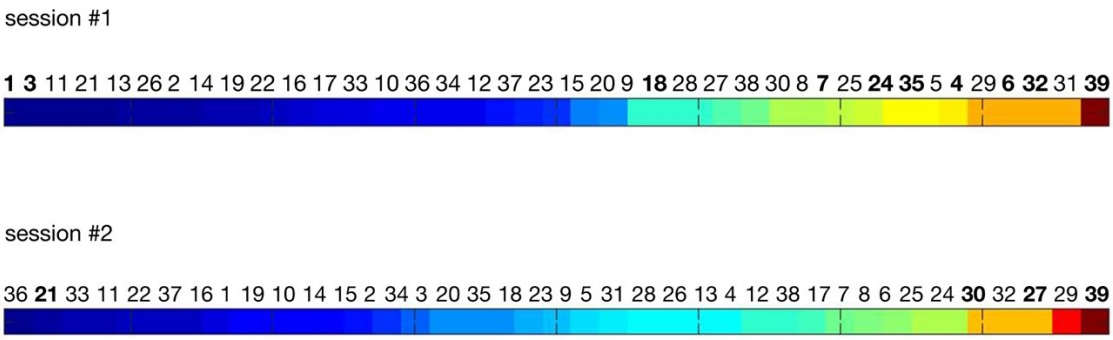

Fig. 22 **Individual stimuli from the stimulation battery rearranged with regard to the overall firing rate evoked in two consecutive sessions.** Numbers in bold indicate stimuli that were clustered into the presumed response modes (shown in Fig. 21).

Unfortunately, no data for sound mixing are available for the FOV described in Fig. 21. Alternatively, we show the second and only FOV subjected to the mixing stimulation directly following the initial detection of modes. As illustrated in Fig. 23C, the two mode-evoking sounds used for the mix stimulation, exhibit "patterns" of activity consisting of strong response in the case of sound#6 and weak response in the case of sound#19, much like the case we described in Fig. 21. According to the analysis determining the fraction of the pure stimulus response in single steps of the mix (Fig. 23D), the strong response evoked by sounds#6 is found in all mix steps except the last one, which represents pure sound#19.

In summary, the used experimental setup combining GCaMP6s with slow acquisition speed did not prove capable of reliably detecting response patterns. Moreover, we believe it is prone to reporting in an all-or-none manner, while lacking sensitivity needed to indicate sparse singular events presumably fundamental to L2/3 coding (Petersen and Crochet, 2013; Sakata and Harris, 2009).

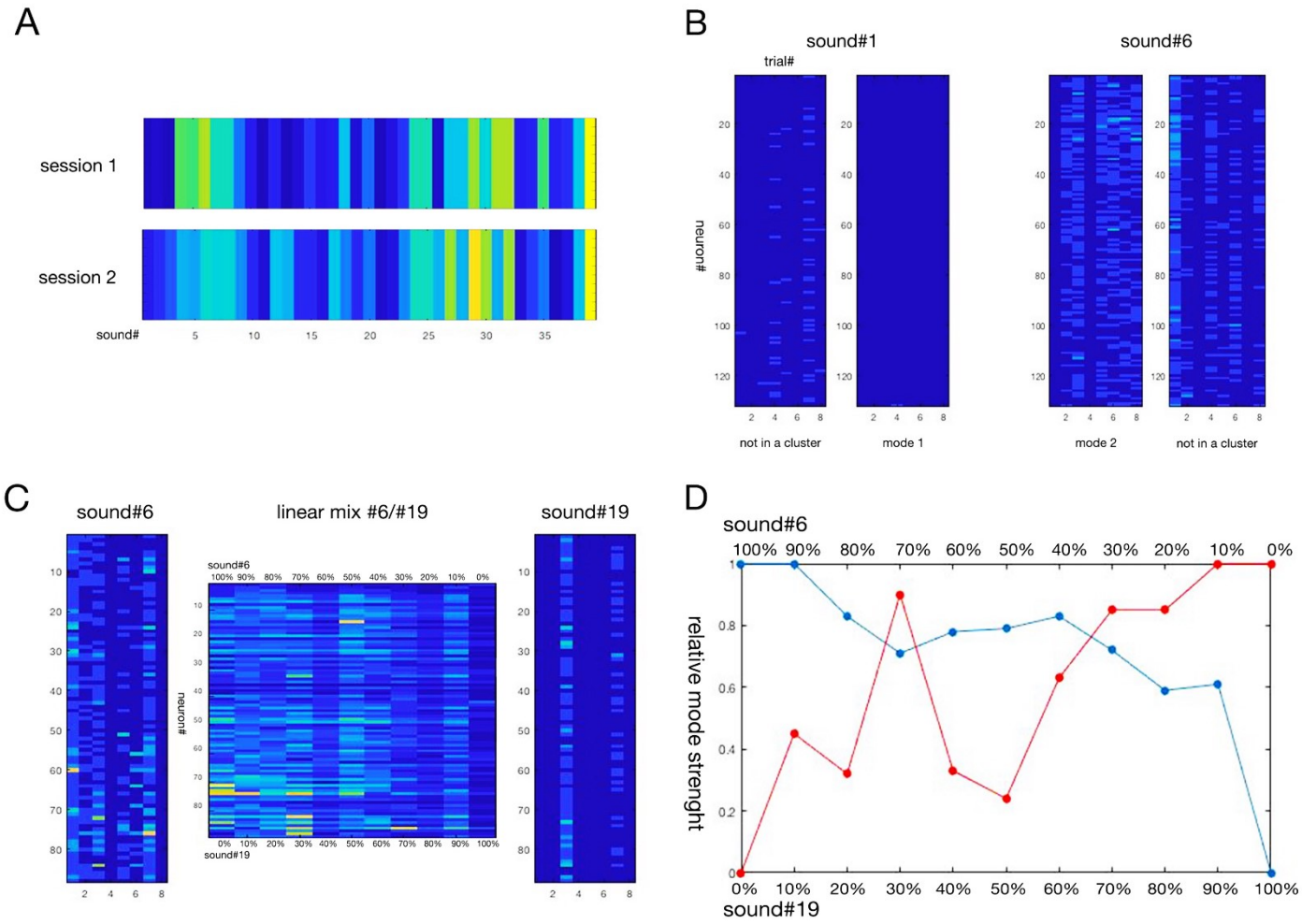

Fig. 23 **Properties of the presumed cortical modes detected using GCaMP6s combined with slow scanning speed**. A: Average population firing rates of neurons described in Fig. 21 evoked by the battery of 39 stimuli. The overall strengths of response of the population to single stimuli are similar across sessions (p=0.39, two-sided Wilcoxon rank sum test). Consequently, there is a pool of high and low firing-rate inducing sounds. B: Single-trial population responses to sounds evoking mode-related "patterns" in one of the sessions but not in the other illustrate the high level of trial-to-trial variability. Sound #1 is a part of the "silent" mode in the first session (*mode 1*) due to its stable lack of firing. However, sparse activity in session 2 causes the failure to pass the autocorrelation threshold, resulting in the filtering of the sound (*not in a cluster*). Sound #6 is a part of the "loud" mode in the first session (*mode 2*). However, the failure to sustain a strong population response across trials has led to the exclusion of sound #6 from mode 2 in session 2 (*not in a cluster*). C: A different FOV in a different animal exhibited similar clustering dynamics including a "silent" mode represented by sound #19 (*right*) and a "loud" mode represented by sound #6 (*left*). A linear intensity mix of these two sounds (11-steps) (*middle*) evoked two modes of response (0.03 autocorrelation threshold). Mode 1 included steps 1-10, while mode 2 consisted of step 11. Average populational responses evoked by the linear mix show that high firing is evoked by all steps containing a fraction of sound #6, while the last step representing pure sound #19 shows a decrease in the overall response. D: The analysis determining the fraction of the pure stimulus response in

single steps of the mix shows that the "mode" of response generated by sound#6 from C is present in all mix steps except step 11 representing the pure sound#19.

5.1.2 GCaMP6f

Due to its fast half-decay time (under 0.2 seconds (Fig. 18)), GCaMP6f was not compatible with the 0.3 second frame period delivered by the original setup. However, our 2PLSM system was recently upgraded with a new x,y-scanning module (a resonant scanner (Sutter)) enabling full-frame, high-speed, high-resolution image acquisition (512x512 at 30fps). Consequently, we were able to order a viral vector enabling the expression of GCaMP6f, for which we developed an application protocol. Based on references from other laboratories, we acquired the AAV9-serotype variant of GCaMP6f-containing viral vector, promising superior spreading of viral transduction, thus requiring less injections (Watakabe et al., 2015), later confirmed in our own experience (Fig. 24). In a further effort to reduce damage infliction, we used an injector enabling controlled injection speed of defined volumes (Nanoject III, Drummond scientific). The final protocol recommends the use of a ~8.10^{11}particles/ml titer applied in 3-4 injections, with the injection volume of 200nl applied at 1nl per second.

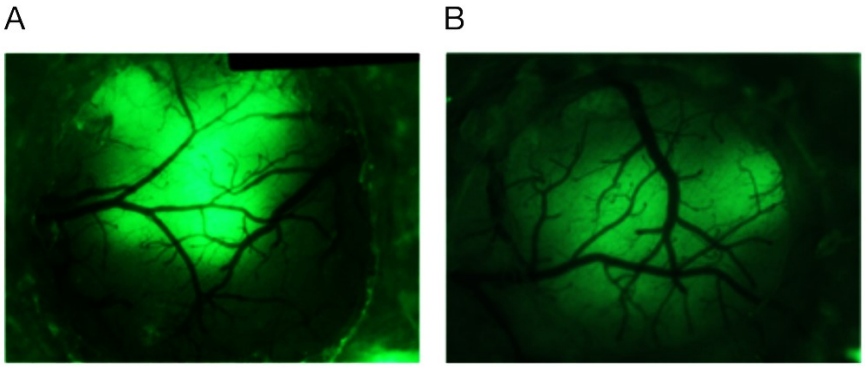

Fig. 24 **An illustration of differences in spreading properties between AAV1 and AAV9 serotypes in mouse AC**. Epifluorescence images of mice expressing A: AAV1.GCaMP6s (9 injection sites) and B: AAV9.GCaMP6f (3 injections).

5.1.2.1 Response modes

Out of the 13 GCaMP6f-expressing mice declared suitable for imaging, 3 exhibited the hypothesized populational dynamics. Firstly, we present data from an animal with tdTomato expression localized in SST+ cells (SST/tdT), containing one FOV exhibiting a single mode of response. The response pattern visualized in the form of plotted single-trial population vectors is consistent between sessions 1 and 2 performed within one hour. In session 1, an additional stimulus (sound#29) has passed the autocorrelation threshold set at 0.1 (Fig. 25).

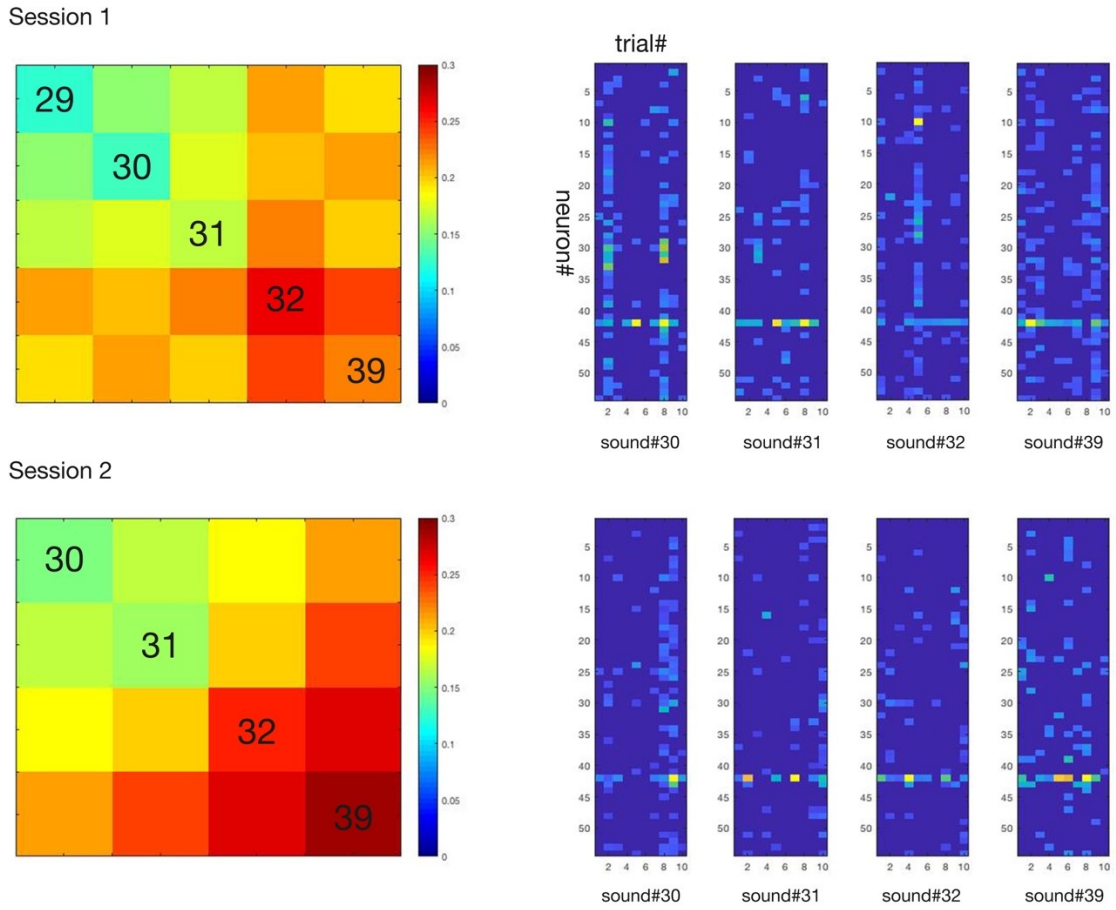

Fig. 25 **A FOV exhibiting a single mode of response stable across consecutive sessions.** The clustered averaged correlation matrices (ACMs) (*left*) of sound evoked population vectors plotted on the *right* reveal, that number of modes of response exhibited by the FOV, as well as the identities of sounds evoking the response mode, are stable across sessions performed within one hour. Sound#29-evoked response in session 2 did not pass the autocorrelation threshold of 0.1.

Our most representative results were acquired from a single mouse (again of the SST/tdT genotype) that contained two FOVs exhibiting clustered population responses. In both cases, the battery of 39 complex stimuli evoked 2 response modes with autocorrelation greater than 0.1 or 0.2 respectively. We observed a simple, but stable pattern of activity in both local populations; data from one of the populations is presented in Fig. 26

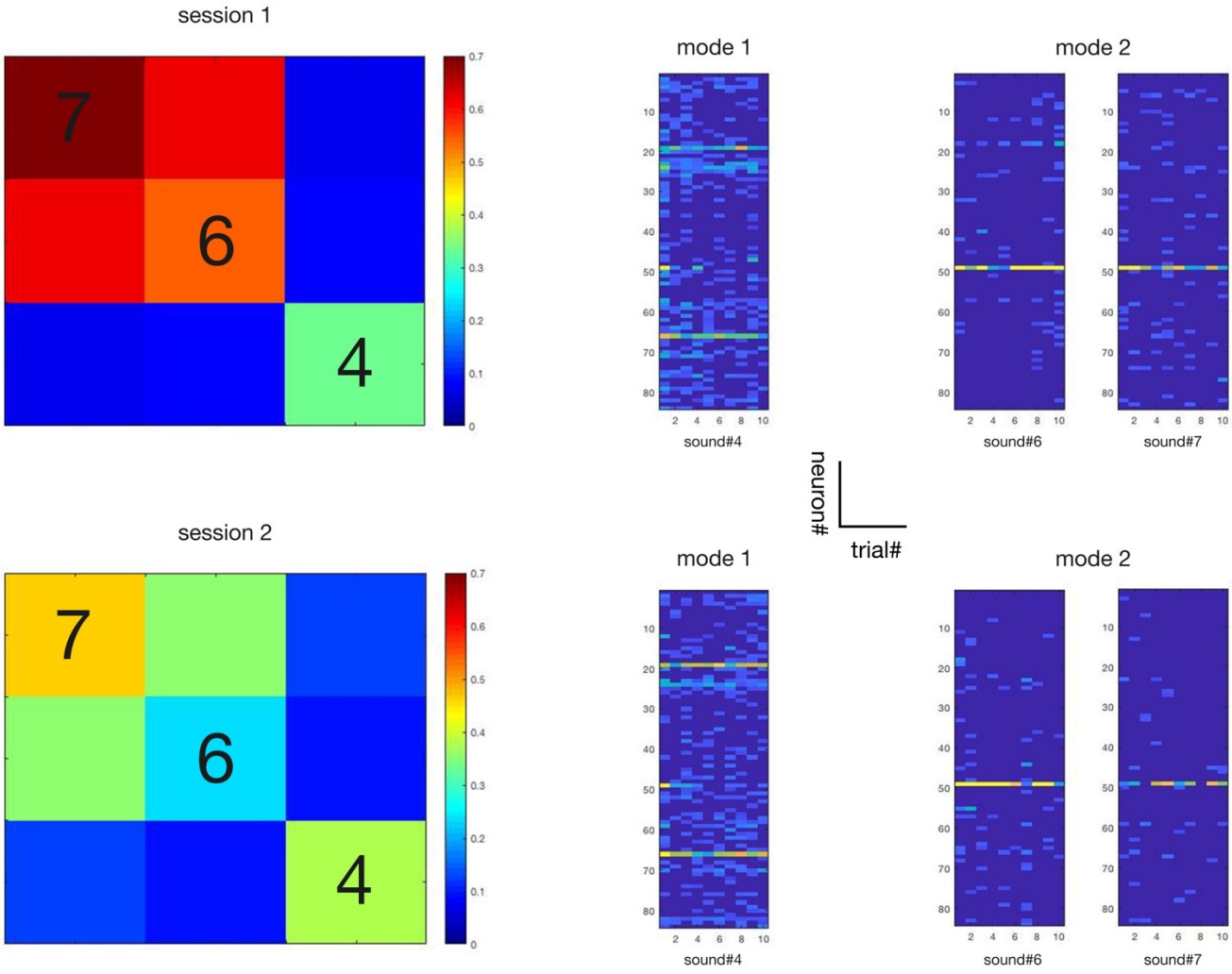

Fig. 26 **A FOV expressing stable multi-pattern activity**. Clustered averaged correlation matrices of two sessions (separated by 20 minutes) revealed a stable number of modes evoked by the same stimuli. Plotted population vectors across trials demonstrate, that the activity patterns evoked by sounds of the same mode (sounds #6 and #7) are similar and that population activity does not differ between sessions performed within one hour.

In order to verify that the observed auditory representation exhibits the reported attractor-like dynamics, we generated a linear intensity mix of sounds #4 and #6. Imaging of the FOV presented in Fig. 26 revealed that the activity evoked by single steps of the mix did include an abrupt change in the representation (Fig. 27C), although separated by steps that did not pass the autocorrelation threshold in cluster calculation (steps 4-8) Fig. 27A). As a form of negative control (Fig. 28), we tested the proposed model in the context of a FOV with a single mode of response (local population described in Fig. 25). A linear mix of sounds evoking the same response pattern produced an uniform population response in all steps of the mix (Fig. 28 *right*). In order to support our observations, we analyzed the relative strength of the response mode in every step of the mix, by determining the fraction of the population response vector evoked by a pure stimulus, present in population responses recorded for single steps (Fig. 28B).

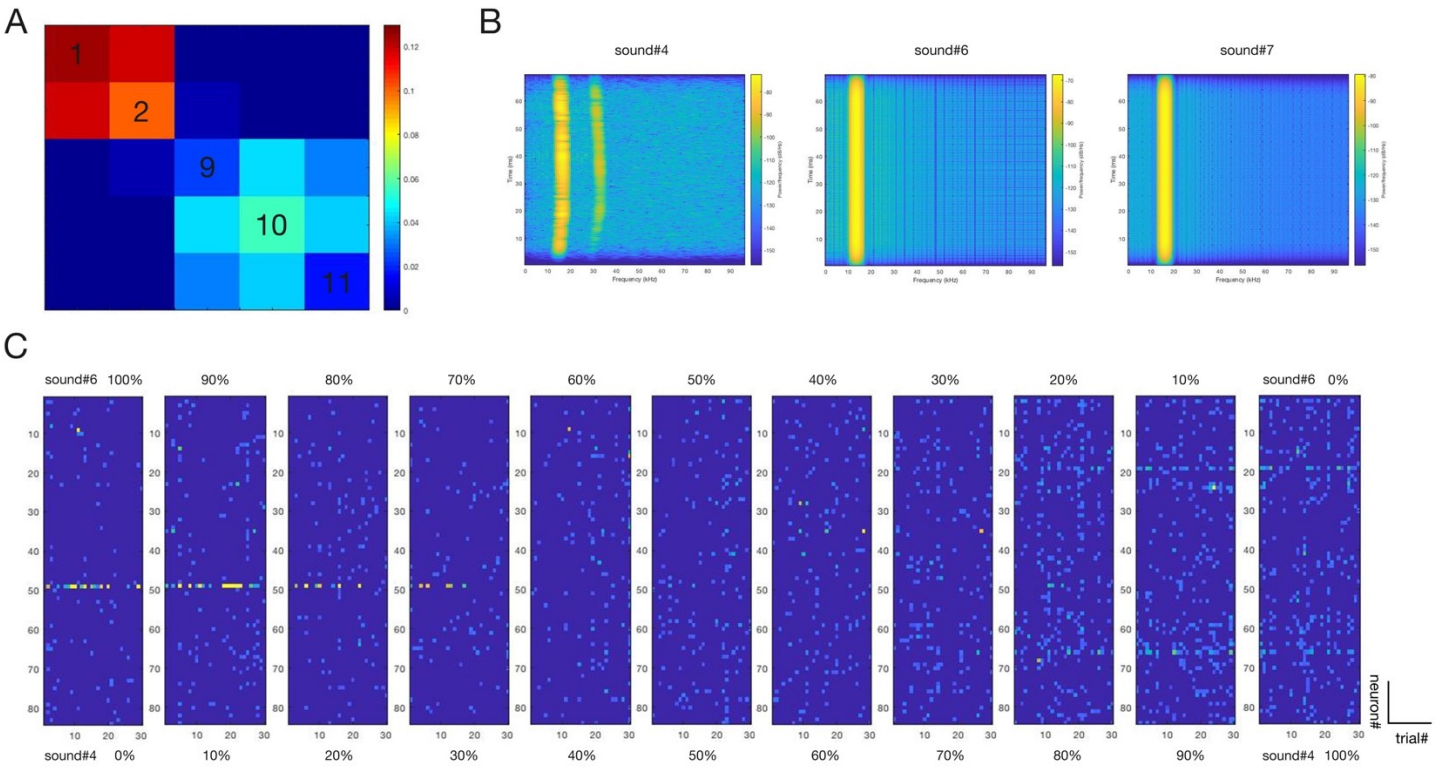

Fig. 27 **Population responses to a linear mix of sounds #4 and #6**. A: An average correlation matrix revealing two modes of activity evoked by single steps of a linear intensity mix of two sounds belonging to different clusters. Steps 3-8 have failed to pass to autocorrelation threshold. B: Spectrograms of sound #4 evoking the first and sounds #6 and #7 evoking the second population response mode described in Fig. 26. C: Population vectors across trials for different steps in the linear intensity mix of sounds #6 and #4. A decrease in the intensity of the evoked representation is observable with lower percentage of the driving stimulus, while steps 5, 6, 7 and 8 lack a visible pattern of activity.

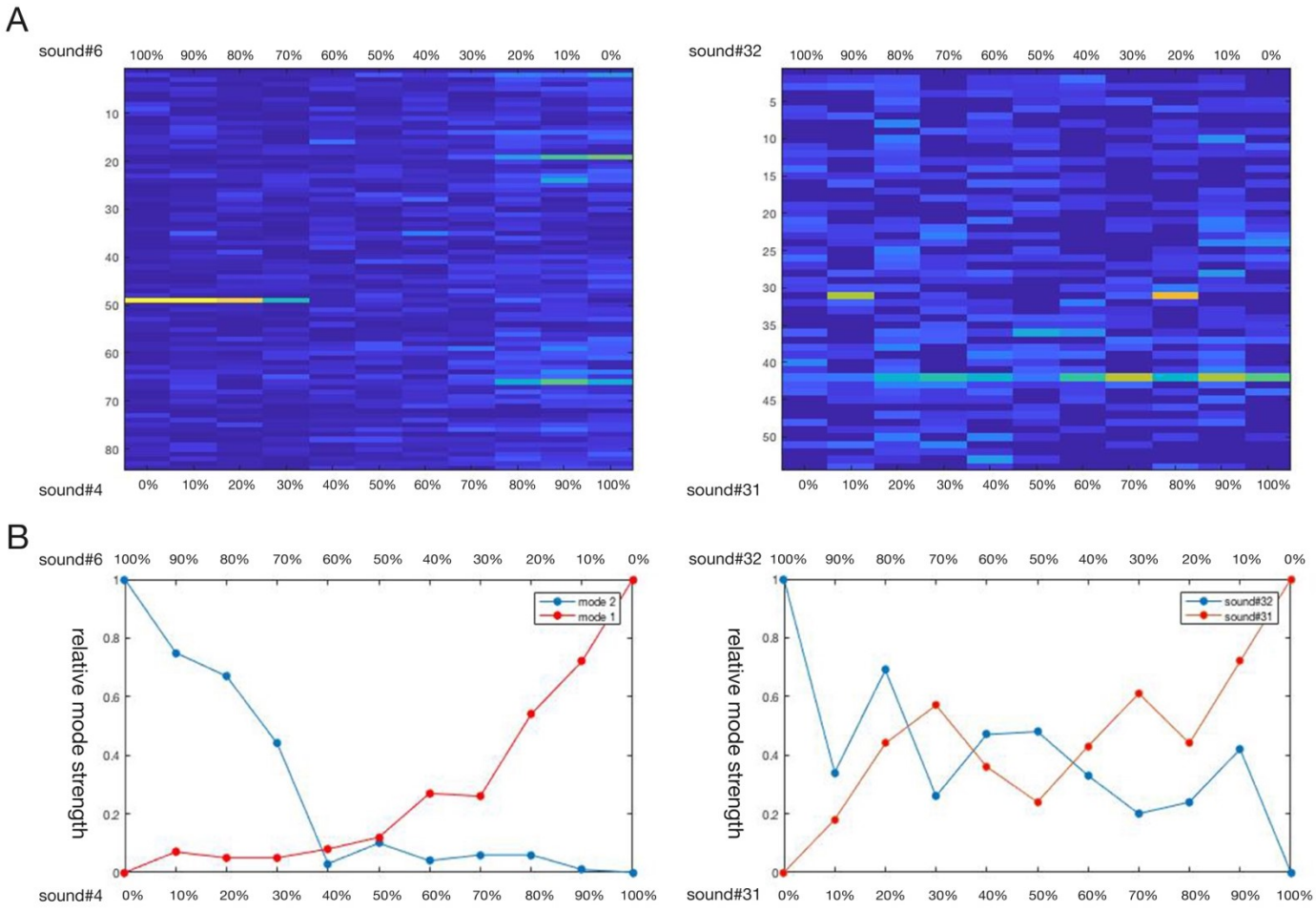

Fig. 28 **Activity recorded in response to linear mixes of sounds evoking two (*left*) and one (*right*) mode of response.** A: Population responses of a FOV averaged across trials in response to single steps of a linear intestity mix of two sounds. *Left*: A mix of two sounds evoking different patterns. An interval of steps evoking no visible pattern of activity divides two regions, where the imaged population responds either by the sound #4-evoked representation or by the sound #6-evoked representation. No intermediate pattern is visible. *Right*: A mix of two sounds evoking the same mode of response (thoroughly presented in Fig. 25). A mostly uniform representation is evoked by all steps of the linear mix battery of sounds #31 and #32. B: Fractions of the respective pure-stimulus population response vectors (mode strength) for each step of the mix. *Left*: Sound#6-evoked mode 2-related reponse pattern disappears from the representation when sound#6 is at 60% (step 5 of the mix). The onset of the sound#4-evoked mode 1 is more challenging to interpret since a low fraction of the response mode is detected from step 6 (50-50 mix). However, it is not until steps 7 and 8 that the mode strength starts to show sings of exponential growth. *Right*: The fraction of the pure stimulus response (sound #31 or #32) in mix steps varies around 0.5, which supports the claim that the reponse pattern evoked by a linear mix of two sounds clustered into the same mode is uniform across mix steps.

Based on our mapping of single-cell tuning, not one of the imaged FOVs was located in the core region of auditory cortex, suggesting that the presented FOVs most likely belong to a higher-order auditory area.

In order to assess the temporal stability of recorded activity patterns, original FOVs exhibiting multiple modes of response were revisited and single neurons were reidentified. However, population responses recorded 24 hours following the first session did not match the earlier results, nor did a novel pattern emerge. Moreover, signs of pathological development restricted to the original FOV suggested that extensive imaging sessions may be damaging. Unfortunately, all FOVs exhibiting 2 or more modes of response were subjected to thorough and long-lasting imaging sessions, in all cases leading to photodamage. Since no further imaging was normally performed in FOVs where the stability of a single-mode behavior was established, a FOV exhibiting a single mode of response was revisited in order to inspect its stability. Despite minor changes in levels of GCaMP-expression, no anatomical differences indicating tissue damage were observed. Moreover, response patterns along with the identities of mode-evoking sounds matched those recorded six days prior to the second session.

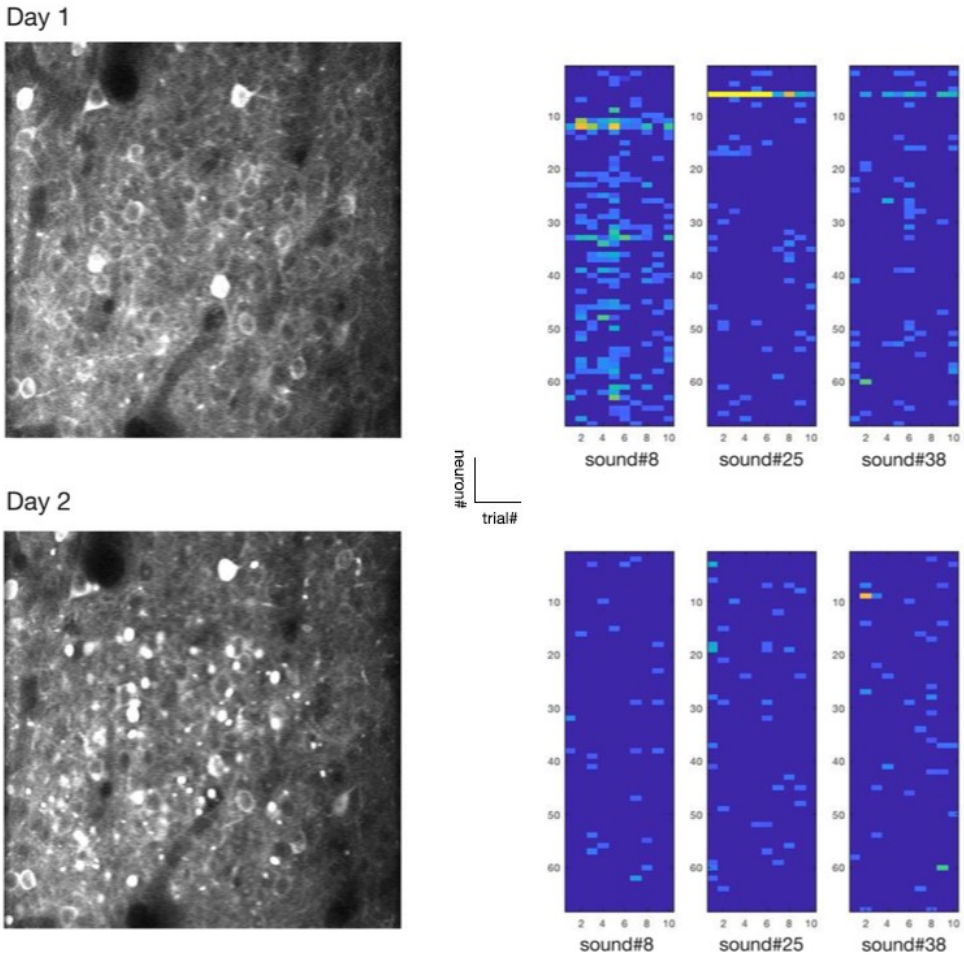

Fig. 29. **Representations of auditory stimuli in the AC showing susceptibility to photodamage induced by extensive imaging**. A second recording session performed ~24 hours after the first was not able to examine the stability of cortical representation of sounds #8, #25 and #35. *Top*: Imaging sessions of Day 1 revealed two stable modes of response repeatedly evoked by the same stimuli. *Bottom*: Sounds #8, #25 and #38 failed to

evoke activity patterns similar to those acquired on Day 1. The overall quality of the recording was partly compromised by numerous fluorescent artifacts, which represent possible markers of photodamage. The situation did not change during later revisits.

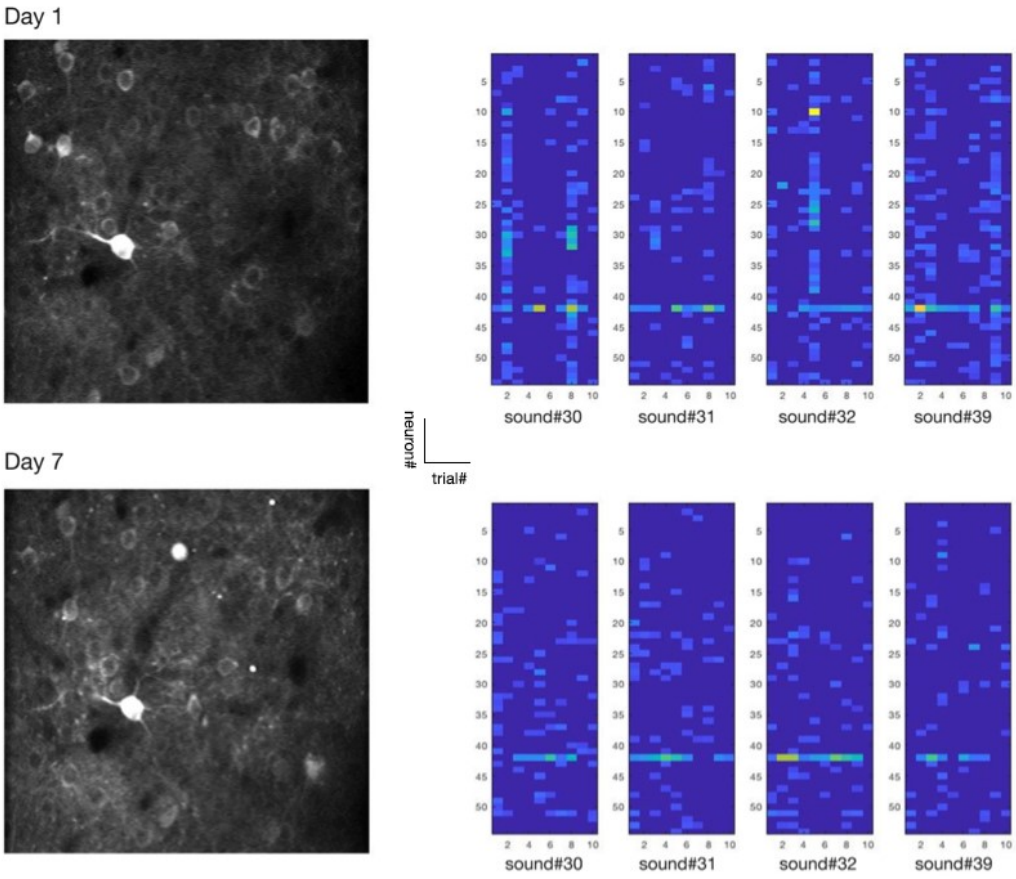

Fig. 30 **Representations of auditory stimuli in the AC showing stability after six days.** Two recording sessions separated by 6 days revealed the consistent nature of mode representation. *Top*: A FOV exhibiting a single mode of response was imaged and a stable pattern of activity was observed across the pool of mode-evoking stimuli. *Bottom*: The original FOV did not exhibit any signs of damage on Day 7 after the initial session. The identities of stimuli evoking the single mode of response were matching those described on Day 1. The underlying activity pattern shared by all mode-evoking stimuli strongly resembles the one described on Day 1.

5.2 The activity of interneurons associated with the switch in cortical representation

The second experimental aim of this thesis was to analyze the activity of different IN subtypes, during the abrupt change in mode representation. Therefore, after every successful identification of a neuronal population exhibiting pattern-switching activity, we immediately performed an another set of recordings capturing the responses of (either PV+ or SST+) interneurons to the same linear mix of sounds. However, since we discovered only three FOVs exhibiting such behavior, the numbers of interneurons recorded under pattern-switching conditions are very low (PV+ INs n= 3 cells, SST+ INs n= 20). Since relevant statistical analysis is largely

incompatible with such small sample size, the following results and interpretations should be considered as preliminary data.

Single-cell averaged correlation matrices (ACMs) demonstrating the similarity in activity evoked by different steps of the linear mix within a single cell, revealed a weak organization into two blocks (no clustering was performed). These blocks may be viewed as a single cell equivalent (Fig. 31A) of the previously discussed modes of population response (such as in Fig. 27). We observed similar organization in a mean ACM obtained by averaging ACMs of all local SST+ INs (Fig. 31B). Interestingly, we observed an overlap, where the stimuli representing borders of the two blocks, evoke activity similar to both modes of SST+ cell-response. These overlapping steps mostly coincide with the steep onset of the sound#4-evoked population pattern we describe in Fig. 27C and Fig. 28 *left*. Moreover, the average correlation coefficient within the overlapping steps seems to be slightly superior to the correlation coefficient exhibited by steps exclusively belonging to one of the blocks (Fig. 31B). The average population firing is stronger (Fig. 31C) in response to steps where the richer response pattern evoked by sound#4 dominates (Fig. 27, Fig. 28). The average firing rate of the whole FOV gradually rises to its maximum during step 11 of mix, representing pure sound#4. However, it seems that the peak in average firing rate of SST+ cells, corresponds to step 9 of the mix (Fig. 31C). We analyzed the response dynamics of SST+ INs of the single-mode FOV (n=6) imaged for temporal stability (Fig. 25 and Fig. 30) in order to provide a negative control. These SST+ cells exhibit a single mode of response, similar among all steps of the linear mix described in Fig. 28 *Right* (Fig. 31D).

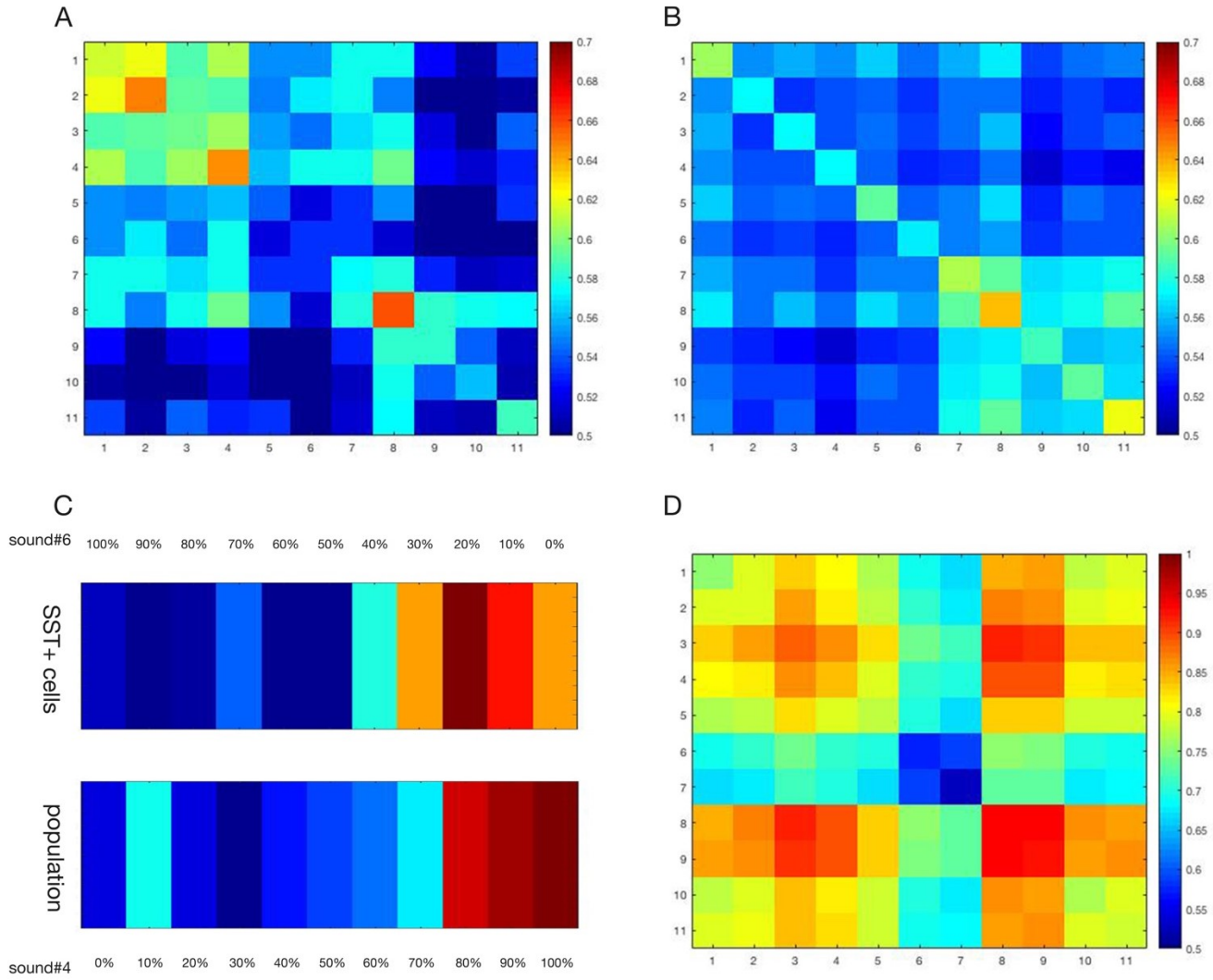

Fig. 31 **Preliminary data acquired from 15 SST+ INs residing within, or in the close vicinity of the FOV** A: An averaged correlation matrix constructed using fluorescence traces of a SST+ cells stimulated by the linear sound mix presented in Fig. 27. The firing profile of this particular cell shows higher similarity when sound#6 is dominant in the mix. However, a faint indication of two clusters of response is visible. Responses evoked by steps #7 and #8 of the mixture show a relatively high level of similarity B: A mean of averaged correlation matrices of single SST+ cells (Fig. 31A) reveals combinations of stimuli most likely to evoke consistent responses in single cells across the population. Weak indications of a two-cluster organization produce an overlap where the highest overall consistency of response is located. Contrary to the SST+ cell described in Fig. 31A, the overall trend in the local SST+ population seems be that higher similarity of responses is exhibited to mix steps dominated by sound#4. C: Average SST+ subpopulation firing rates in response to single steps of the linear mix stimulation battery described in Fig. 27, in the context of the whole FOV. Steps of the mix where sound#4 dominates, provoke stronger firing in both local SST+ cells (*top*) and the imaged population as a whole (*bottom*). In the case of the whole FOV, the intensity of activity reaches its maximum with step 11 representing pure sound#4. However, the activity of the SST+ subpopulation reaches its peak during step 9. D: An averaged

correlation matrix of SST+ cells residing within a FOV exhibiting single-mode behavior. The population responses of these cells produce a single mode of activity common to all steps of the linear mix described in Fig. 28 *right*. No clustering was performed on any of these ACMs.

All scripts used in the analysis-pipeline along with a dataset containing preprocessed recordings of neurons and SST+ cells from the FOV described in Fig. 25, Fig. 26, Fig. 30A,B and C are available for review at https://github.com/2pLabIEM/clustering.

6 Discussion

The main experimental aim of this thesis was to establish a protocol enabling chronic examination of population coding in the auditory cortex of mice. In 2012, Bathellier et al. provided data supporting a model of perceptual categorization in the auditory cortex relying on attractor-like dynamics of local neuronal populations (Bathellier et al., 2012). The original study employed 2PLSM calcium imaging using a synthetic calcium indicator providing reliable spike detection (Stosiek et al., 2003). However, such synthetic dyes are incompatible with chronic experiments, as they would require repeated re-administration. In 2013, Chen et al. introduced GCaMP6, an advanced genetically-encoded calcium indicator, which became the most commonly used probe for two-photon *in vivo* calcium imaging. However, due to its cytosolic localization properties, GCaMP6-based calcium imaging requires raster scanning, which is significantly slower compared to the linescan mode supported by OGB-1 (the synthetic indicator used in the original study). The reduction in the acquisition speed is particularly significant (30-fold decrease) in the case of older 2PLSM setups relying on x-y scanning provided by two galvanometric mirrors.

In our first attempt to observe the hypothesized dynamic, we performed calcium imaging of mice expressing GCaMP6s at slow acquisition speed (3Hz). Two out of the 17 imaged mice were consistent in exhibiting two or more modes of activity, in response to a battery of 39 complex sounds. We determined that the identities of sounds evoking different modes were largely variable, however did not migrate between modes. This suggested, that there were two pools of stimuli, random representatives of which appeared in the clustered correlation matrix across different sessions. The visualization of single-trial population vectors (Fig. 21) revealed that the two modes of response are represented by a “pattern” of high overall activity on one side, and a weak population response on the other. The high similarity ($p=0.39$, two-sided Wilcoxon rank sum test) of average population firing rates across two sessions (Fig. 23A) suggested, that the two previously hypothesized pools of stimuli, may represent sounds evoking strong activity and sounds evoking a weak response. We tried to examine this notion by organizing the battery of stimuli based on the amount of activity evoked by each stimulus across trials. While the sounds of the quiet mode (mode 1) placed reliably as the lowest-firing evoking stimuli, the sounds of mode two exhibited a slightly larger spread (Fig. 22). Furthermore, differences we observed in single-trial response patterns evoked by a sound when part of a cluster and when not part of a cluster suggested, that the consistently high (or low) activity across trials is the main prerequisite required for

appearance in the ACM (Fig. 23B). The observation of high trial-to-trial variability in the activity of single L2/3 neurons supports the previously reported results (Bathellier et al., 2012; Hromádka et al., 2008). Moreover, when presented with a linear intensity mix of sound#6 from the "loud" mode and sound#19 from the "quiet" mode, the response "pattern" represented by high overall activity seems to be prominent in all steps where a percentage of sound 1 is present in the mix (Fig. 23C, Fig. 23D). In summary, these results provide very limited information about the cortical modes of response. Our sole relevant conclusion therefore is, that GCaMP6s-based calcium imaging combined with slow acquisition speed does not enable reliable reporting of population coding in the context of L2/3 of the auditory cortex of mice.

GCaMP6s produces strong and long-lasting (half-decay time above 0.5s) changes of fluorescence in response to single action potentials (Fig. 18). Due to the long decay-time and high calcium affinity, high-frequency activity leads to reliable signal summation, quickly reaching saturation. Consequently, GCaMP6s can mask the underlying faster spiking pattern, in a situation when large depolarizations evoke strong and long-lasting fluorescence. Setups with slow scanning speeds are more likely to detect these incidents, over brief events appearing and disappearing in a timeframe similar to their frame period. Therefore, setups with slow acquisition speed using GCaM6s, may exhibit high-pass filtering and consequent limited firing rate sensitivity. In the case of strong response-evoking complex stimuli, the sensitivity is effectively limited to whether the neuron is firing, or not. Experiments aiming to describe tuning features of single neurons usually search for stimuli that generate strong responses and therefore are compatible with such setting. However, the detection of response patterns evoked by complex stimuli relies on the ability to assess the overall firing profile of the population. The activity in local, highly interconnected neuronal populations is of recurrent nature (Douglas et al., 1995; Wang, 2008). Therefore, it is likely that a response-pattern-evoking sound, efficiently stimulating a subset of neurons in the FOV, generates at least some activity in all neurons of the local network through recurrent excitation which can be inherently overshot by slow image acquisition and calcium reporting with long fluorescence decay. Consequently, a probe with properties enabling the reporting of different firing rates, is essential for successful response pattern detection.

The half decay-time of GCaMP6f is under 200ms and its affinity to calcium is lower than that of GCaMP6s (Chen et al., 2013). Consequently GCaMP6f-based reporting of neural activity is more reliable in terms of spike detection from multi-spike recordings, creating a larger range of firing rates (dynamic range) that can be distinguished. However, again due to its fast decay-time, GCaMP6f is largely incompatible with slow-scanning 2PLSM setups. Fortunately, a resonant scanner module was installed in April 2018, effectively increasing the scanning speed of our setup to 30 Hz in high (512x512) resolution, which rendered the 2PLSM setup compatible with GCaM6f-based calcium imaging. The subsequent acquisition of a new GCaMP6f-containing AAV vector provided us with an opportunity to explore different serotype options suitable for use in the neocortex. We selected the AAV9 serotype due to the promise of superior neocortical spread supported by several personal and published references (Watakabe et al., 2015). Our application protocol developed for optimal expression (covering the cranial window) of GCaMP6f delivered in an AAV9-based viral vector proposes 3-4 injections of 200nl at 1nl per second (Fig. 24B). The AAV1-based GCaMP6s-containing vectors required 7-9 80nl

injections in order to cover a reasonable part of the cranial window (Fig. 24A). Therefore, the use of a AAV9-based vector significantly reduced the number of injections required for viral delivery, consequently reducing the amount of inflicted mechanical trauma.

All of our further demonstrated results were acquired from three mice expressing the GCaMP6f calcium indicator. Although sample sizes in *in vivo* studies are generally small (10 mice per group), our sample size (n=3) is even smaller (mainly caused by the low yield of the surgical procedure) and therefore our results are, without a question, insufficient in terms of robustness of produced data. Consequently, results and interpretations discussed in the following paragraphs are to be regarded as a proof-of-concept followed by preliminary data.

In total, we were able to locate three fields of view (FOVs) exhibiting two modes of response to a battery of complex acoustic stimuli. In all cases, the identities of mode-evoking sounds proved to remain consistent between consecutive sessions performed within one hour. Visualizations of activity patterns underlying single response modes suggest, that the population activity is conserved across trials, between immediately succeeding sessions and between sounds of the same mode (Fig. 25, Fig. 26). In the next step, we generated a stimulation battery consisting of a 11-step linear intensity mix of two sounds selected based on their capacity to evoke a different mode of response. In all cases, an ACM describing the response of the population to the linear mix, clustered the evoked activity patterns into two modes (demonstrated in Fig. 27A). However, in each multi-mode FOV, we observed at least one step between the representations of the original stimuli, that did not cross the autocorrelation threshold (six steps in Fig. 27). This lack of representation may be interpreted as the failure to perceive any of the original sounds in the respective mix steps. Alternatively, our setup may simply lack the sensitivity required in order to detect the faint representation evoked during these mix steps. We used a linear mix of sounds evoking a single response mode from the FOV described in Fig. 25, in order to examine the consistency of the model. The neuronal population exhibited a single mode of response across all mix steps, thus increasing the validity of the concept through the use of a negative control (Fig. 28). Moreover, as we show in single trial population vectors of Fig. 27 or averaged population vectors of Fig. 28 *left*, the nature of the pattern underlying the sound#4-evoked mode 1 is more complex than that of the sound#6-evoked mode 2. This notion is also supported by the gradual increase in average firing rate of the population, positively correlating with the percentage of sound#4 present in the a step (Fig. 31C *bottom*). Since highly-interconnected sister PCs do exhibit a level of colocalization (Yu et al., 2012b), it is likely to expect that cells of a single functional population would dominate a certain spatial domain. Bathellier et al., propose that the "centers of mass" of the response patterns they observed were separated by at least 50μm (Bathellier et al., 2012). Provided a FOV is not big enough to cover multiple domains at the same time, one cortical mode may evoke a response pattern seemingly more complex (in terms of the number of actively participating cells) than the other. This notion can be illustrated by the plotted single trial population vectors of sound#4 (a complex mode of response) compared to those of sounds#6 and #7 (a simple mode of response) we show in Fig. 26, or of sound#8 (a complex mode of response) compared to those of sounds #25 and #38 (a simple mode of response) we present in Fig. 29. However, this could be hypothetically determined solely by the absence of additional mode 2-related cells

localized outside of the FOV. Moreover, the absence of other mode 2-related cells may generate the gap with no clear activity pattern such as we observed in Fig. 27. It is possible that cells outside of our FOV participating in the response pattern underlying mode 2 were still responding to mix steps during the apparently silent gap, and thus were blocking the onset of the sound#4-related mode 1. Its onset is more likely to mark the actual switch since more cells of our FOV participate in its population response.

GCaMP expression is relatively stable over longer periods of time (several weeks in our experience), which supports experimental protocols aiming to revisit the previously imaged FOVs in order to assess the temporal stability of the observed neuronal behavior. However, our attempts to examine the temporal stability of FOVs exhibiting multiple modes of response were largely unsuccessful. The failure to acquire recordings of necessary quality was mainly caused by damage-induced anatomical changes in the FOV. Large fluorescent artifacts directly interfering with fluorescent signal acquisition are presumably markers of photodamage, inflicted through extensive imaging during the first session (Fig. 29). Furthermore, a decrease in intracellular fluorescence intensity may indicate pathological changes in cellular physiology, which, if true, are very likely to affect the electrical properties of the cell. All FOVs exhibiting two modes of response were thoroughly imaged during the first session, and later developed anatomical symptoms indicating tissue damage. Due to the amount of damage-related evidence, we find it is most likely that the failure to observe similar response patterns upon revisiting, is a false-negative and therefore does not qualify as proof of mode instability. FOVs exhibiting a single, stable mode of response were subject to significantly shorter imaging sessions and lacked signs of damage when revisited. Our recordings of carefully reidentified neurons revealed population responses largely similar to those recorded during the first session six days prior. A matching group of stimuli evoked a single cluster of activity, represented by a response pattern matching its counterpart observed during session 1 (Fig. 30). These results may indicate that, under physiological conditions, cortical representations of acoustic stimuli remain stable at least for one week. Our results are therefore theoretically in accord with studies performed in the barrel cortex ((Margolis et al., 2012; Peron et al., 2015) and motor cortex (Peters et al., 2014) of the mouse, which reported neuronal representations consistent over the course of multiple weeks. However, a recent study concerning the initially stable representations recorded in the posterior parietal cortex reported, that these are likely to disappear after over a week (Driscoll et al., 2017). Our future experiments will therefore aim to examine the temporal stability of auditory representation during longer time frames (one month).

The second objective of this thesis was to describe the activity of single interneuronal subtypes during changes in perceptual representation. Therefore, all of the imaged mice exhibited interneuron-specific expression of a red fluorescent marker. In addition to the small number of suitable FOVs (n=3), two of these populations did not contain a relevant subpopulation of tdTomato-expressing cells (n=3, n=5) residing within the borders of the FOV or in its close vicinity. We observed the presented dynamics in a subpopulation of 15 SST+ cells located inside the FOV (described in Fig. 26 and Fig. 27), or within a 20μm wide radius along each axis. The expression of GCaMP is usually lower in tdTomato-positive cells, but remains relatively consistent across the labeled subpopulation. In addition, GCaMP6f-mediated spike extraction is prone to ignore a small percentage of APs. Consequently, the spiking pattern extracted from fluorescent traces of SST+ cells was very

sparse, while a significant part of the activity profile was lost during analysis. These incomplete spiking patterns proved incompatible with cross-correlation and similarity detection. Since the overall level of GCaMP expression across the SST+ population was relatively stable, we presumed that the amount of fluorescence generated by one cell in response to a single action potential should be very similar to the amount generated by all other cells in response to the same event. Consequently, we analyzed the activity of SST+ cells using fluorescent traces directly.

If not stated otherwise, we based all our following interpretations on results acquired from responses of the local SST+ subpopulation to the linear intensity mix of sounds #4 and #6 presented in Fig. 27. An averaged correlation matrix (ACM) constructed via cross-correlation of 250ms-long time bins from stimulus-evoked fluorescent traces of a single cell (Fig. 31A), provided insight about intra- and inter-stimulus response similarity at single-cell level. In order to examine if the organization of responses of SST+ INs to the linear mix is, to any extent, consistent across the SST+ subpopulation, we constructed a mean ACM averaging ACMs of all SST+ cells (Fig.31B). The main purpose of the mean ACM is to represent the organization of response patterns exhibited by an average SST+ cell that can be found within the spatial context of the FOV. In our opinion, the mean ACM presented in Fig. 31B reveals a weak, but evident organization of mix-evoked activity into two blocks, although no hierarchal clustering was performed. Moreover, we believe that there is an overlap observable (steps 7 and 8). This could mean that the mix-step-evoked activity profiles belonging to the overlap are similar to both blocks of response patterns at the same time (Fig. 31B). Based on these preliminary results, we hypothesize that the activity of single SST+ INs possibly reflects three states of the local network. Firstly, the two blocks of SST+ response (steps 1-8 and steps 7-11 of the linear mix, Fig. 31B) seem to correlate with the population response modes of the surrounding principal cells (Fig. 27, Fig. 28). Secondly, a transient increase in the response consistency of single SST+ cells is observable during the transition between these two blocks, and therefore may be related to the transition between cortical representations, which cannot be precisely determined due to the large gap between the significant onset of both representations (visible in Fig. 27C and analyzed in Fig. 28B). Moreover, the difference in average firing rate in response to single steps of the linear mix between SST+ cells and the whole population (mostly comprised of L2/3 excitatory pyramidal cells), further suggests that SST+ INs do play a, possibly substantial, role in the categorization of auditory stimuli. A similar conclusion was drawn by a study performed on a primate model, where it was based on the observation that interneurons of the auditory cortex exhibit higher selectivity for auditory categories, compared to the local pyramids (Tsunada et al., 2012). In addition, the notion that inhibitory interneurons play a pivotal role in the neocortical processing of auditory stimuli is generally accepted in different areas of auditory research (Schinkel-Bielefeld et al., 2012; Wu et al., 2008).

The quality and size of interpretations that can be directly postulated based on the acquired dataset, is objectively limited. We believe that in order to effectively study the role of inhibitory interneurons, an upgraded, hypothesis-driven experimental protocol is required. Therefore, we assembled a set of speculative hypotheses

proposing a simplified model describing the role of SST+ INs in the transition between representations of auditory percepts based on the acquired preliminary data.

The conserved response pattern of local PCs exhibited across stimuli evoking the same mode of response, should create a specific but consistent pattern of excitation upon each local SST+ interneuron. Consequently, this wiring-determined, mode-specific footprint of depolarization should be unique for every IN and could force a given SST+ IN into firing in a certain manner when the cortical mode is represented. We propose that the two clusters visible in the mean ACM (Fig. 31B) could demonstrate the presence of such footprints, which would in turn suggests, that the local subpopulation of SST+ INs is targeted by two mode-determined functional subpopulations of local principal cells (PCs). Such wiring does not contradict with the reported role of SST+ INs in feedforward, feedback and lateral inhibition (Adesnik et al., 2012; Phillips et al., 2017; Silberberg and Markram, 2007). In an attempt to provide a negative control, we examined the responses of a local SST+ population residing within a FOV with one mode of response (FOV presented in Fig. 25 and Fig. 30). Our results indicate that these cells exhibited a single pattern of activity across all steps of the mix (Fig. 31D), supporting the notion that modes of response exhibited by local SST+ INs are forced upon them by local PCs. As possibly assumable from Fig. 27C and Fig. 28 *left*, the intensity of the response pattern increases with the percentage of the pattern-driving stimulus presented in the mix. The local pattern evoked by sound#4 of mode 1 is significantly more complex than the locally observable pattern underlying mode 2 (illustrated by the visualization of single trial population vectors in Fig. 26). Therefore, the amount of input onto local SST+ cells generated by the response pattern of the first mode (evoked by sound#4) should be larger than that of mode 2 (evoked by sounds#6 and #7). The average SST+ population firing rate across single steps of the linear mixture mostly supports this notion, since mix steps evoking a detectable sound#4-response pattern (representing the more (locally) complex representation) are coupled with higher SST+ firing rate than others. The efficiency of the more complex pattern in generating high firing-rate may be supported by the facilitating nature of SST+ INs input synapses (Silberberg and Markram, 2007). In summary, our results indicate that SST+ cells of the imaged FOV seem to be preferably targeted by mode 1-related PCs, presumably dominating in the local spatial domain (supported by the gradually increasing population firing rate we show in Fig. 31C *bottom*). Their high firing rate accompanying the presence of the mode 1-related representation pattern (Fig. 31C *top*, (Fig. 27 and Fig. 28 for the onset of mode 1)), could provide lateral inhibition, effectively silencing cells participating in the representation of mode 2. These results support the hypothesis that SST+ INs promote a winner-takes-all environment, effectively enabling attractor-like dynamics between cell assemblies (Silberberg, 2008; Tremblay et al., 2016).

Moreover, we believe our results suggest that the mixture-step stimuli creating the overlap between two modes of SST+ response exhibit a superior level of inter-trial consistency (Fig. 31B, steps 7 and 8). We hypothesize that the two blocks of SST+ cell response and the increase in synchronicity located in the overlap may represent functional consequences of the underlying attractor network state. Strong representation of a stimulus dominant in the mixture step should provoke stronger activity in the local fraction of SST+ INs (such as in Fig. 31C). As noted before, our results presented in Fig. 27 and Fig. 28 suggest that the intensity of stimulus

representation rises with the percentage of the driving stimulus in the mix. Due to the facilitating nature of input synapses on SST+ INs (Reyes et al., 1998; Silberberg and Markram, 2007), their strength of response should rise nonlinearly with rising intensity of the cortical mode . Therefore, the firing rate of the local subpopulation of SST+ INs should rise exponentially on both ends of the mix, while the "middle" (dependent on the location of the abrupt transition) steps should provoke the least amount of activity. Our results exhibit such exponential rise on one end of the mix (Fig. 31C). As postulated above, this could be a direct consequence of the small area covered by the FOV, capturing the fraction of the SST+ subpopulation mostly targeted by mode 1-related PCs. Moreover, in contrast to the local PC population imaged in the FOV, the peak in firing rate is not located in the last step of the mix but in step 9 instead (Fig. 31C). This could possibly suggest, that the activity of SST+ INs is modulated in cases of clearly perceived stimuli. Therefore, it might prove interesting to examine the firing properties of SST+IN-targeting Vip+ bipolar cells during clearly represented stimuli since these are implicated in spatially confined disinhibition (M. M. Karnani et al., 2016). Based on the activity profile displayed in Fig. 31, we might speculate that the two blocks of SST+ cell response visible in Fig. 31B represent a pattern of SST+ IN activity driven by strong excitatory input of the currently dominating representation. Consequently, the two blocks of Fig. 31B could represent two basins of attraction of the local network. Furthermore, we propose that the peak in inter-trial consistency of response-evoked SST+ activity (steps #7 and #8 in Fig. 31B) might have been caused by the lack of bursting activity, otherwise provoked by strong input summation and facilitating synapses of SST+ INs. The summation of a high number of EPSP may partially compromise the temporal reliability of translation of the mode-specific excitation footprint into the firing output of the SST+ IN. The supposed lack of such unreliability in steps 7 and 8 could hypothetically mean that no response mode is overly dominant during the given mixture steps, and that the nature of the representation (the basin of attraction) is determined, based on small and precise differences in activity within the local SST+ subpopulation. Therefore, this state of the network could possibly represent a peak in a simple energy landscape located between two basins of attraction (Fig. 14). In summary, the absence of strong inhibition driven by either of the modes of response could create a network state, where spatially-determined fractions of single SST+ INs can precisely compare the intensity of the arriving excitatory input while reliably selecting the dominant representation. A graphical representation fitted with our data is provided in order demonstrate the described model (Fig. 32).

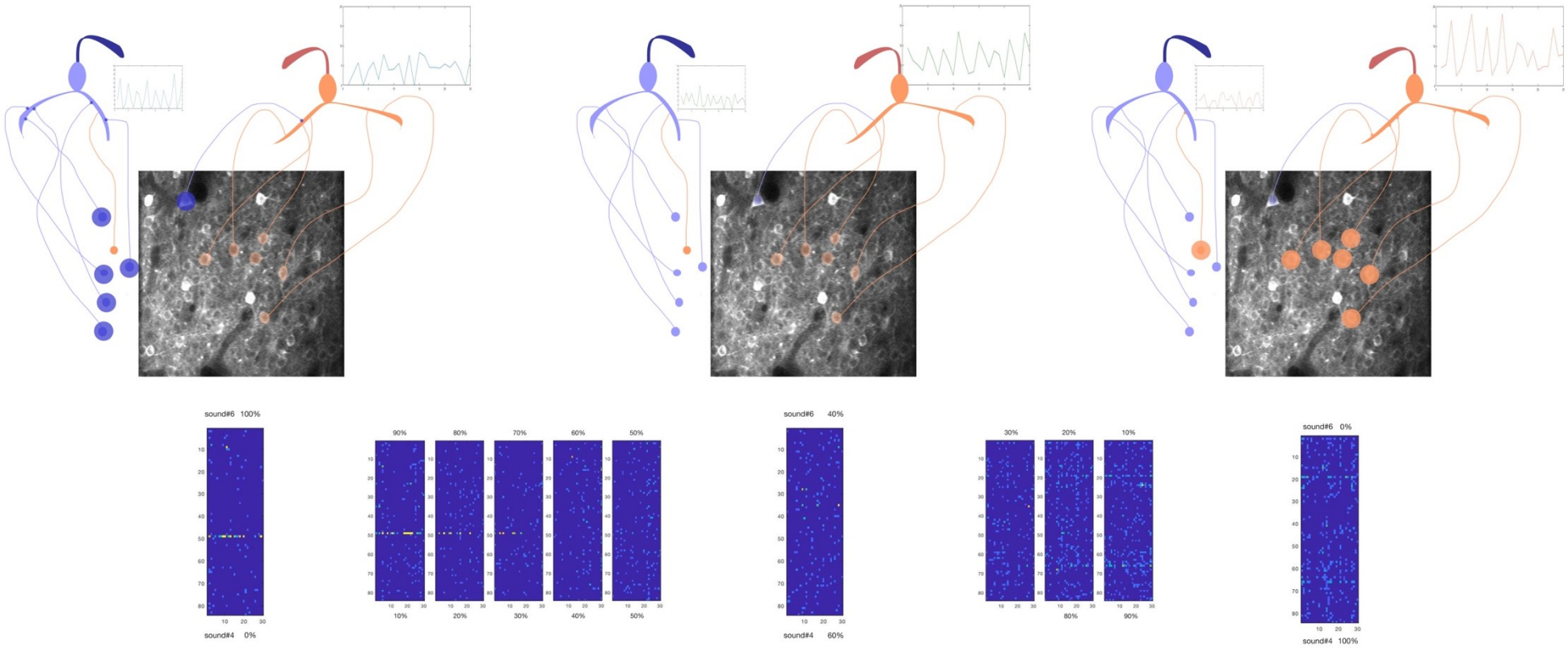

Fig. 32 **A graphical representation of the model of action proposed for SST+ INs based on the acquired preliminary data.** We propose that the local FOV (described in Fig. 26) is dominated by the representation of sound#4 due to its more complex response pattern. Since a FOV represents a random selection from the local population, it is likely that additional mode one- and mode two-recruited cells are present outside of its borders (blue cells). Local SST+ INs are likely to be primarily targeted by local PCs. PCs participating in mode-related response patterns are spatially clustered since their centers of mass were reported to be located at least 50µm apart (Bathellier et al., 2012). Consequently, single SST+ INs receive input primarily from the locally dominant representation (represented the blue and orange subpopulation). Strong representation of a response mode will provoke strong depolarization of local SST+ cells (*left, right*). These will respond with bursting activity providing strong feedback inhibition, silencing any competing representations. The bursting nature of SST+ firing introduces an increase in the temporal variability of spikes as illustrated by the fluorescence traces. We propose that the higher similarity of responses evoked by steps #7 and #8 displayed in Fig. 31B, is a direct consequence of the absence of a dominating representation capable of evoking bursting activity. The firing profile of individual SST+ INs becomes more reliable in translating the incoming input, which could suggest that precise comparison of the intensity of both representations takes place during these mix-steps (*middle*).

In terms of further outlook, we plan to primarily concentrate on the completion of the second experimental aim of this text, which proved too challenging to achieve in a two-year time frame. We plan to perform additional experiments in order to increase the sample size and validity of our results and interpretations. We also hope to acquire data regarding the activity of PV+ and Vip+ neocortical cells during the observed switch in population coding, in order to describe their role in the dynamics of presumed neural correlates of perceptual categorization. Furthermore, we would like to redesign our imaging protocol in order to enable the assessment of temporal stability of the observed population coding.

In conclusion, we developed an experimental protocol enabling chronic observation of population coding similar to that described by Bathellier and colleagues in 2012. This, in our view, classifies as proof-of-concept, meaning the first experimental aim of this thesis can be considered completed even in spite of the small sample size. On the other hand, results obtained with regard to the role of inhibitory interneurons in population coding, do not meet the standards of a solid scientific study. Therefore, all of our hypotheses postulated in order to interpret the observed activity can be rightfully criticized as speculations. However, we believe that the acquired evidence does qualify as preliminary data, laying ground for further hypothesis-driven research. Although the second experimental aim of this thesis cannot be considered as successfully completed, we believe that the results presented in this study hold value in providing guidelines for design of future experiments aiming to test the validity of our assumptions on larger samples.

7 References

Adesnik, H., Bruns, W., Taniguchi, H., Huang, Z.J., Scanziani, M., 2012. A neural circuit for spatial summation in visual cortex. Nature 490, 226–231. https://doi.org/10.1038/nature11526

Aertsen, A.M., Olders, J.H., Johannesma, P.I., 1981. Spectro-temporal receptive fields of auditory neurons in the grassfrog. III. Analysis of the stimulus-event relation for natural stimuli. Biol. Cybern. 39, 195–209.

Aizenberg, M., Mwilambwe-Tshilobo, L., Briguglio, J.J., Natan, R.G., Geffen, M.N., 2015. Bidirectional Regulation of Innate and Learned Behaviors That Rely on Frequency Discrimination by Cortical Inhibitory Neurons. PLOS Biol. 13, e1002308. https://doi.org/10.1371/journal.pbio.1002308

Alagha, K., Palot, A., Sofalvi, T., Pahus, L., Gouitaa, M., Tummino, C., Martinez, S., Charpin, D., Bourdin, A., Chanez, P., 2014. Long-acting muscarinic receptor antagonists for the treatment of chronic airway diseases. Ther. Adv. Chronic Dis. 5, 85–98. https://doi.org/10.1177/2040622313518227

Alonso, J.-M., Swadlow, H.A., 2005. Thalamocortical Specificity and the Synthesis of Sensory Cortical Receptive Fields. J. Neurophysiol. 94, 26–32. https://doi.org/10.1152/jn.01281.2004

Amitai, Y., Gibson, J.R., Beierlein, M., Patrick, S.L., Ho, A.M., Connors, B.W., Golomb, D., 2002. The Spatial Dimensions of Electrically Coupled Networks of Interneurons in the Neocortex. J. Neurosci. 22, 4142–4152. https://doi.org/10.1523/JNEUROSCI.22-10-04142.2002

Anderson, L.A., Christianson, G.B., Linden, J.F., 2009. Mouse auditory cortex differs from visual and somatosensory cortices in the laminar distribution of cytochrome oxidase and acetylcholinesterase. Brain Res. 1252, 130–142. https://doi.org/10.1016/j.brainres.2008.11.037

Andoni, S., Li, N., Pollak, G.D., 2007. Spectrotemporal Receptive Fields in the Inferior Colliculus Revealing Selectivity for Spectral Motion in Conspecific Vocalizations. J. Neurosci. 27, 4882–4893. https://doi.org/10.1523/JNEUROSCI.4342-06.2007

Arai, Y., Pierani, A., 2014. Development and evolution of cortical fields. Neurosci. Res. 86, 66–76. https://doi.org/10.1016/j.neures.2014.06.005

Arif, S.H., 2009. A Ca(2+)-binding protein with numerous roles and uses: parvalbumin in molecular biology and physiology. BioEssays News Rev. Mol. Cell. Dev. Biol. 31, 410–421. https://doi.org/10.1002/bies.200800170

Atiani, S., Elhilali, M., David, S.V., Fritz, J.B., Shamma, S.A., 2009. Task Difficulty and Performance Induce Diverse Adaptive Patterns in Gain and Shape of Primary Auditory Cortical Receptive Fields. Neuron 61, 467–480. https://doi.org/10.1016/j.neuron.2008.12.027

Baba, H., Tsukano, H., Hishida, R., Takahashi, K., Horii, A., Takahashi, S., Shibuki, K., 2016. Auditory cortical field coding long-lasting tonal offsets in mice. Sci. Rep. 6, 34421. https://doi.org/10.1038/srep34421

Bai, W.-Z., Ishida, M., Arimatsu, Y., 2004. Chemically defined feedback connections from infragranular layers of sensory association cortices in the rat. Neuroscience 123, 257–267.

Ballesteros-Yáñez, I., Benavides-Piccione, R., Elston, G.N., Yuste, R., DeFelipe, J., 2006. Density and morphology of dendritic spines in mouse neocortex. Neuroscience 138, 403–409. https://doi.org/10.1016/j.neuroscience.2005.11.038

Barlow, H.B., 1972. Single Units and Sensation: A Neuron Doctrine for Perceptual Psychology? Perception 1, 371–394. https://doi.org/10.1068/p010371

Barnstedt, O., Keating, P., Weissenberger, Y., King, A.J., Dahmen, J.C., 2015. Functional Microarchitecture of the Mouse Dorsal Inferior Colliculus Revealed through In Vivo Two-Photon Calcium Imaging. J. Neurosci. 35, 10927–10939. https://doi.org/10.1523/JNEUROSCI.0103-15.2015

Bar-Yam, Y., 1997. Dynamics of complex systems, Studies in nonlinearity. Addison-Wesley, Reading, Mass.

Bathellier, B., Ushakova, L., Rumpel, S., 2012. Discrete Neocortical Dynamics Predict Behavioral Categorization of Sounds. Neuron 76, 435–449. https://doi.org/10.1016/j.neuron.2012.07.008

Bayraktar, T., Welker, E., Freund, T.F., Zilles, K., Staiger, J.F., 2000. Neurons immunoreactive for vasoactive intestinal polypeptide in the rat primary somatosensory cortex: Morphology and spatial relationship to barrel-related columns. J. Comp. Neurol. 420, 291–304. https://doi.org/10.1002/(SICI)1096-9861(20000508)420:3<291::AID-CNE2>3.0.CO;2-H

Beierlein, M., Gibson, J.R., Connors, B.W., 2003. Two Dynamically Distinct Inhibitory Networks in Layer 4 of the Neocortex. J. Neurophysiol. 90, 2987–3000. https://doi.org/10.1152/jn.00283.2003

Bizley, J.K., Cohen, Y.E., 2013. The what, where and how of auditory-object perception. Nat. Rev. Neurosci. 14, 693–707. https://doi.org/10.1038/nrn3565

Bockamp, E., Maringer, M., Spangenberg, C., Fees, S., Fraser, S., Eshkind, L., Oesch, F., Zabel, B., 2002. Of mice and models: improved animal models for biomedical research. Physiol. Genomics 11, 115–132. https://doi.org/10.1152/physiolgenomics.00067.2002

Bortone, D.S., Olsen, S.R., Scanziani, M., 2014. Translaminar Inhibitory Cells Recruited by Layer 6 Corticothalamic Neurons Suppress Visual Cortex. Neuron 82, 474–485. https://doi.org/10.1016/j.neuron.2014.02.021

Bourassa, J., Deschˆnes, M., 1995. Corticothalamic projections from the primary visual cortex in rats: a single fiber study using biocytin as an anterograde tracer. Neuroscience 66, 253–263. https://doi.org/10.1016/0306-4522(95)00009-8

Brazeau, P., Vale, W., Burgus, R., Ling, N., Butcher, M., Rivier, J., Guillemin, R., 1973. Hypothalamic polypeptide that inhibits the secretion of immunoreactive pituitary growth hormone. Science 179, 77–79.

Buchanan, K.A., Blackman, A.V., Moreau, A.W., Elgar, D., Costa, R.P., Lalanne, T., Tudor Jones, A.A., Oyrer, J., Sjöström, P.J., 2012. Target-Specific Expression of Presynaptic NMDA Receptors in Neocortical Microcircuits. Neuron 75, 451–466. https://doi.org/10.1016/j.neuron.2012.06.017

Büning, H., Perabo, L., Coutelle, O., Quadt-Humme, S., Hallek, M., 2008. Recent developments in adeno-associated virus vector technology. J. Gene Med. 10, 717–733. https://doi.org/10.1002/jgm.1205

Buzsáki, G., 2004. Large-scale recording of neuronal ensembles. Nat. Neurosci. 7, 446–451. https://doi.org/10.1038/nn1233

Buzsáki, G., Wang, X.-J., 2012. Mechanisms of Gamma Oscillations. Annu. Rev. Neurosci. 35, 203–225. https://doi.org/10.1146/annurev-neuro-062111-150444

Callaway, E.M., 2004. Feedforward, feedback and inhibitory connections in primate visual cortex. Neural Netw. 17, 625–632. https://doi.org/10.1016/j.neunet.2004.04.004

Caputi, A., Rozov, A., Blatow, M., Monyer, H., 2009. Two Calretinin-Positive GABAergic Cell Types in Layer 2/3 of the Mouse Neocortex Provide Different Forms of Inhibition. Cereb. Cortex 19, 1345–1359. https://doi.org/10.1093/cercor/bhn175

Cauli, B., Tong, X.-K., Rancillac, A., Serluca, N., Lambolez, B., Rossier, J., Hamel, E., 2004. Cortical GABA Interneurons in Neurovascular Coupling: Relays for Subcortical Vasoactive Pathways. J. Neurosci. 24, 8940–8949. https://doi.org/10.1523/JNEUROSCI.3065-04.2004

Cauller, L., 1995. Layer I of primary sensory neocortex: where top-down converges upon bottom-up. Behav. Brain Res. 71, 163–170. https://doi.org/10.1016/0166-4328(95)00032-1

Cetas, J.S., de Venecia, R.K., McMullen, N.T., 1999. Thalamocortical afferents of Lorente de Nó: medial geniculate axons that project to primary auditory cortex have collateral branches to layer I. Brain Res. 830, 203–208.

Chen, C.-C., Abrams, S., Pinhas, A., Brumberg, J.C., 2009. Morphological heterogeneity of layer VI neurons in mouse barrel cortex. J. Comp. Neurol. 512, 726–746. https://doi.org/10.1002/cne.21926

Chen, T.-W., Wardill, T.J., Sun, Y., Pulver, S.R., Renninger, S.L., Baohan, A., Schreiter, E.R., Kerr, R.A., Orger, M.B., Jayaraman, V., Looger, L.L., Svoboda, K., Kim, D.S., 2013. Ultra-sensitive fluorescent proteins for imaging neuronal activity. Nature 499, 295–300. https://doi.org/10.1038/nature12354

Chiu, C.Q., Lur, G., Morse, T.M., Carnevale, N.T., Ellis-Davies, G.C.R., Higley, M.J., 2013. Compartmentalization of GABAergic Inhibition by Dendritic Spines. Science 340, 759–762. https://doi.org/10.1126/science.1234274

Chklovskii, D.B., Schikorski, T., Stevens, C.F., 2002. Wiring Optimization in Cortical Circuits. Neuron 34, 341–347. https://doi.org/10.1016/S0896-6273(02)00679-7

Choi, J.-H., Yu, N.-K., Baek, G.-C., Bakes, J., Seo, D., Nam, H.J., Baek, S.H., Lim, C.-S., Lee, Y.-S., Kaang, B.-K., 2014. Optimization of AAV expression cassettes to improve packaging capacity and transgene expression in neurons. Mol. Brain 7, 17. https://doi.org/10.1186/1756-6606-7-17

Chorev, E., Epsztein, J., Houweling, A.R., Lee, A.K., Brecht, M., 2009. Electrophysiological recordings from behaving animals—going beyond spikes. Curr. Opin. Neurobiol. 19, 513–519. https://doi.org/10.1016/j.conb.2009.08.005

Christianson, G.B., Sahani, M., Linden, J.F., 2011. Depth-Dependent Temporal Response Properties in Core Auditory Cortex. J. Neurosci. Off. J. Soc. Neurosci. 31, 12837–12848. https://doi.org/10.1523/JNEUROSCI.2863-11.2011

Christianson, G.B., Sahani, M., Linden, J.F., 2008. The Consequences of Response Nonlinearities for Interpretation of Spectrotemporal Receptive Fields. J. Neurosci. 28, 446–455. https://doi.org/10.1523/JNEUROSCI.1775-07.2007
Colonnier, M., 1968. Synaptic patterns on different cell types in the different laminae of the cat visual cortex. An electron microscope study. Brain Res. 9, 268–287. https://doi.org/10.1016/0006-8993(68)90234-5
Combs, C.A., 2010. Fluorescence Microscopy: A Concise Guide to Current Imaging Methods. Curr. Protoc. Neurosci. Editor. Board Jacqueline N Crawley Al 0 2, Unit2.1. https://doi.org/10.1002/0471142301.ns0201s50
Constantinople, C.M., Bruno, R.M., 2013. Deep Cortical Layers are Activated Directly by Thalamus. Science 340, 1591–1594. https://doi.org/10.1126/science.1236425
Costa, A.D., M, N.M., Martin, K., 2010. Whose cortical column would that be? Front. Neuroanat. 4. https://doi.org/10.3389/fnana.2010.00016
Costa, N.M. da, Martin, K.A.C., 2011. How Thalamus Connects to Spiny Stellate Cells in the Cat's Visual Cortex. J. Neurosci. 31, 2925–2937. https://doi.org/10.1523/JNEUROSCI.5961-10.2011
Couey, J.J., Witoelar, A., Zhang, S.-J., Zheng, K., Ye, J., Dunn, B., Czajkowski, R., Moser, M.-B., Moser, E.I., Roudi, Y., Witter, M.P., 2013. Recurrent inhibitory circuitry as a mechanism for grid formation. Nat. Neurosci. 16, 318–324. https://doi.org/10.1038/nn.3310
Dantzker, J.L., Callaway, E.M., 2000. Laminar sources of synaptic input to cortical inhibitory interneurons and pyramidal neurons. Nat. Neurosci. 3, 701–707. https://doi.org/10.1038/76656
DeFelipe, J., Ballesteros-Yáñez, I., Inda, M.C., Muñoz, A., 2006. Double-bouquet cells in the monkey and human cerebral cortex with special reference to areas 17 and 18, in: Progress in Brain Research. Elsevier, pp. 15–32. https://doi.org/10.1016/S0079-6123(06)54002-6
DeFelipe, J., Fariñas, I., 1992. The pyramidal neuron of the cerebral cortex: Morphological and chemical characteristics of the synaptic inputs. Prog. Neurobiol. 39, 563–607. https://doi.org/10.1016/0301-0082(92)90015-7
Del Río, J.A., Heimrich, B., Borrell, V., Förster, E., Drakew, A., Alcántara, S., Nakajima, K., Miyata, T., Ogawa, M., Mikoshiba, K., Derer, P., Frotscher, M., Soriano, E., 1997. A role for Cajal–Retzius cells and reelin in the development of hippocampal connections. Nature 385, 70–74. https://doi.org/10.1038/385070a0
Deneux, T., Kempf, A., Daret, A., Ponsot, E., Bathellier, B., 2016. Temporal asymmetries in auditory coding and perception reflect multi-layered nonlinearities. Nat. Commun. 7, 12682. https://doi.org/10.1038/ncomms12682
Denk, W., Strickler, J., Webb, W., 1990. Two-photon laser scanning fluorescence microscopy. Science 248, 73–76. https://doi.org/10.1126/science.2321027
Dennison-Cavanagh, M.E., Papadopoulos, G., Parnavelas, J.G., 1993. The emergence of the cortical GABAergic neuron: with particular reference to some peptidergic subpopulations. J. Neurocytol. 22, 805–814. https://doi.org/10.1007/BF01181325
Derry, S., Wiffen, P.J., Moore, R.A., Quinlan, J., 2014. Topical lidocaine for neuropathic pain in adults 52.
Deschênes, M., Veinante, P., Zhang, Z.W., 1998. The organization of corticothalamic projections: reciprocity versus parity. Brain Res. Brain Res. Rev. 28, 286–308.
Douglas, R.J., Koch, C., Mahowald, M., Martin, K.A., Suarez, H.H., 1995. Recurrent excitation in neocortical circuits. Science 269, 981–985.
Douglas, R.J., Martin, K.A.C., 2007. Mapping the Matrix: The Ways of Neocortex. Neuron 56, 226–238. https://doi.org/10.1016/j.neuron.2007.10.017
Douglas, R.J., Martin, K.A.C., 2004. NEURONAL CIRCUITS OF THE NEOCORTEX. Annu. Rev. Neurosci. 27, 419–451. https://doi.org/10.1146/annurev.neuro.27.070203.144152
Douglas, R.J., Martin, K.A.C., Whitteridge, D., 1989. A Canonical Microcircuit for Neocortex. Neural Comput. 1, 480–488. https://doi.org/10.1162/neco.1989.1.4.480
Driscoll, L.N., Pettit, N.L., Minderer, M., Chettih, S.N., Harvey, C.D., 2017. Dynamic Reorganization of Neuronal Activity Patterns in Parietal Cortex. Cell 170, 986-999.e16. https://doi.org/10.1016/j.cell.2017.07.021
Drobizhev, M., Makarov, N.S., Tillo, S.E., Hughes, T.E., Rebane, A., 2011. Two-photon absorption properties of fluorescent proteins. Nat. Methods 8, 393–399. https://doi.org/10.1038/nmeth.1596

Dumville, J.C., McFarlane, E., Edwards, P., Lipp, A., Holmes, A., Liu, Z., 2015. Preoperative skin antiseptics for preventing surgical wound infections after clean surgery. Cochrane Database Syst. Rev. https://doi.org/10.1002/14651858.CD003949.pub4
Dunn, A.K., Wallace, V.P., Coleno, M., Berns, M.W., Tromberg, B.J., 2000. Influence of optical properties on two-photon fluorescence imaging in turbid samples 39, 1194–1201. https://doi.org/10.1364/AO.39.001194
Eggermont, J.J., 2011. Context dependence of spectro-temporal receptive fields with implications for neural coding. Hear. Res. 271, 123–132. https://doi.org/10.1016/j.heares.2010.01.014
Erickson, R.P., Woodbury, M.A., Doetsch, G.S., 1996. Distributed neural coding based on fuzzy logic. Inf. Sci. 95, 103–112. https://doi.org/10.1016/S0020-0255(96)00127-2
Estebanez, L., Boustani, S.E., Destexhe, A., Shulz, D.E., 2012. Correlated input reveals coexisting coding schemes in a sensory cortex. Nat. Neurosci. 15, 1691–1699. https://doi.org/10.1038/nn.3258
Fanselow, E.E., Richardson, K.A., Connors, B.W., 2008. Selective, State-Dependent Activation of Somatostatin-Expressing Inhibitory Interneurons in Mouse Neocortex. J. Neurophysiol. 100, 2640–2652. https://doi.org/10.1152/jn.90691.2008
Feldmeyer, D., 2012. Excitatory neuronal connectivity in the barrel cortex. Front. Neuroanat. 6. https://doi.org/10.3389/fnana.2012.00024
Férézou, I., Cauli, B., Hill, E.L., Rossier, J., Hamel, E., Lambolez, B., 2002. 5-HT3 Receptors Mediate Serotonergic Fast Synaptic Excitation of Neocortical Vasoactive Intestinal Peptide/Cholecystokinin Interneurons. J. Neurosci. 22, 7389–7397. https://doi.org/10.1523/JNEUROSCI.22-17-07389.2002
Fino, E., Yuste, R., 2011. Dense Inhibitory Connectivity in Neocortex. Neuron 69, 1188–1203. https://doi.org/10.1016/j.neuron.2011.02.025
Frégnac, Y., Bathellier, B., 2015. Cortical Correlates of Low-Level Perception: From Neural Circuits to Percepts. Neuron 88, 110–126. https://doi.org/10.1016/j.neuron.2015.09.041
Freund, T.F., 2003. Interneuron Diversity series: Rhythm and mood in perisomatic inhibition. Trends Neurosci. 26, 489–495. https://doi.org/10.1016/S0166-2236(03)00227-3
Freund, T.F., Katona, I., 2007. Perisomatic Inhibition. Neuron 56, 33–42. https://doi.org/10.1016/j.neuron.2007.09.012
Fu, Y., Tucciarone, J.M., Espinosa, J.S., Sheng, N., Darcy, D.P., Nicoll, R.A., Huang, Z.J., Stryker, M.P., 2014. A Cortical Circuit for Gain Control by Behavioral State. Cell 156, 1139–1152. https://doi.org/10.1016/j.cell.2014.01.050
Gahete, M.D., Cordoba-Chacón, J., Duran-Prado, M., Malagón, M.M., Martinez-Fuentes, A.J., Gracia-Navarro, F., Luque, R.M., Castaño, J.P., 2010. Somatostatin and its receptors from fish to mammals: Gahete et al. Ann. N. Y. Acad. Sci. 1200, 43–52. https://doi.org/10.1111/j.1749-6632.2010.05511.x
Gähwiler, B.H., Brown, D.A., 1985. GABAB-receptor-activated K+ current in voltage-clamped CA3 pyramidal cells in hippocampal cultures. Proc. Natl. Acad. Sci. 82, 1558–1562. https://doi.org/10.1073/pnas.82.5.1558
Galarreta, M., Erdélyi, F., Szabó, G., Hestrin, S., 2004. Electrical Coupling among Irregular-Spiking GABAergic Interneurons Expressing Cannabinoid Receptors. J. Neurosci. 24, 9770–9778. https://doi.org/10.1523/JNEUROSCI.3027-04.2004
Galarreta, M., Hestrin, S., 1999. A network of fast-spiking cells in the neocortex connected by electrical synapses. Nature 402, 72–75. https://doi.org/10.1038/47029
Garcia-Munoz, M., Arbuthnott, G.W., 2015. Basal ganglia-thalamus and the “crowning enigma.” Front. Neural Circuits 9, 71. https://doi.org/10.3389/fncir.2015.00071
Gentet, L.J., Kremer, Y., Taniguchi, H., Huang, Z.J., Staiger, J.F., Petersen, C.C.H., 2012. Unique functional properties of somatostatin-expressing GABAergic neurons in mouse barrel cortex. Nat. Neurosci. 15, 607–612. https://doi.org/10.1038/nn.3051
Gibson, J.R., Beierlein, M., Connors, B.W., 1999. Two networks of electrically coupled inhibitory neurons in neocortex. Nature 402, 75–79. https://doi.org/10.1038/47035
Gilbert, C.D., Kelly, J.P., 1975. The projections of cells in different layers of the cat’s visual cortex. J. Comp. Neurol. 163, 81–105. https://doi.org/10.1002/cne.901630106
Gilbert, C.D., Sigman, M., 2007. Brain States: Top-Down Influences in Sensory Processing. Neuron 54, 677–696. https://doi.org/10.1016/j.neuron.2007.05.019
Gilbert, C.D., Wiesel, T.N., 1989. Columnar Specificity of Intrinsic Horizontal and Corticocortical Connections in Cat Visual Cortex 11.

Gilbert, C.D., Wiesel, T.N., 1983. Functional Organization of the Visual Cortex, in: Progress in Brain Research. Elsevier, pp. 209–218. https://doi.org/10.1016/S0079-6123(08)60022-9
Gilbert, C.D., Wiesel, T.N., 1979. Morphology and intracortical projections of functionally characterised neurones in the cat visual cortex. Nature 280, 120–125.
Gonchar, Y., Burkhalter, A., 2003. Distinct GABAergic Targets of Feedforward and Feedback Connections Between Lower and Higher Areas of Rat Visual Cortex. J. Neurosci. 23, 10904–10912. https://doi.org/10.1523/JNEUROSCI.23-34-10904.2003
Gonzalez-Burgos, G., 2010. GABA Transporter GAT1: A Crucial Determinant of GABAB Receptor Activation in Cortical Circuits?, in: Blackburn, T.P. (Ed.), Advances in Pharmacology, GABAReceptor Pharmacology. Academic Press, pp. 175–204. https://doi.org/10.1016/S1054-3589(10)58008-6
Gray, E.G., 1959. Electron Microscopy of Synaptic Contacts on Dendrite Spines of the Cerebral Cortex. Nature 183, 1592–1593. https://doi.org/10.1038/1831592a0
Grewe, B.F., Langer, D., Kasper, H., Kampa, B.M., Helmchen, F., 2010. High-speed in vivo calcium imaging reveals neuronal network activity with near-millisecond precision. Nat. Methods 7, 399–405. https://doi.org/10.1038/nmeth.1453
Groh, A., Meyer, H.S., Schmidt, E.F., Heintz, N., Sakmann, B., Krieger, P., 2010. Cell-Type Specific Properties of Pyramidal Neurons in Neocortex Underlying a Layout that Is Modifiable Depending on the Cortical Area. Cereb. Cortex 20, 826–836. https://doi.org/10.1093/cercor/bhp152
Grynkiewicz, G., Poenie, M., TsienB, R.Y., 1985. A New Generation of Ca2+ Indicatorswith Greatly Improved Fluorescence Properties. J. Biol. Chem. 260, 3440,3450.
Guo, J., Anton, E.S., 2014. Decision making during interneuron migration in the developing cerebral cortex. Trends Cell Biol. 24, 342–351. https://doi.org/10.1016/j.tcb.2013.12.001
Gupta, A., 2000. Organizing Principles for a Diversity of GABAergic Interneurons and Synapses in the Neocortex. Science 287, 273–278. https://doi.org/10.1126/science.287.5451.273
Hallman, L.E., Schofield, B.R., Lin, C.S., 1988. Dendritic morphology and axon collaterals of corticotectal, corticopontine, and callosal neurons in layer V of primary visual cortex of the hooded rat. J. Comp. Neurol. 272, 149–160. https://doi.org/10.1002/cne.902720111
Hefti, B.J., Smith, P.H., 2000. Anatomy, Physiology, and Synaptic Responses of Rat Layer V Auditory Cortical Cells and Effects of Intracellular GABA $_A$ Blockade. J. Neurophysiol. 83, 2626–2638. https://doi.org/10.1152/jn.2000.83.5.2626
Helmchen, F., Denk, W., 2005. Deep tissue two-photon microscopy. Nat. Methods 2, 932–940. https://doi.org/10.1038/nmeth818
Helmstaedter, M., Staiger, J.F., Sakmann, B., Feldmeyer, D., 2008. Efficient Recruitment of Layer 2/3 Interneurons by Layer 4 Input in Single Columns of Rat Somatosensory Cortex. J. Neurosci. 28, 8273–8284. https://doi.org/10.1523/JNEUROSCI.5701-07.2008
Hestrin, S., Armstrong, W.E., 1996. Morphology and Physiology of Cortical Neurons in Layer I. J. Neurosci. 16, 5290–5300. https://doi.org/10.1523/JNEUROSCI.16-17-05290.1996
Holtmaat, A., Bonhoeffer, T., Chow, D.K., Chuckowree, J., De Paola, V., Hofer, S.B., Hübener, M., Keck, T., Knott, G., Lee, W.-C.A., Mostany, R., Mrsic-Flogel, T.D., Nedivi, E., Portera-Cailliau, C., Svoboda, K., Trachtenberg, J.T., Wilbrecht, L., 2009. Long-term, high-resolution imaging in the mouse neocortex through a chronic cranial window. Nat. Protoc. 4, 1128–1144. https://doi.org/10.1038/nprot.2009.89
Hopfield, J.J., 1982. Neural networks and physical systems with emergent collective computational abilities. Proc. Natl. Acad. Sci. U. S. A. 79, 2554–2558.
Horton, J.C., Adams, D.L., 2005. The cortical column: a structure without a function. Philos. Trans. R. Soc. Lond. B Biol. Sci. 360, 837–862. https://doi.org/10.1098/rstb.2005.1623
Howard, A., Tamas, G., Soltesz, I., 2005. Lighting the chandelier: new vistas for axo-axonic cells. Trends Neurosci. 28, 310–316. https://doi.org/10.1016/j.tins.2005.04.004
Hromádka, T., DeWeese, M.R., Zador, A.M., 2008. Sparse Representation of Sounds in the Unanesthetized Auditory Cortex. PLoS Biol. 6. https://doi.org/10.1371/journal.pbio.0060016
Hu, H., Jonas, P., 2014. A supercritical density of Na^+ channels ensures fast signaling in GABAergic interneuron axons. Nat. Neurosci. 17, 686–693. https://doi.org/10.1038/nn.3678
Hubel, D.H., Wiesel, T.N., 1974. Uniformity of monkey striate cortex: A parallel relationship between field size, scatter, and magnification factor. J. Comp. Neurol. 158, 295–305. https://doi.org/10.1002/cne.901580305

Hubel, D.H., Wiesel, T.N., 1962. Receptive fields, binocular interaction and functional architecture in the cat's visual cortex. J. Physiol. 160, 106–154. https://doi.org/10.1113/jphysiol.1962.sp006837
Hull, C., Isaacson, J.S., Scanziani, M., 2009. Postsynaptic Mechanisms Govern the Differential Excitation of Cortical Neurons by Thalamic Inputs. J. Neurosci. 29, 9127–9136. https://doi.org/10.1523/JNEUROSCI.5971-08.2009
Isaacson, J.S., Scanziani, M., 2011. How Inhibition Shapes Cortical Activity. Neuron 72, 231–243. https://doi.org/10.1016/j.neuron.2011.09.027
Issa, J.B., Haeffele, B.D., Agarwal, A., Bergles, D.E., Young, E.D., Yue, D.T., 2014. Multiscale Optical Ca2+ Imaging of Tonal Organization in Mouse Auditory Cortex. Neuron 83, 944–959. https://doi.org/10.1016/j.neuron.2014.07.009
Ji, X., Zingg, B., Mesik, L., Xiao, Z., Zhang, L.I., Tao, H.W., 2016. Thalamocortical Innervation Pattern in Mouse Auditory and Visual Cortex: Laminar and Cell-Type Specificity. Cereb. Cortex N. Y. NY 26, 2612–2625. https://doi.org/10.1093/cercor/bhv099
Jiang, X., Shen, S., Cadwell, C.R., Berens, P., Sinz, F., Ecker, A.S., Patel, S., Tolias, A.S., 2015. Principles of connectivity among morphologically defined cell types in adult neocortex. Science 350, aac9462. https://doi.org/10.1126/science.aac9462
Jiang, X., Wang, G., Lee, A.J., Stornetta, R.L., Zhu, J.J., 2013. The organization of two new cortical interneuronal circuits. Nat. Neurosci. 16, 210–218. https://doi.org/10.1038/nn.3305
Jones, E.G., Wise, S.P., 1977. Size, laminar and columnar distribution of efferent cells in the sensory-motor cortex of monkeys. J. Comp. Neurol. 175, 391–437. https://doi.org/10.1002/cne.901750403
Kapfer, C., Glickfeld, L.L., Atallah, B.V., Scanziani, M., 2007. Supralinear increase of recurrent inhibition during sparse activity in the somatosensory cortex. Nat. Neurosci. 10, 743–753. https://doi.org/10.1038/nn1909
Karnani, M. M., Jackson, J., Ayzenshtat, I., Hamzehei Sichani, A., Manoocheri, K., Kim, S., Yuste, R., 2016. Opening Holes in the Blanket of Inhibition: Localized Lateral Disinhibition by VIP Interneurons. J. Neurosci. 36, 3471–3480. https://doi.org/10.1523/JNEUROSCI.3646-15.2016
Karnani, Mahesh M., Jackson, J., Ayzenshtat, I., Tucciarone, J., Manoocheri, K., Snider, W.G., Yuste, R., 2016. Cooperative Subnetworks of Molecularly Similar Interneurons in Mouse Neocortex. Neuron 90, 86–100. https://doi.org/10.1016/j.neuron.2016.02.037
Karra, D., Dahm, R., 2010. Transfection Techniques for Neuronal Cells. J. Neurosci. 30, 6171–6177. https://doi.org/10.1523/JNEUROSCI.0183-10.2010
Karube, F., Kubota, Y., Kawaguchi, Y., 2004. Axon Branching and Synaptic Bouton Phenotypes in GABAergic Nonpyramidal Cell Subtypes. J. Neurosci. 24, 2853–2865. https://doi.org/10.1523/JNEUROSCI.4814-03.2004
Kasper, E.M., Larkman, A.U., Lübke, J., Blakemore, C., 1994. Pyramidal neurons in layer 5 of the rat visual cortex. I. Correlation among cell morphology, intrinsic electrophysiological properties, and axon targets. J. Comp. Neurol. 339, 459–474. https://doi.org/10.1002/cne.903390402
Kato, H.K., Gillet, S.N., Isaacson, J.S., 2015. Flexible Sensory Representations in Auditory Cortex Driven by Behavioral Relevance. Neuron 88, 1027–1039. https://doi.org/10.1016/j.neuron.2015.10.024
Katz, L.C., 1987. Local circuitry of identified projection neurons in cat visual cortex brain slices. J. Neurosci. 7, 1223–1249. https://doi.org/10.1523/JNEUROSCI.07-04-01223.1987
Kätzel, D., Zemelman, B.V., Buetfering, C., Wölfel, M., Miesenböck, G., 2011. The columnar and laminar organization of inhibitory connections to neocortical excitatory cells. Nat. Neurosci. 14, 100–107. https://doi.org/10.1038/nn.2687
Kawaguchi, Y., 1997. Selective Cholinergic Modulation of Cortical GABAergic Cell Subtypes. J. Neurophysiol. 78, 1743–1747. https://doi.org/10.1152/jn.1997.78.3.1743
Kawaguchi, Y., 1995. Physiological subgroups of nonpyramidal cells with specific morphological characteristics in layer II/III of rat frontal cortex. J. Neurosci. 15, 2638–2655. https://doi.org/10.1523/JNEUROSCI.15-04-02638.1995
Kawaguchi, Y., Karube, F., Kubota, Y., 2006. Dendritic Branch Typing and Spine Expression Patterns in Cortical Nonpyramidal Cells. Cereb. Cortex 16, 696–711. https://doi.org/10.1093/cercor/bhj015
Kawaguchi, Y., Kubota, Y., 1997. GABAergic cell subtypes and their synaptic connections in rat frontal cortex. Cereb. Cortex N. Y. N 1991 7, 476–486.
Kawaguchi, Y., Shindou, T., 1998. Noradrenergic excitation and inhibition of GABAergic cell types in rat frontal cortex. J. Neurosci. 18, 6963–6976.

Keimpema, E., Straiker, A., Mackie, K., Harkany, T., Hjerling-Leffler, J., 2012. Sticking out of the crowd: the molecular identity and development of cholecystokinin-containing basket cells. J. Physiol. 590, 703–714. https://doi.org/10.1113/jphysiol.2011.224386

Kerr, J.N.D., Greenberg, D., Helmchen, F., 2005. Imaging input and output of neocortical networks in vivo. Proc. Natl. Acad. Sci. 102, 14063–14068. https://doi.org/10.1073/pnas.0506029102

Kim, E.J., Juavinett, A.L., Kyubwa, E.M., Jacobs, M.W., Callaway, E.M., 2015. Three Types of Cortical Layer 5 Neurons That Differ in Brain-wide Connectivity and Function. Neuron 88, 1253–1267. https://doi.org/10.1016/j.neuron.2015.11.002

Kim, J., Matney, C.J., Blankenship, A., Hestrin, S., Brown, S.P., 2014. Layer 6 Corticothalamic Neurons Activate a Cortical Output Layer, Layer 5a. J. Neurosci. 34, 9656–9664. https://doi.org/10.1523/JNEUROSCI.1325-14.2014

Kirkcaldie, M.T.K., 2012. Chapter 4 - Neocortex, in: Watson, C., Paxinos, G., Puelles, L. (Eds.), The Mouse Nervous System. Academic Press, San Diego, pp. 52–111. https://doi.org/10.1016/B978-0-12-369497-3.10004-4

Knöpfel, T., Díez-García, J., Akemann, W., 2006. Optical probing of neuronal circuit dynamics: genetically encoded versus classical fluorescent sensors. Trends Neurosci. 29, 160–166. https://doi.org/10.1016/j.tins.2006.01.004

Kubota, Y., 2014. Untangling GABAergic wiring in the cortical microcircuit. Curr. Opin. Neurobiol. 26, 7–14. https://doi.org/10.1016/j.conb.2013.10.003

Kubota, Y., Hattori, R., Yui, Y., 1994. Three distinct subpopulations of GABAergic neurons in rat frontal agranular cortex. Brain Res. 649, 159–173. https://doi.org/10.1016/0006-8993(94)91060-X

Kuhlman, S.J., Huang, Z.J., 2008. High-Resolution Labeling and Functional Manipulation of Specific Neuron Types in Mouse Brain by Cre-Activated Viral Gene Expression. PLoS ONE 3. https://doi.org/10.1371/journal.pone.0002005

Kwan, A.C., Dan, Y., 2012. Dissection of Cortical Microcircuits by Single-Neuron Stimulation In Vivo. Curr. Biol. 22, 1459–1467. https://doi.org/10.1016/j.cub.2012.06.007

Kwon, H.J., Ma, S., Huang, Z., 2011. Radial glia regulate Cajal–Retzius cell positioning in the early embryonic cerebral cortex. Dev. Biol. 351, 25–34. https://doi.org/10.1016/j.ydbio.2010.12.026

Larkum, M., 2013. A cellular mechanism for cortical associations: an organizing principle for the cerebral cortex. Trends Neurosci. 36, 141–151. https://doi.org/10.1016/j.tins.2012.11.006

Larkum, M.E., Waters, J., Sakmann, B., Helmchen, F., 2007. Dendritic Spikes in Apical Dendrites of Neocortical Layer 2/3 Pyramidal Neurons. J. Neurosci. 27, 8999–9008. https://doi.org/10.1523/JNEUROSCI.1717-07.2007

Lee, A.J., Wang, G., Jiang, X., Johnson, S.M., Hoang, E.T., Lanté, F., Stornetta, R.L., Beenhakker, M.P., Shen, Y., Julius Zhu, J., 2015. Canonical Organization of Layer 1 Neuron-Led Cortical Inhibitory and Disinhibitory Interneuronal Circuits. Cereb. Cortex N. Y. NY 25, 2114–2126. https://doi.org/10.1093/cercor/bhu020

Lee, S., Hjerling-Leffler, J., Zagha, E., Fishell, G., Rudy, B., 2010. The Largest Group of Superficial Neocortical GABAergic Interneurons Expresses Ionotropic Serotonin Receptors. J. Neurosci. 30, 16796–16808. https://doi.org/10.1523/JNEUROSCI.1869-10.2010

Lee, S., Kruglikov, I., Huang, Z.J., Fishell, G., Rudy, B., 2013. A disinhibitory circuit mediates motor integration in the somatosensory cortex. Nat. Neurosci. 16, 1662–1670. https://doi.org/10.1038/nn.3544

Liguz-Lecznar, M., Urban-Ciecko, J., Kossut, M., 2016. Somatostatin and Somatostatin-Containing Neurons in Shaping Neuronal Activity and Plasticity. Front. Neural Circuits 10. https://doi.org/10.3389/fncir.2016.00048

Lima, A.D.D., Morrison, J.H., 1989. Ultrastructural analysis of somatostatin-immunoreactive neurons and synapses in the temporal and occipital cortex of the macaque monkey. J. Comp. Neurol. 283, 212–227. https://doi.org/10.1002/cne.902830205

Lin, M.Z., Schnitzer, M.J., 2016. Genetically encoded indicators of neuronal activity. Nat. Neurosci. 19, 1142–1153. https://doi.org/10.1038/nn.4359

Loebel, A., Nelken, I., Tsodyks, M., 2007. Processing of Sounds by Population Spikes in a Model of Primary Auditory Cortex. Front. Neurosci. 1, 197–209. https://doi.org/10.3389/neuro.01.1.1.015.2007

Lund, J.S., Hawken, M.J., Parker, A.J., 1988. Local circuit neurons of macaque monkey striate cortex: II. Neurons of laminae 5B and 6. J. Comp. Neurol. 276, 1–29. https://doi.org/10.1002/cne.902760102

Lund, J.S., Yoshioka, T., 1991. Local circuit neurons of macaque monkey striate cortex: III. Neurons of laminae 4B, 4A, and 3B. J. Comp. Neurol. 311, 234–258. https://doi.org/10.1002/cne.903110206
Lüscher, C., Jan, L.Y., Stoffel, M., Malenka, R.C., Nicoll, R.A., 1997. G Protein-Coupled Inwardly Rectifying K+ Channels (GIRKs) Mediate Postsynaptic but Not Presynaptic Transmitter Actions in Hippocampal Neurons. Neuron 19, 687–695. https://doi.org/10.1016/S0896-6273(00)80381-5
Lütcke, H., Helmchen, F., 2011. Two-photon imaging and analysis of neural network dynamics. Rep. Prog. Phys. 74, 086602. https://doi.org/10.1088/0034-4885/74/8/086602
Ma, J., Yao, X.-H., Fu, Y., Yu, Y.-C., 2014. Development of Layer 1 Neurons in the Mouse Neocortex. Cereb. Cortex 24, 2604–2618. https://doi.org/10.1093/cercor/bht114
Ma, Y., Hu, H., Berrebi, A.S., Mathers, P.H., Agmon, A., 2006. Distinct Subtypes of Somatostatin-Containing Neocortical Interneurons Revealed in Transgenic Mice. J. Neurosci. 26, 5069–5082. https://doi.org/10.1523/JNEUROSCI.0661-06.2006
Maass, W., Joshi, P., Sontag, E.D., 2007. Computational aspects of feedback in neural circuits. PLoS Comput. Biol. 3, e165. https://doi.org/10.1371/journal.pcbi.0020165
Machens, C.K., Wehr, M.S., Zador, A.M., 2004. Linearity of cortical receptive fields measured with natural sounds. J. Neurosci. Off. J. Soc. Neurosci. 24, 1089–1100. https://doi.org/10.1523/JNEUROSCI.4445-03.2004
Mank, M., Griesbeck, O., 2008. Genetically Encoded Calcium Indicators. Chem. Rev. 108, 1550–1564. https://doi.org/10.1021/cr078213v
Margolis, D.J., Lütcke, H., Schulz, K., Haiss, F., Weber, B., Kügler, S., Hasan, M.T., Helmchen, F., 2012. Reorganization of cortical population activity imaged throughout long-term sensory deprivation. Nat. Neurosci. 15, 1539–1546. https://doi.org/10.1038/nn.3240
Marín-Padilla, M., 1998. Cajal–Retzius cells and the development of the neocortex. Trends Neurosci. 21, 64–71. https://doi.org/10.1016/S0166-2236(97)01164-8
Markram, H., Lübke, J., Frotscher, M., Roth, A., Sakmann, B., 1997. Physiology and anatomy of synaptic connections between thick tufted pyramidal neurones in the developing rat neocortex. J. Physiol. 500, 409–440.
Markram, H., Toledo-Rodriguez, M., Wang, Y., Gupta, A., Silberberg, G., Wu, C., 2004. Interneurons of the neocortical inhibitory system. Nat. Rev. Neurosci. 5, 793–807. https://doi.org/10.1038/nrn1519
Meng, X., Winkowski, D.E., Kao, J.P.Y., Kanold, P.O., 2017. Sublaminar Subdivision of Mouse Auditory Cortex Layer 2/3 Based on Functional Translaminar Connections. J. Neurosci. Off. J. Soc. Neurosci. 37, 10200–10214. https://doi.org/10.1523/JNEUROSCI.1361-17.2017
Meyer, H.S., Schwarz, D., Wimmer, V.C., Schmitt, A.C., Kerr, J.N.D., Sakmann, B., Helmstaedter, M., 2011. Inhibitory interneurons in a cortical column form hot zones of inhibition in layers 2 and 5A. Proc. Natl. Acad. Sci. 108, 16807–16812. https://doi.org/10.1073/pnas.1113648108
Miles, R., Tóth, K., Gulyás, A.I., Hájos, N., Freund, T.F., 1996. Differences between Somatic and Dendritic Inhibition in the Hippocampus. Neuron 16, 815–823. https://doi.org/10.1016/S0896-6273(00)80101-4
Miller, E.K., Nieder, A., Freedman, D.J., Wallis, J.D., 2003. Neural correlates of categories and concepts. Curr. Opin. Neurobiol. 13, 198–203.
Mitchison, G., 1991. Neuronal branching patterns and the economy of cortical wiring. Proc R Soc Lond B 245, 151–158. https://doi.org/10.1098/rspb.1991.0102
Mountcastle, V.B., 1997. The columnar organization of the neocortex. Brain J. Neurol. 120 (Pt 4), 701–722.
Mountcastle, V.B., 1957. Modality and topographic properties of single neurons of cat's somatic sensory cortex. J. Neurophysiol. 20, 408–434. https://doi.org/10.1152/jn.1957.20.4.408
Muñoz, W., Rudy, B., 2014. Spatiotemporal specificity in cholinergic control of neocortical function. Curr. Opin. Neurobiol. 26, 149–160. https://doi.org/10.1016/j.conb.2014.02.015
Muralidhar, S., Wang, Y., Markram, H., 2014. Synaptic and cellular organization of layer 1 of the developing rat somatosensory cortex. Front. Neuroanat. 7. https://doi.org/10.3389/fnana.2013.00052
Murphy, E.H., Berman, N., 2004. The rabbit and the cat: A comparison of some features of response properties of single cells in the primary visual cortex. J. Comp. Neurol. 188, 401–427. https://doi.org/10.1002/cne.901880305
Nakai, J., Ohkura, M., Imoto, K., 2001. A high signal-to-noise Ca(2+) probe composed of a single green fluorescent protein. Nat. Biotechnol. 19, 137–141. https://doi.org/10.1038/84397
Nelken, I., 2004. Processing of complex stimuli and natural scenes in the auditory cortex. Curr. Opin. Neurobiol. 14, 474–480. https://doi.org/10.1016/j.conb.2004.06.005

Nelken, I., Fishbach, A., Las, L., Ulanovsky, N., Farkas, D., 2003. Primary auditory cortex of cats: feature detection or something else? Biol. Cybern. 89, 397–406. https://doi.org/10.1007/s00422-003-0445-3

Niessing, J., Friedrich, R.W., 2010. Olfactory pattern classification by discrete neuronal network states. Nature 465, 47–52. https://doi.org/10.1038/nature08961

Novák, O., Zelenka, O., Hromádka, T., Syka, J., 2016. Immediate manifestation of acoustic trauma in the auditory cortex is layer specific and cell type dependent. J. Neurophysiol. 115, 1860–1874. https://doi.org/10.1152/jn.00810.2015

Oberlaender, M., de Kock, C.P.J., Bruno, R.M., Ramirez, A., Meyer, H.S., Dercksen, V.J., Helmstaedter, M., Sakmann, B., 2012. Cell Type–Specific Three-Dimensional Structure of Thalamocortical Circuits in a Column of Rat Vibrissal Cortex. Cereb. Cortex N. Y. NY 22, 2375–2391. https://doi.org/10.1093/cercor/bhr317

O'Connor, D.H., Peron, S.P., Huber, D., Svoboda, K., 2010. Neural Activity in Barrel Cortex Underlying Vibrissa-Based Object Localization in Mice. Neuron 67, 1048–1061. https://doi.org/10.1016/j.neuron.2010.08.026

Ogawa, M., Miyata, T., Nakajima, K., Yagyu, K., Seike, M., Ikenaka, K., Yamamoto, H., Mikoshiba, K., 1995. The reeler gene-associated antigen on Cajal-Retzius neurons is a crucial molecule for laminar organization of cortical neurons. Neuron 14, 899–912.

Oláh, S., Füle, M., Komlósi, G., Varga, C., Báldi, R., Barzó, P., Tamás, G., 2009. Regulation of cortical microcircuits by unitary GABA-mediated volume transmission. Nature 461, 1278–1281. https://doi.org/10.1038/nature08503

Oláh, S., Komlósi, G., Szabadics, J., Varga, C., Tóth, É., Barzó, P., Tamás, G., 2007. Output of neurogliaform cells to various neuron types in the human and rat cerebral cortex. Front. Neural Circuits 1. https://doi.org/10.3389/neuro.04.004.2007

Packer, A.M., Yuste, R., 2011. Dense, unspecific connectivity of neocortical parvalbumin-positive interneurons: a canonical microcircuit for inhibition? J. Neurosci. Off. J. Soc. Neurosci. 31, 13260–13271. https://doi.org/10.1523/JNEUROSCI.3131-11.2011

Papp, E., Leinekugel, X., Henze, D.A., Lee, J., Buzsáki, G., 2001. The apical shaft of CA1 pyramidal cells is under GABAergic interneuronal control. Neuroscience 102, 715–721.

Paredes, R.M., Etzler, J.C., Watts, L.T., Lechleiter, J.D., 2008. Chemical Calcium Indicators. Methods San Diego Calif 46, 143–151. https://doi.org/10.1016/j.ymeth.2008.09.025

Peron, S.P., Freeman, J., Iyer, V., Guo, C., Svoboda, K., 2015. A Cellular Resolution Map of Barrel Cortex Activity during Tactile Behavior. Neuron 86, 783–799. https://doi.org/10.1016/j.neuron.2015.03.027

Peters, A.J., Chen, S.X., Komiyama, T., 2014. Emergence of reproducible spatiotemporal activity during motor learning. Nature 510, 263–267. https://doi.org/10.1038/nature13235

Petersen, C.C.H., Crochet, S., 2013. Synaptic Computation and Sensory Processing in Neocortical Layer 2/3. Neuron 78, 28–48. https://doi.org/10.1016/j.neuron.2013.03.020

Pfeffer, C.K., Xue, M., He, M., Huang, Z.J., Scanziani, M., 2013. Inhibition of inhibition in visual cortex: the logic of connections between molecularly distinct interneurons. Nat. Neurosci. 16, 1068–1076. https://doi.org/10.1038/nn.3446

Phillips, E.A.K., Schreiner, C.E., Hasenstaub, A.R., 2017. Cortical Interneurons Differentially Regulate the Effects of Acoustic Context. Cell Rep. 20, 771–778. https://doi.org/10.1016/j.celrep.2017.07.001

Pi, H.-J., Hangya, B., Kvitsiani, D., Sanders, J.I., Huang, Z.J., Kepecs, A., 2013. Cortical interneurons that specialize in disinhibitory control. Nature 503, 521–524. https://doi.org/10.1038/nature12676

Pinto, D.J., Brumberg, J.C., Simons, D.J., 2000. Circuit Dynamics and Coding Strategies in Rodent Somatosensory Cortex. J. Neurophysiol. 83, 1158–1166. https://doi.org/10.1152/jn.2000.83.3.1158

Pinto, D.J., Hartings, J.A., Brumberg, J.C., Simons, D.J., 2003. Cortical Damping: Analysis of Thalamocortical Response Transformations in Rodent Barrel Cortex. Cereb. Cortex 13, 33–44. https://doi.org/10.1093/cercor/13.1.33

Pologruto, T.A., Yasuda, R., Svoboda, K., 2004. Monitoring Neural Activity and [Ca2+] with Genetically Encoded Ca2+ Indicators. J. Neurosci. 24, 9572–9579. https://doi.org/10.1523/JNEUROSCI.2854-04.2004

Pouille, F., 2001. Enforcement of Temporal Fidelity in Pyramidal Cells by Somatic Feed-Forward Inhibition. Science 293, 1159–1163. https://doi.org/10.1126/science.1060342

Pouille, F., Scanziani, M., 2004. Routing of spike series by dynamic circuits in the hippocampus. Nature 429, 717–723. https://doi.org/10.1038/nature02615

Priebe, N.J., Ferster, D., 2012. Mechanisms of Neuronal Computation in Mammalian Visual Cortex. Neuron 75, 194–208. https://doi.org/10.1016/j.neuron.2012.06.011
Prönneke, A., Scheuer, B., Wagener, R.J., Möck, M., Witte, M., Staiger, J.F., 2015. Characterizing VIP Neurons in the Barrel Cortex of VIPcre/tdTomato Mice Reveals Layer-Specific Differences. Cereb. Cortex N. Y. NY 25, 4854–4868. https://doi.org/10.1093/cercor/bhv202
Rakic, P., 1972. Mode of cell migration to the superficial layers of fetal monkey neocortex. J. Comp. Neurol. 145, 61–83. https://doi.org/10.1002/cne.901450105
Ramos, R.L., Tam, D.M., Brumberg, J.C., 2008. Physiology and morphology of callosal projection neurons in mouse. Neuroscience 153, 654–663. https://doi.org/10.1016/j.neuroscience.2008.02.069
Redish, A.D., 1999. Beyond the cognitive map: from place cells to episodic memory. MIT Press, Cambridge, Mass.
Reyes, A., Lujan, R., Rozov, A., Burnashev, N., Somogyi, P., Sakmann, B., 1998. Target-cell-specific facilitation and depression in neocortical circuits. Nat. Neurosci. 1, 279–285. https://doi.org/10.1038/1092
Richardson, R.J., Blundon, J.A., Bayazitov, I.T., Zakharenko, S.S., 2009. Connectivity patterns revealed by mapping of active inputs on dendrites of thalamorecipient neurons in the auditory cortex. J. Neurosci. Off. J. Soc. Neurosci. 29, 6406–6417. https://doi.org/10.1523/JNEUROSCI.0258-09.2009
Robles, L., Ruggero, M.A., 2001. Mechanics of the Mammalian Cochlea. Physiol. Rev. 81, 1305–1352.
Rothschild, G., Nelken, I., Mizrahi, A., 2010. Functional organization and population dynamics in the mouse primary auditory cortex. Nat. Neurosci. 13, 353–360. https://doi.org/10.1038/nn.2484
Roux, L., Buzsáki, G., 2015. Tasks for inhibitory interneurons in intact brain circuits. Neuropharmacology 88, 10–23. https://doi.org/10.1016/j.neuropharm.2014.09.011
Royer, S., Zemelman, B.V., Losonczy, A., Kim, J., Chance, F., Magee, J.C., Buzsáki, G., 2012. Control of timing, rate and bursts of hippocampal place cells by dendritic and somatic inhibition. Nat. Neurosci. 15, 769–775. https://doi.org/10.1038/nn.3077
Rubio-Garrido, P., Pérez-de-Manzo, F., Porrero, C., Galazo, M.J., Clascá, F., 2009. Thalamic Input to Distal Apical Dendrites in Neocortical Layer 1 Is Massive and Highly Convergent. Cereb. Cortex 19, 2380–2395. https://doi.org/10.1093/cercor/bhn259
Rudy, B., Fishell, G., Lee, S., Hjerling-Leffler, J., 2011. Three Groups of Interneurons Account for Nearly 100% of Neocortical GABAergic Neurons. Dev. Neurobiol. 71, 45–61. https://doi.org/10.1002/dneu.20853
Russ, B.E., Lee, Y.-S., Cohen, Y.E., 2007. Neural and behavioral correlates of auditory categorization. Hear. Res. 229, 204–212. https://doi.org/10.1016/j.heares.2006.10.010
Rust, N.C., Schwartz, O., Movshon, J.A., Simoncelli, E.P., 2005. Spatiotemporal Elements of Macaque V1 Receptive Fields. Neuron 46, 945–956. https://doi.org/10.1016/j.neuron.2005.05.021
Sakata, S., Harris, K.D., 2009. Laminar Structure of Spontaneous and Sensory-Evoked Population Activity in Auditory Cortex. Neuron 64, 404–418. https://doi.org/10.1016/j.neuron.2009.09.020
Sawatari, H., Tanaka, Y., Takemoto, M., Nishimura, M., Hasegawa, K., Saitoh, K., Song, W.-J., 2011. Identification and characterization of an insular auditory field in mice: Insular auditory field in mice. Eur. J. Neurosci. 34, 1944–1952. https://doi.org/10.1111/j.1460-9568.2011.07926.x
Scanziani, M., 2000. GABA Spillover Activates Postsynaptic GABAB Receptors to Control Rhythmic Hippocampal Activity. Neuron 25, 673–681. https://doi.org/10.1016/S0896-6273(00)81069-7
Schiller, J., Schiller, Y., Stuart, G., Sakmann, B., 1997. Calcium action potentials restricted to distal apical dendrites of rat neocortical pyramidal neurons. J. Physiol. 505, 605–616.
Schinkel-Bielefeld, N., David, S.V., Shamma, S.A., Butts, D.A., 2012. Inferring the role of inhibition in auditory processing of complex natural stimuli. J. Neurophysiol. 107, 3296–3307. https://doi.org/10.1152/jn.01173.2011
Seger, C.A., Miller, E.K., 2010. Category Learning in the Brain. Annu. Rev. Neurosci. 33, 203–219. https://doi.org/10.1146/annurev.neuro.051508.135546
Seitelberger, F., 1997. Theodor Meynert (1833-1892), pioneer and visionary of brain research. J. Hist. Neurosci. 6, 264–274. https://doi.org/10.1080/09647049709525713
Shipp, S., 2007. Structure and function of the cerebral cortex. Curr. Biol. 17, R443–R449. https://doi.org/10.1016/j.cub.2007.03.044
Silberberg, G., 2008. Polysynaptic subcircuits in the neocortex: spatial and temporal diversity. Curr. Opin. Neurobiol. 18, 332–337. https://doi.org/10.1016/j.conb.2008.08.009

Silberberg, G., Markram, H., 2007. Disynaptic inhibition between neocortical pyramidal cells mediated by Martinotti cells. Neuron 53, 735–746. https://doi.org/10.1016/j.neuron.2007.02.012
Simon, A., Oláh, S., Molnár, G., Szabadics, J., Tamás, G., 2005. Gap-Junctional Coupling between Neurogliaform Cells and Various Interneuron Types in the Neocortex. J. Neurosci. 25, 6278–6285. https://doi.org/10.1523/JNEUROSCI.1431-05.2005
Sjöström, P.J., Turrigiano, G.G., Nelson, S.B., 2001. Rate, Timing, and Cooperativity Jointly Determine Cortical Synaptic Plasticity. Neuron 32, 1149–1164. https://doi.org/10.1016/S0896-6273(01)00542-6
Skoglund, T., 1997. The existence of a layer IV in the rat motor cortex. Cereb. Cortex 7, 178–180. https://doi.org/10.1093/cercor/7.2.178
Smith, P.H., Populin, L.C., 2001. Fundamental differences between the thalamocortical recipient layers of the cat auditory and visual cortices. J. Comp. Neurol. 436, 508–519.
Snow, L.A., McConnico, R.S., Morgan, T.W., Hartmann, E., Davidson, J.R., Hosgood, G., 2014. Carprofen-induced oxidative stress in mitochondria of the colonic mucosa of the dog. Can. J. Vet. Res. 78, 183–192.
Somogyi, P., 1977. A specific 'axo-axonal' interneuron in the visual cortex of the rat. Brain Res. 136, 345–350. https://doi.org/10.1016/0006-8993(77)90808-3
Somogyi, P., Freund, T.F., Cowey, A., 1982. The axo-axonic interneuron in the cerebral cortex of the rat, cat and monkey. Neuroscience 7, 2577–2607. https://doi.org/10.1016/0306-4522(82)90086-0
Song, S., Sjöström, P.J., Reigl, M., Nelson, S., Chklovskii, D.B., 2005. Highly Nonrandom Features of Synaptic Connectivity in Local Cortical Circuits. PLoS Biol. 3. https://doi.org/10.1371/journal.pbio.0030068
Staiger, J.F., Flagmeyer, I., Schubert, D., Zilles, K., Kötter, R., Luhmann, H.J., 2004. Functional diversity of layer IV spiny neurons in rat somatosensory cortex: quantitative morphology of electrophysiologically characterized and biocytin labeled cells. Cereb. Cortex N. Y. N 1991 14, 690–701. https://doi.org/10.1093/cercor/bhh029
Stiebler, I., Neulist, R., Fichtel, I., Ehret, G., 1997. The auditory cortex of the house mouse: left-right differences, tonotopic organization and quantitative analysis of frequency representation. J. Comp. Physiol. A 181, 559–571. https://doi.org/10.1007/s003590050140
Stosiek, C., Garaschuk, O., Holthoff, K., Konnerth, A., 2003. In vivo two-photon calcium imaging of neuronal networks. Proc. Natl. Acad. Sci. 100, 7319–7324. https://doi.org/10.1073/pnas.1232232100
Szabadics, J., 2006. Excitatory Effect of GABAergic Axo-Axonic Cells in Cortical Microcircuits. Science 311, 233–235. https://doi.org/10.1126/science.1121325
Szabadics, J., Tamás, G., Soltesz, I., 2007. Different transmitter transients underlie presynaptic cell type specificity of GABAA,slow and GABAA,fast. Proc. Natl. Acad. Sci. 104, 14831–14836. https://doi.org/10.1073/pnas.0707204104
Szentágothai, J., Arbib, M.A., 1974. Conceptual models of neural organization. Neurosci. Res. Program Bull. 12, 305–510.
Tai, Y., Janas, J.A., Wang, C.-L., Van Aelst, L., 2014. Regulation of Chandelier Cell Cartridge and Bouton Development via DOCK7-Mediated ErbB4 Activation. Cell Rep. 6, 254–263. https://doi.org/10.1016/j.celrep.2013.12.034
Tamamaki, N., Nakamura, K., Okamoto, K., Kaneko, T., 2001. Radial glia is a progenitor of neocortical neurons in the developing cerebral cortex. Neurosci. Res. 41, 51–60.
Tamamaki, N., Yanagawa, Y., Tomioka, R., Miyazaki, J.-I., Obata, K., Kaneko, T., 2003. Green fluorescent protein expression and colocalization with calretinin, parvalbumin, and somatostatin in the GAD67-GFP knock-in mouse. J. Comp. Neurol. 467, 60–79. https://doi.org/10.1002/cne.10905
Tamás, G., Andrea Lőrincz, Anna Simon, János Szabadics, 2003. Identified Sources and Targets of Slow Inhibition in the Neocortex. Sci. New Ser. 299, 1902–1905.
Taniguchi, H., He, M., Wu, P., Kim, S., Paik, R., Sugino, K., Kvitsani, D., Fu, Y., Lu, J., Lin, Y., Miyoshi, G., Shima, Y., Fishell, G., Nelson, S.B., Huang, Z.J., 2011. A Resource of Cre Driver Lines for Genetic Targeting of GABAergic Neurons in Cerebral Cortex. Neuron 71, 995–1013. https://doi.org/10.1016/j.neuron.2011.07.026
Taniguchi, H., Lu, J., Huang, Z.J., 2013. The Spatial and Temporal Origin of Chandelier Cells in Mouse Neocortex. Science 339, 70–74. https://doi.org/10.1126/science.1227622
Tasic, B., Menon, V., Nguyen, T.N., Kim, T.K., Jarsky, T., Yao, Z., Levi, B., Gray, L.T., Sorensen, S.A., Dolbeare, T., Bertagnolli, D., Goldy, J., Shapovalova, N., Parry, S., Lee, C., Smith, K., Bernard, A., Madisen, L., Sunkin, S.M., Hawrylycz, M., Koch, C., Zeng, H., 2016. Adult mouse cortical cell

taxonomy revealed by single cell transcriptomics. Nat. Neurosci. 19, 335–346. https://doi.org/10.1038/nn.4216
The Petilla Interneuron Nomenclature Group (PING), 2008. Petilla terminology: nomenclature of features of GABAergic interneurons of the cerebral cortex. Nat. Rev. Neurosci. 9, 557–568. https://doi.org/10.1038/nrn2402
Theunissen, F.E., Elie, J.E., 2014. Neural processing of natural sounds 15, 355–366. https://doi.org/10.1038/nrn3731
Theunissen, F.E., Sen, K., Doupe, A.J., 2000. Spectral-Temporal Receptive Fields of Nonlinear Auditory Neurons Obtained Using Natural Sounds. J. Neurosci. 20, 2315–2331. https://doi.org/10.1523/JNEUROSCI.20-06-02315.2000
Thomson, A.M., 2010. Neocortical Layer 6, A Review. Front. Neuroanat. 4. https://doi.org/10.3389/fnana.2010.00013
Thomson, A.M., 2003. Presynaptic Frequency- and Pattern-Dependent Filtering. J. Comput. Neurosci. 15, 159–202. https://doi.org/10.1023/A:1025812808362
Thomson, A.M., Lamy, C., 2007. Functional maps of neocortical local circuitry. Front. Neurosci. 1. https://doi.org/10.3389/neuro.01.1.1.002.2007
Tomek, J., Novak, O., Syka, J., 2013. Two-Photon Processor and SeNeCA: a freely available software package to process data from two-photon calcium imaging at speeds down to several milliseconds per frame. J. Neurophysiol. 110, 243–256. https://doi.org/10.1152/jn.00087.2013
Trachtenberg, J.T., Chen, B.E., Knott, G.W., Feng, G., Sanes, J.R., Welker, E., Svoboda, K., 2002. Long-term in vivo imaging of experience-dependent synaptic plasticity in adult cortex. Nature 420, 788–794. https://doi.org/10.1038/nature01273
Tremblay, R., Lee, S., Rudy, B., 2016. GABAergic Interneurons in the Neocortex: From Cellular Properties to Circuits. Neuron 91, 260–292. https://doi.org/10.1016/j.neuron.2016.06.033
Tsukano, H., Horie, M., Bo, T., Uchimura, A., Hishida, R., Kudoh, M., Takahashi, K., Takebayashi, H., Shibuki, K., 2015. Delineation of a frequency-organized region isolated from the mouse primary auditory cortex. J. Neurophysiol. 113, 2900–2920. https://doi.org/10.1152/jn.00932.2014
Tsunada, J., Lee, J.H., Cohen, Y.E., 2012. Differential representation of auditory categories between cell classes in primate auditory cortex. J. Physiol. 590, 3129–3139. https://doi.org/10.1113/jphysiol.2012.232892
Tsurufwi, S., Kurihara, A., Ojima, F., 1984. Mechanisms of Anti-inflammatory Action of Dexamethasone: Blockade by Hydrocortisone Mesylate and Actinomycin D of the Inhibitory Eftect of Dexamethasone on Leukocyte Infiltration in Inflammatory Sites 229, 7.
Ulanovsky, N., Las, L., Farkas, D., Nelken, I., 2004. Multiple time scales of adaptation in auditory cortex neurons. J. Neurosci. Off. J. Soc. Neurosci. 24, 10440–10453. https://doi.org/10.1523/JNEUROSCI.1905-04.2004
Umetsu, Y., Tenno, T., Goda, N., Shirakawa, M., Ikegami, T., Hiroaki, H., 2011. Structural difference of vasoactive intestinal peptide in two distinct membrane-mimicking environments. Biochim. Biophys. Acta BBA - Proteins Proteomics 1814, 724–730. https://doi.org/10.1016/j.bbapap.2011.03.009
Vogelstein, J.T., Packer, A.M., Machado, T.A., Sippy, T., Babadi, B., Yuste, R., Paninski, L., 2010. Fast Nonnegative Deconvolution for Spike Train Inference From Population Calcium Imaging. J. Neurophysiol. 104, 3691–3704. https://doi.org/10.1152/jn.01073.2009
Wang, Q., Webber, R.M., Stanley, G.B., 2010. Thalamic synchrony and the adaptive gating of information flow to cortex. Nat. Neurosci. 13, 1534–1541. https://doi.org/10.1038/nn.2670
Wang, X.-J., 2008. Decision Making in Recurrent Neuronal Circuits. Neuron 60, 215–234. https://doi.org/10.1016/j.neuron.2008.09.034
Wang, Y., 2002. Anatomical, Physiological, Molecular and Circuit Properties of Nest Basket Cells in the Developing Somatosensory Cortex. Cereb. Cortex 12, 395–410. https://doi.org/10.1093/cercor/12.4.395
Wang, Y., Toledo-Rodriguez, M., Gupta, A., Wu, C., Silberberg, G., Luo, J., Markram, H., 2004. Anatomical, physiological and molecular properties of Martinotti cells in the somatosensory cortex of the juvenile rat. J. Physiol. 561, 65–90. https://doi.org/10.1113/jphysiol.2004.073353
Watakabe, A., Ohtsuka, M., Kinoshita, M., Takaji, M., Isa, K., Mizukami, H., Ozawa, K., Isa, T., Yamamori, T., 2015. Comparative analyses of adeno-associated viral vector serotypes 1, 2, 5, 8 and 9 in marmoset, mouse and macaque cerebral cortex. Neurosci. Res. 93, 144–157. https://doi.org/10.1016/j.neures.2014.09.002

West, D.C., Mercer, A., Kirchhecker, S., Morris, O.T., Thomson, A.M., 2006. Layer 6 cortico-thalamic pyramidal cells preferentially innervate interneurons and generate facilitating EPSPs. Cereb. Cortex N. Y. N 1991 16, 200–211. https://doi.org/10.1093/cercor/bhi098

White, C.M., Ji, S., Cai, H., Maudsley, S., Martin, B., 2010. Therapeutic potential of vasoactive intestinal peptide and its receptors in neurological disorders. CNS Neurol. Disord. Drug Targets 9, 661–666.

Wilent, W.B., Contreras, D., 2005. Dynamics of excitation and inhibition underlying stimulus selectivity in rat somatosensory cortex. Nat. Neurosci. 8, 1364–1370. https://doi.org/10.1038/nn1545

Wills, T.J., Lever, C., Cacucci, F., Burgess, N., O'Keefe, J., 2005. Attractor Dynamics in the Hippocampal Representation of the Local Environment. Science 308, 873–876. https://doi.org/10.1126/science.1108905

Winkowski, D.E., Kanold, P.O., 2013. Laminar transformation of frequency organization in auditory cortex. J. Neurosci. Off. J. Soc. Neurosci. 33, 1498–1508. https://doi.org/10.1523/JNEUROSCI.3101-12.2013

Woodruff, A.R., McGarry, L.M., Vogels, T.P., Inan, M., Anderson, S.A., Yuste, R., 2011. State-Dependent Function of Neocortical Chandelier Cells. J. Neurosci. 31, 17872–17886. https://doi.org/10.1523/JNEUROSCI.3894-11.2011

Wu, G.K., Arbuckle, R., Liu, B., Tao, H.W., Zhang, L.I., 2008. Lateral Sharpening of Cortical Frequency Tuning by Approximately Balanced Inhibition. Neuron 58, 132–143. https://doi.org/10.1016/j.neuron.2008.01.035

Xu, H., Jeong, H.-Y., Tremblay, R., Rudy, B., 2013. Neocortical Somatostatin-Expressing GABAergic Interneurons Disinhibit the Thalamorecipient Layer 4. Neuron 77, 155–167. https://doi.org/10.1016/j.neuron.2012.11.004

Xu, X., Roby, K.D., Callaway, E.M., 2010. Immunochemical characterization of inhibitory mouse cortical neurons: Three chemically distinct classes of inhibitory cells. J. Comp. Neurol. 518, 389–404. https://doi.org/10.1002/cne.22229

Yamawaki, N., Borges, K., Suter, B.A., Harris, K.D., Shepherd, G.M.G., 2014. A genuine layer 4 in motor cortex with prototypical synaptic circuit connectivity. eLife 3. https://doi.org/10.7554/eLife.05422

Yavorska, I., Wehr, M., 2016. Somatostatin-Expressing Inhibitory Interneurons in Cortical Circuits. Front. Neural Circuits 10. https://doi.org/10.3389/fncir.2016.00076

Yu, Y.-C., Bultje, R.S., Wang, X., Shi, S.-H., 2009. Specific synapses develop preferentially among sister excitatory neurons in the neocortex. Nature 458, 501–504. https://doi.org/10.1038/nature07722

Yu, Y.-C., He, S., Chen, S., Fu, Y., Brown, K.N., Yao, X.-H., Ma, J., Gao, K.P., Sosinsky, G.E., Huang, K., Shi, S.-H., 2012a. Preferential electrical coupling regulates neocortical lineage-dependent microcircuit assembly. Nature 486, 113–117. https://doi.org/10.1038/nature10958

Yu, Y.-C., He, S., Chen, S., Fu, Y., Brown, K.N., Yao, X.-H., Ma, J., Gao, K.P., Sosinsky, G.E., Huang, K., Shi, S.-H., 2012b. Preferential electrical coupling regulates neocortical lineage-dependent microcircuit assembly. Nature 486, 113–117. https://doi.org/10.1038/nature10958

Yuan, F., Salehi, H.A., Boucher, Y., Vasthare, U.S., Tuma, R.F., Jain, R.K., 1994. Vascular Permeability and Microcirculation of Gliomas and Mammary Carcinomas Transplanted in Rat and Mouse Cranial Windows 6.

Yuste, R., 2005. Origin and Classification of Neocortical Interneurons. Neuron 48, 524–527. https://doi.org/10.1016/j.neuron.2005.11.012

Yuste, R., Gutnick, M.J., Saar, D., Delaney, K.R., Tank, D.W., 1994. Ca2+ accumulations in dendrites of neocortical pyramidal neurons: an apical band and evidence for two functional compartments. Neuron 13, 23–43.

Zeisel, A., Munoz-Manchado, A.B., Codeluppi, S., Lonnerberg, P., La Manno, G., Jureus, A., Marques, S., Munguba, H., He, L., Betsholtz, C., Rolny, C., Castelo-Branco, G., Hjerling-Leffler, J., Linnarsson, S., 2015. Cell types in the mouse cortex and hippocampus revealed by single-cell RNA-seq. Science 347, 1138–1142. https://doi.org/10.1126/science.aaa1934

Zhang, K., 1996. Representation of spatial orientation by the intrinsic dynamics of the head-direction cell ensemble: a theory. J. Neurosci. 16, 2112–2126. https://doi.org/10.1523/JNEUROSCI.16-06-02112.1996

Zhang, S., Xu, M., Kamigaki, T., Do, J.P.H., Chang, W.-C., Jenvay, S., Miyamichi, K., Luo, L., Dan, Y., 2014. Long-range and local circuits for top-down modulation of visual cortex processing. Science 345, 660–665. https://doi.org/10.1126/science.1254126

Zhou, Y., Mesik, L., Sun, Y.J., Liang, F., Xiao, Z., Tao, H.W., Zhang, L.I., 2012. Generation of Spike Latency Tuning by Thalamocortical Circuits in Auditory Cortex. J. Neurosci. 32, 9969–9980. https://doi.org/10.1523/JNEUROSCI.1384-12.2012

Zhu, Y., Stornetta, R.L., Zhu, J.J., 2004. Chandelier Cells Control Excessive Cortical Excitation: Characteristics of Whisker-Evoked Synaptic Responses of Layer 2/3 Nonpyramidal and Pyramidal Neurons. J. Neurosci. 24, 5101–5108. https://doi.org/10.1523/JNEUROSCI.0544-04.2004

Zipfel, W.R., Williams, R.M., Webb, W.W., 2003. Nonlinear magic: multiphoton microscopy in the biosciences. Nat. Biotechnol. 21, 1369–1377. https://doi.org/10.1038/nbt899

Zufferey, R., Donello, J.E., Trono, D., Hope, T.J., 1999. Woodchuck Hepatitis Virus Posttranscriptional Regulatory Element Enhances Expression of Transgenes Delivered by Retroviral Vectors. J. Virol. 73, 2886–2892.